Universidade do Minho
Escola de Ciências

Isabel Carina Simões da Silva

Biological characterization of coatings based on titanium dioxide doped with metallic elements for antimicrobial applications

Abril de 2013

Isabel Carina Simões da Silva **Biological characterization of coatings based on titanium dioxide doped with metallic elements for antimicrobial applications**

UMinho | 2013

Universidade do Minho
Escola de Ciências

Isabel Carina Simões da Silva

Biological characterization of coatings based on titanium dioxide doped with metallic elements for antimicrobial applications

Dissertação de Mestrado
Mestrado em Biofísica e Bionanossistemas

Trabalho realizado sob a orientação do
Professor Doutor Joaquim Carneiro
e da
Professora Doutora Célia Pais

Abril de 2013

"What we know is a drop, what we ignore is an ocean"

Isaac Newton

I dedicate this work to my

grandfather Joaquim.

AGRADECIMENTOS

Todo o meu trabalho de investigação não teria sido possível sem a presença de fantásticas pessoas que me acompanharam ao longo deste percurso. Um muito obrigado não chegará para agradecer todo o apoio, dedicação e respeito que sempre demonstraram por mim e pelo meu trabalho.

Em primeiro quero agradecer aos meus orientadores, Professor Doutor Joaquim Carneiro do Departamento de Física, e Professora Doutora Célia Pais do Departamento de Biologia, da Universidade do Minho, por toda a dedicação, disponibilidade e apoio incansável que sempre me demonstraram. Por toda a bondade e conhecimento que me conseguiram transmitir tão claramente. Aumentaram ainda mais o meu gosto pela investigação onde descobri uma área fascinante: a nanotecnologia.

Gostaria também de agradecer à Professora Doutora Paula Sampaio do Departamento de Biologia e ao Doutor Pedro Carvalho do Departamento de Física, da Universidade do Minho. Foram como meus segundos orientadores devido ao facto de estarem constantemente presentes em cada barreira e desafio, sempre prestáveis a me apoiar e ajudar.

Quero agradecer também à Universidade do Minho, ao Departamento de Física e ao Departamento de Biologia pela disponibilidade na realização deste meu trabalho.

É com enorme agrado que agradeço à Mestre Sofia Azevedo do Departamento de Física da Universidade do Minho, pelo trabalho incansável para comigo, pela força, determinação, empenho e conhecimento extraordinário que possui e demonstrou-me a cada passinho. Pelos "sermões" que nunca me faltaram mas também pelas palavras de incentivo: Fizeram falta!

De maneira nenhuma poderei esquecer de agradecer à Mestre Filipa Fernandes do Departamento de Física da Universidade do Minho, por todo o companheirismo, toda a bondade, sempre prestável e com um sorriso de encorajamento em cada desafio. Pelos dias ao meu lado em trabalhos de caracterização necessários para a realização do meu trabalho.

Aos meus colegas do Departamento de Biologia da Universidade do Minho, Catarina Carneiro, Catarina Vaz, Joana Pereira, Filipa Vale e Manoel Oliveira que me acolheram de braços abertos de forma tão sincera e calorosa no seu espacinho onde todos tínhamos a mesma paixão e gosto pela investigação. Por toda a amizade e cumplicidade que se formou ao longo deste percurso. "A "Micro II" é a nossa segunda casa".

Quero agradecer também a todos os técnicos, tanto do Departamento de Física como do de Biologia, que sempre estiveram presentes para me ajudar no que necessitava. Agradeço principalmente à técnica Manuela Rodrigues, do Departamento de Biologia, pelo fornecimento dos microorganismos que utilizei neste trabalho e ao Engenheiro José Santos, do laboratório de filmes finos II do Departamento de Física, pelo apoio e presença constante no laboratório!

Como é óbvio quero agradecer aos meus colegas de mestrado, Rita Rodrigues, Henrique Cachetas, Ivo Lopes, José do Egipto, Jorge Rodrigues, João Martins e Pedro Mendes. Este obrigado é por estes dois anos onde nos aprofundamos em tantos conhecimentos, pelas tardes e noites de trabalhos intensos, pela força e determinação que cada um me demonstrou à sua maneira. Pelas gargalhadas e simpatia que nunca faltou neste grupo. Desde já desejo a maior sorte a todos vocês!

E por fim mas não menos importante, muito pelo contrário, quero agradecer à minha família, especialmente às três pessoas mais importantes da minha vida, à minha mãe Ana, ao meu pai Alberto e ao meu irmão Carlos, por nunca me desampararem em nenhum momento, por tanto esforço e coragem, por tanto amor e carinho e principalmente por sempre acreditarem em mim e naquilo que sonho. Um agradecimento especial ao Tiago por estar ao meu lado constantemente e por compreender e ouvir sempre os meus desvaneios e mau humor com palavras de incentivo e força. Vocês são o meu porto de abrigo.

A todos eles o meu sincero Obrigado!

ABSTRACT

The use of semiconductors for processes of self-cleaning, air and water depollution as well as surface disinfection has triggered a great interest in the scientific community. One of the most used semiconductor materials is titanium dioxide (TiO_2) due to their large photocatalytic effect, higher oxidation strength, chemical stability non-toxicity and availability, among others. This oxide has been highly researched and was found that it is capable of decomposing various organic and inorganic compounds.

Most of these studies were conducted under ultraviolet light (UV), since TiO_2 has a photocatalytic activity and a relatively high chemical stability under UV radiation. The process has several advantages and one of them is the ability to combine processes involving biological decontamination methods, which makes this semiconductor capable of removing a wide range of bacteria, viruses, fungi, algae, protozoa, etc. (antimicrobial effect).

Despite the advantages of this process we can notice two important limitations. Firstly, only 5% of the solar spectrum comprises ultraviolet radiation; secondly, the direct UV radiation is harmful to human's health. Based on these limitations, the researchers have been studying methods that enable the use of TiO_2 under the presence of visible light. This effect can be achieved by doping TiO_2 with some metallic elements. Having this in mind some research groups have been focusing on the antimicrobial applications of this semiconductor material. Thus, the main goal of this work was the production of TiO_2 thin films and TiO_2 thin films doped with two different metals (iron and silver) with photocatalytic activity and, consequently, antimicrobial proprieties.

The thin films were deposited on glass and cotton substrates by DC magnetron sputtering method. The studies of morphological characterization of the surface were performed using SEM and AFM techniques. The thin films crystalline structure was evaluated by XRD technique. Through UV-Vis spectroscopy it was possible to study their optical proprieties (namely transmittance). The thin films photocatalytic ability was assessed the photodegradation of methylene blue aqueous solution (organic dye) under UV irradiation. The thin films antimicrobial properties were tested by studying there effect on the growth of a strain of *Escherichia coli* bacteria. The TiO_2 thin films doped with silver were the ones that presented the higher photocatalytic and antimicrobial performance, showing around 10% of photodegradation yield and presented the higher inhibition of bacterial growth.

RESUMO

A utilização de semicondutores para processos de auto-limpeza, desinfecção de superfícies, do ar e da água, tem suscitado um grande interesse no mundo científico. Um dos semicondutores mais utilizado é o dióxido de titânio (TiO_2) devido ao seu elevado efeito fotocatalítico, elevada capacidade de oxidação, estabilidade química, disponibilidade e não-toxicidade, entre outros. Este material semicondutor tem sido extremamente investigado e verificou-se que é capaz de decompor vários tipos de compostos orgânicos e inorgânicos.

A maioria destes estudos foram realizados sob a ação de luz ultravioleta (UV), uma vez que o TiO_2 apresenta uma actividade fotocatalítica e uma estabilidade química relativamente elevada sob a radiação UV. O processo apresenta diversas vantagens sendo uma delas a possibilidade de combinar processos de descontaminação biológica, tornando este semicondutor capaz de eliminar uma vasta gama de bactérias, vírus, fungos, algas, protozoários, etc. (efeito antimicrobiano).

Embora o processo apresente diversas vantagens, observam-se duas importantes limitações. Em primeiro lugar, apenas 5% do espectro solar compreende a radiação ultra-violeta, e em segundo lugar a radiação UV é prejudicial para a saúde do ser humano. Tendo em consideração estas limitações, vários grupos de investigação têm estudado métodos alternativos que possam ser capazes de permitir a utilização de TiO_2 na presença da luz visível. Um dos métodos utilizados consiste na dopagem do TiO_2 com elementos metálicos. Tendo em consideração o exposto, alguns grupos de investigação têm direcionado os seus trabalhos na utilização deste material semicondutor ao estudo de aplicações antimicrobianas. Neste sentido, o principal objetivo deste trabalho visou a produção de filmes finos de TiO_2 e filmes finos de TiO_2 dopados com dois metais diferentes (ferro e prata) com atividade fotocatalítica e propriedades antimicrobianas.

Os filmes finos foram depositados em substratos de vidro e de algodão pelo método de pulverização catódica em magnetrão utilizando fonte DC. Os estudos de caracterização morfológica da superfície foram realizados pela utilização de microscopia electrónica de varrimento (do inglês *Scanning Electron Microscopy*, SEM) e microscopia de força atómica (do inglês *Atomic Force Microscopy*, AFM). A estrutura cristalina dos filmes finos foi avaliada pela técnica de Difração de Raios-X (do inglês *X-ray difraction,* XRD).

Através da utilização dr espectroscopia UV-Vis foi possível estudar as propriedades ópticas dos filmes finos produzidos (nomeadamente a transmitância). A atividade fotocatalítica dos filmes finos foi avaliada através da medição da fotodegradação de uma solução aquosa de azul de metileno (corante orgânico) sob iradiação de luz UV. As propriedades antimicrobianas dos filmes finos foram estudadadas através da observação das curvas de crescimento da bactéria *E. coli*. Os filmes finos de TiO_2 dopados com prata foram aqueles que apresentaram os maiores desempenhos fotocatalítico e antimicrobiano, apresentando um rendimento de fotodegradação de aproximadamente 10% e a maior inibição do crescimento bacteriano.

TABLE OF CONTENTS

LIST OF ABBREVIATIONS AND SYMBOLS

µm	Micrometer
AFM	Atomic Force Microscopy
Ag	Silver
Al_20_3	Aluminum Oxide or Alumina
Ar	Argon
Au	Gold
BSE	Backscattered electrons
C	Carbon
CB	Conduction Band
CBM	Conventional balanced magnetrons
CO_2	Carbon Dioxide
Cu	Copper
CVD	Chemical Vapor Deposition
DC	Direct Current
DNA	Deoxyribonucleic Acid
DRIs	Device-Related Infections
E. Coli	*Escherichia coli*
EDX	Energy Dispersive X-ray
Eg	Band Gap Energy
eV	Electron Volt
Fe	Iron
H^+	Hidrogen
hkl	Miller indices
H_20	Water

H_2O_2	Hydrogen Peroxide
IM	Inner Membrane
LB	Luria-Bertani medium
M	Metal
MB	Methylene blue
N	Outer magnet
NaCl	Sodium Chloride
Nd	Neodymium
Ni	Nickel
NiO	Nickel Oxide
nm	Nanometer
NPs	Nanoparticles
O_2^-	Superoxide Radical
OH	Hydroxyl Radical
OOH	Hydroperoxyl
OM	Outer Membrane
Pd	Palladium
PG	Peptidoglycan
PM	Planar magnetron
PVD	Physical Vapor Deposition
PZC	Point of zero charge
RF	Radio frequency
ROS	Reactive Oxygen Species
S	Inner magnet
SC	Semiconductor
SE	Secondary electrons

SEM	Scanning Electron Microscopy
Si_3N_4	Silicon nitride
SiO_2	Silicon Dioxide or Silica
Sn	Tin
SPM	Scanning probe microscopes
STM	Scanning tunneling microscopy
SZM	Structure zones models
T_h	Homologous temperature
T_m	Melting temperature
T_s	Temperature normalized
TiO_2	Titanium Dioxide or Titania
UBM	Unbalanced magnetrons
UV	Ultraviolet
UVA	Ultraviolet Type A
UV-Vis-Nir	Ultraviolet-Visible-Near Infra-Red zone
VB	Valence Band
XRD	X-Ray Diffraction
ZnO	Zinc Oxide
ZrO_2	Zirconium Dioxide or Zirconia
$h\upsilon$	Photon energy
e^-	Electron
h^+	Hole
(e^-/ h^+)	Electron/hole pair
θ	Angle
d	Distance
γ_{SL}	Tensions between solid and liquid

γ_{SV}	Tensions between solid and vapor
γ_{LV}	Tensions between liquid and vapor
λ	Wavelength
F	Force
K	Spring Constant
T	Transmittance
A	Absorbance
TA	Total surface area
cm	Centimeters
W	Walt
V	Volt
η	Yield
k	Photodegradation rate

LIST OF FIGURES

LIST OF TABLES

CHAPTER I

INTRODUCTION AND OBJECTIVES

CHAPTER I – INTRODUCTION

1.1 – GENERAL

The origin of Nanotechnology dates back to 1959, where Richard Freynman proposed the direct manipulation of individual atoms as a very powerful physico-chemical tool very powerful. However, the term nanotechnology was created by Norio Taniguchi of Tokyo University, in 1974. This term was defined as the precision production of materials with nanometer scale. Furthermore, Eric Drexler in 1986, mentioned the term "nanotechnology" in his book "Engines of Creation: The Coming Era of Nanotechnology" [1].

Nanotechnology studies the characterization, production and application of structures, equipment, devices and systems in scale ranging from individual molecules or molecules of approximately 100 nanometers, as well as the junction of the nanostructures for systems with larger dimensions [1].

A nanometer (nm) is one thousand millionth of a meter. The size of a DNA molecule is in the range of 100 nm and is slightly lower than that of a virus. A single human hair is about 80,000nm diameter. A red blood cell is approximately 7,000 nm wide diameter and water molecule almost 0.3nm [2]. See the comparison of scale in Figure 1.

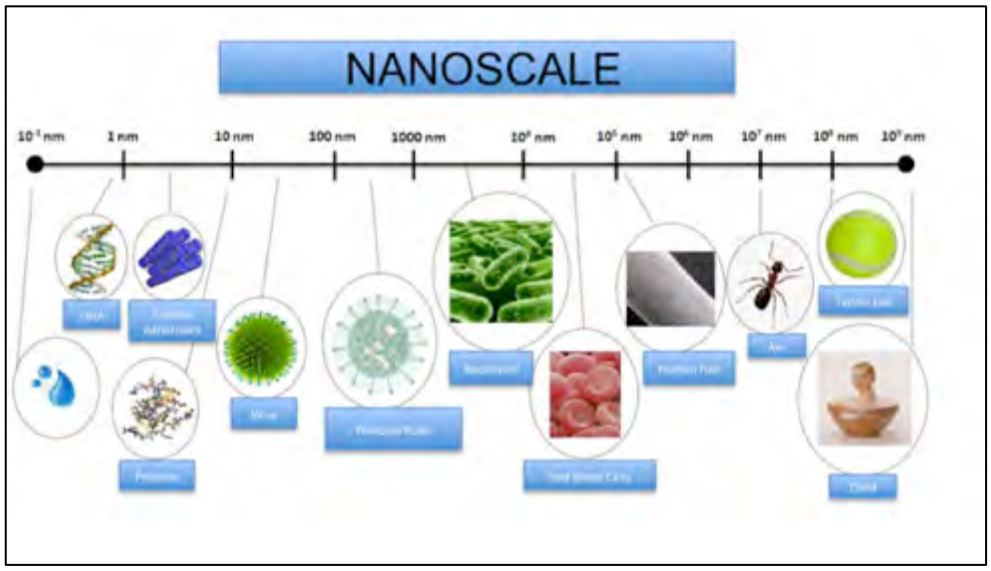

Figure 1: Representation of the dimensions of some typical species, in its various scales (adapted from [2]).

Nanomaterials have been used over time in various applications ranging from window glass and sunglasses lens (see Figure 2) to car bumpers and paints. Nowadays, applications have increased in several areas, such as the manufacture of other materials, computers chips, in medical diagnosis and health care, biotechnology, exploration, security, energy, among others [3].

In the next 10 to 15 years, nanotechnology will have a significant impact on the economy and society, and ever more with utmost importance so that new scientific and technological advances are achieved.

Figure 2: Thin films in glass and sunglasses [4, 5].

Currently, scientific research in the field of nanotechnology has attracted growing interest because of its several applications, either through design of new products, materials characterization, production and application of structures, devices and systems in nanometer scale [6, 7].

In fact, applications of nanomaterials, especially of nanoparticles (NPs), in areas related to therapeutics and diagnosis, such as pathogen detection, drug delivery, disease diagnosis and imaging, among others, are in continuous progress. Alongside with the nanoparticles, thin films coatings have been used to design and create advanced nanocoating systems with significantly optimized or enhanced properties of great interest to health, food and biomedical industry [8].

Thin films are use for more than half a century. Their applications are found in the making of electronic devices, instrument coating, optical coatings and decorative parts.

Initially the thin films were used for decorative effects but currently these coatings are used for materials protection and manufacture of sensors, conductors, resistors of microelectronic circuits [9]; protection of metals against corrosion [10]; solid lubricants [11]; are also used to the protection of plastic packaging for food and optical coatings [12]; tool coatings to enhance their hardness [13]; photovoltaic devices for solar energy conversion [14], among many other applications.

The name "thin film" is given to a coating with thickness of up to 300 μm, but this doesn't include coatings of paints and varnishes that, in general, are ticker. These coatings can be made from various types of materials, including metals, metal oxides or organic substances [15]. In Figure 3 is shown a thin film of a metal oxide - TiO_2, in glass substrate.

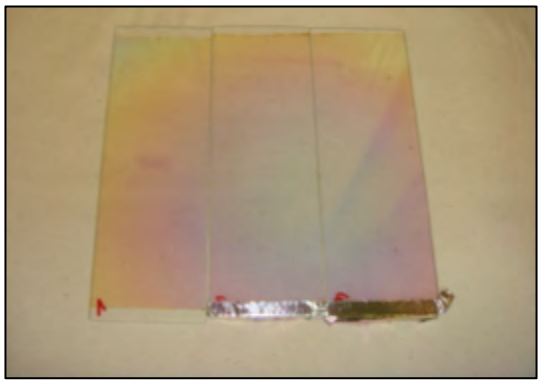

Figure 3: TiO_2 thin film in glass substrate.

It is very important that a thin film presents all, or the majority, of the following properties mentioned below:

- Should be chemically stable in the environment in which it will be used;

- Should be strongly adherent to the surface (substrate), since they are extremely fragile;
- Should have a uniform thickness;
- Must be pure or have controllable composition;
- Should have low defect density [16].

Normally the properties of a material in the form of a thin film differ substantially from the properties of the same material in its solid state due to the influence of the surface, the relation between surface and volume is much greater in the case of the film. On the other hand thin films properties depends on the deposition processes that are used [15]. Thin films can be obtained by a variety of techniques, such as: deposition from liquids; chemical deposition from the vapor phase, a process called CVD (Chemical Vapor Deposition); and by physical deposition from the vapor phase, a process denominated PVD (Physical Vapor Deposition). In this last case species are physically torn apart from a target by temperature (evaporation) or by impact of ions (Sputtering) and are transported to the substrate where they condense into a thin film [15].

In Chapter III Sputtering process will be explained in detail, since the process was used in this laboratory work for the production of thin films.

Since 2010, nanotechnology use became common in many manufactured goods, for example, in electronics and informatics applications, as the production of microprocessors and memory chips, which became available in the market in 2009. Finally, the applications in health-care became more significant with the application of the nano-enabled pharmaceuticals and medical devices [17]. These devices have become of greater importance for human health care and, because of that, its demand in the market has increased over the past three decades. Medical devices such as heart valves, vascular grafts, various catheters and orthopedic fixation screws, are of the must importance because they are used to save lives and to restore the quality of life of many people [18].

These medical devices present a problem. They can be infected by bacteria contamination and cause serious problems or even be fatal for the patient. These

devices are called device-related infections (DRIs), that consist in the proliferation of bacteria and their attaching to the surface of the medical devices and implants [19]. As soon as planktonic bacteria, that circulate in the vascular system, are attached on to the implant surface, they multiply and form a biofilm that eventually leads to an infection (see Figure 4).

Besides the bacterial colonies that are formed in the device, they will also multiply and form an exocellular polysaccharide matrix, which protects them against antibiotics and the host body's innate defense system [20]. This makes it very difficult to remove these bacterial colonies in medical devices. Thus a promising strategy studied by scientists for reducing the occurrence of DRIs is to prevent the attachment of bacteria to the surfaces of the devices. This caused an increase in scientific research and development of thin coatings capable of conferring resistance to bacterial colonization, in the various biomedical devices, it have been studied [18].

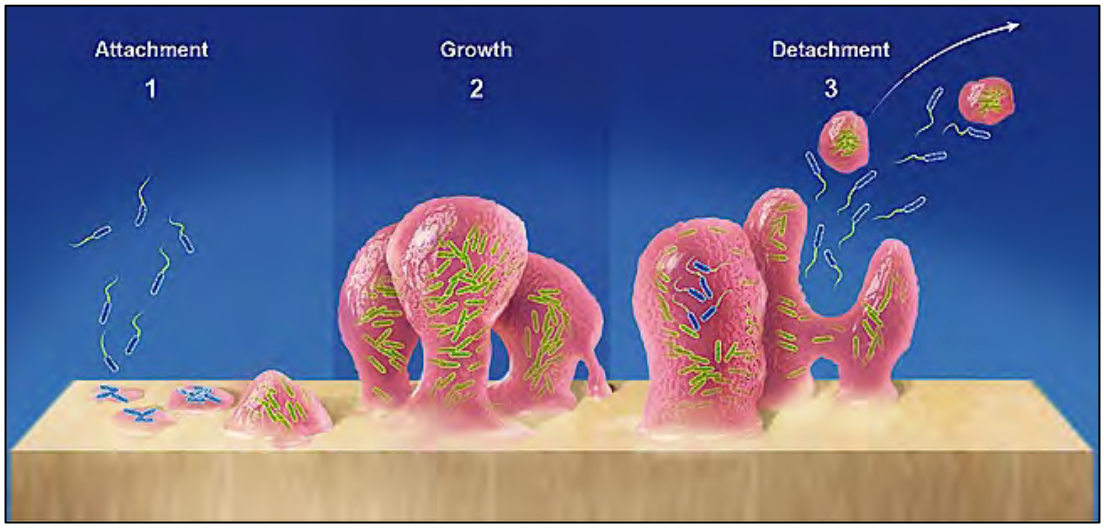

Figure 4: Illustration of the formation of a biofilm.

One of the approaches is the study of the modification of the device surface properties, by chemical and structural composition, and the study of new surfaces, with the aim of preventing bacterial proliferation, control of microorganisms size, shape and organization in the device. There are several methods for modifying the surface of a material capable of presenting antibacterial properties [21]. By

observing Figure 5, it is possible visualize a schematic of different methods for surface coatings with antibacterial properties.

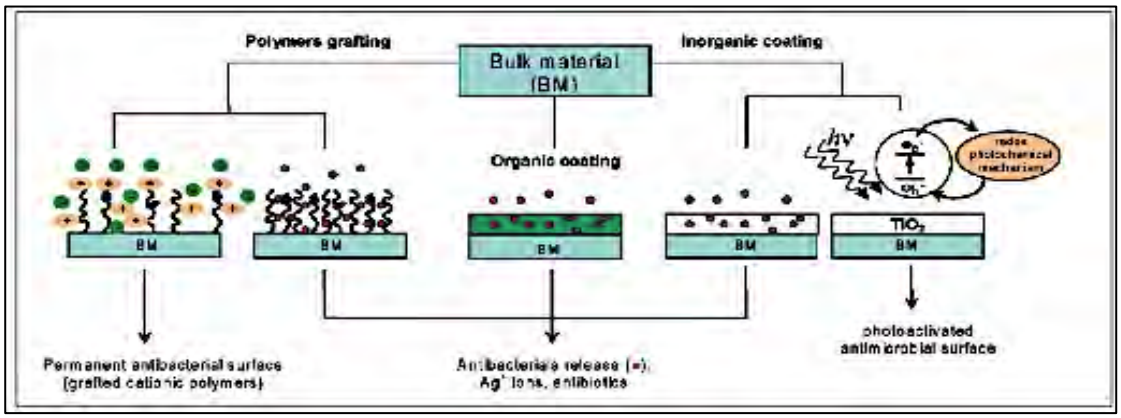

Figure 5: Schematic view of various methods for surface modification of medical devices with antibacterial properties [21].

One approach to modify the material surface and to combat the growth of microorganisms is based on inorganic coatings, in which there is a release of antimicrobial compounds and an intrinsic antibacterial activity. With this purpose are studied materials such as SiO_2, Al_2O_3, ZnO, TiO_2, etc. These materials are used by scientists due to their availability and easy handling, low toxicity, low cost, favorable mechanical strength, thermal stability, high surface area, and allow adsorption of various solids and organic ligands on their surface [22]. Between these inorganics materials, TiO_2 has received increasing attention by researchers, due to its strong oxidizing power, non-toxicity and long-lasting properties physical and chemical stability, low cost and broad-spectrum antibiosis [23]. So, the TiO_2 has been widely used in the sterilization of medical devices and air-conditioning filters owing to its self-sterilizing property. Lastly the TiO_2 has been widely used for the decomposition of organic compounds and microbial organisms, such as cancer cells, viruses and bacteria [23].

In this study, all the attention was focused in the TiO_2 coatings, one of the most attractive antimicrobial materials.

1.2 – MOTIVATION AND OBJECTIVES

The main objective of this work is the production of TiO_2 thin films with the ability to present antimicrobial activity. It is common knowledge in the scientific world that the TiO_2 semiconductor is an excellent photocatalyst when irradiated with UV light. Despite this advantage it is not to be expected that, for example, surgical rooms will have a large number of UV lamps, due to their high cost and the extended human exposure is unhealthy. Thus, in this work it was intended to study the activity of TiO_2 thin films and their doping with metallic elements that use UV irradiation to activate the TiO_2 photocatalysts.

Under this context, the work performed in this master thesis combined the production of TiO_2 thin films and TiO_2 thin films doped with iron and silver by the using DC magnetron sputtering deposition method and the study of their physical and biological properties. A study such as the effect of different thicknesses, morphology and dopant concentration effects in some biological functions was evaluated. *Escherichia coli* was the bacteria used throughout this study.

After the production of TiO_2, Fe- and Ag-doped TiO_2 thin films by DC magnetron sputtering method, the produced samples were characterized in order to evaluate their structural (by X-Ray Diffraction - XRD), surface (by Scanning Electron Microscopy - SEM and Atomic Force Microscopy - AFM) and optical properties (with UV-Vis Spectroscopy). The thin film's photocatalytic activity was assessed by measuring the variation on the absorbance spectra of methylene blue aqueous solution over time under UV irradiation.

1.3 – THESIS ORGANIZATION

This thesis is structured in seven chapters, each one corresponding to different subjects. In the first chapter it is made a very brief introduction of the work, describing personal and scientific motivations to do it, the reason why and how the development of thin films are important for improvement of human health and, of

course, the main goals of this project. In chapter 2 we present an overview of the bibliographical review where it is possible to find information regarding thin films; mainly titanium dioxide thin films and its photocatalytic/antimicrobial properties. In chapter 3 and 4 will be presented some theoretical principles of production techniques (Magnetron Sputtering) and characterization ones (XRD, SEM, AFM, Contact Angle Measurements and Optical Spectroscopy). In chapter 5 are presented the details regarding the experimental procedure. In chapter 6 are presented all the results and their discussion. Finally, in chapter 7 and 8 will be presented the main conclusions and future perspectives, respectively.

CHAPTER II

BIBLIOGRAPHIC REVIEW

CHAPTER II – BIBLIOGRAPHIC REVIEW

2.1 – INTRODUCTION

In this chapter will be described the main characteristics of a semiconductor with high interest in photocatalytic protocols: TiO_2. The characteristics of TiO_2 are depicted as well as the photocatalytic process. Lastly, are listed some of the applications that this oxide is associated with, reinforcing the interest in antimicrobial applications.

2.2 – SEMICONDUCTORS

A large number of the research being done is focused on semiconductor photocatalysts due to their use in the solar energy conversion, environmental purification, water splitting, air and water purification and surface/soil sterilization [24].

A semiconductor (SC) is characterized by a band energetic structure where the valence band (VB) is completely filled with electrons at low energy levels and a conduction band (CB) with higher and unoccupied energy states (Figure 6). The region between these two bands is called a band gap [21, 24]. In this band gap there are some sub-bands that are closely related to surface defects and surface states. The energy of the band gap (Eg) corresponds to the energy difference between the CB and the VB [24].

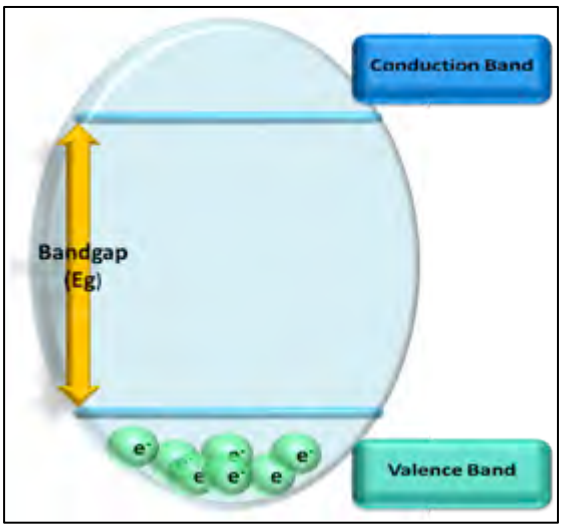

Figure 6: Schematic representation of a semiconductor [25].

When the SC is photo-irradiated with a photon with energy hν equal or higher than the band gap energy, the electrons (e^-) of the VB are promoted to CB (via photon-excitation) and a hole (h^+) is formed in VB (26) (see Figure 7).

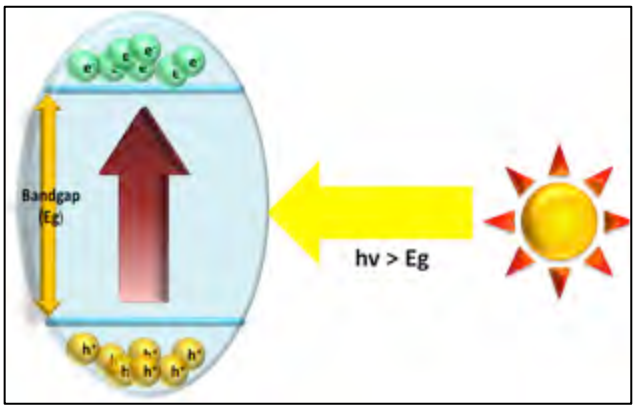

Figure 7: Schematic representation of a semiconductor after photon-irradiation [25].

After the jump of electrons from the VB to the CB there is the formation of the electron-hole pair (e^-/h^+). This can then result with one rapid recombination or with charge trapping in a picoseconds time, and is due to this process that the semiconductor works as a photocatalyst, which becomes of great interest for a wide range of processes and applications [21].

2.3 – TITANIUM DIOXIDE

2.3.1 – GENERAL DESCRIPTION

Titanium dioxide (titania, TiO_2) is undoubtedly the most used semiconductor used due to its chemical stability, non-volatile nature, low thermal conductivity, refractory character, relatively low cost, non-toxicity and high photoactivity. TiO_2 is also the semiconductor selected for organic applications since its doping with metallic elements correspond to a strategy to increased the λ radiation absorption [27–29]. TiO_2 is amphoteric (although being more acidic than alkaline), it is commonly a crystalline material with seven reported polymorphs, from which four are natural and the others ones are synthetic. Of the four natural polymorphs there are three main polymorphs: Anatase (crystal system: tetragonal), Rutile (crystal system: tetragonal) and Brookite (crystal system: orthorhombic) [30]. However, the anatase and rutile forms, of this semiconductor, are the most studied and used in numerous applications. By another hand, the brookite phase is less studied due to its rareness [31]. Both rutile and anatase unit cell can be described as one titanium atom surrounded by six oxygen atoms in octahedral configurations. The structures of the two crystalline forms are distinguished by the distortion of their octahedra and by their geometric arrangement. In rutile phase each octahedron is in contact with 10 neighbors' octahedra, while in the anatase phase each octahedron is in contact with 8 neighbors octahedral [32].

Figure 8 shows the crystal structures of TiO_2 in the anatase, rutile and brookite phases.

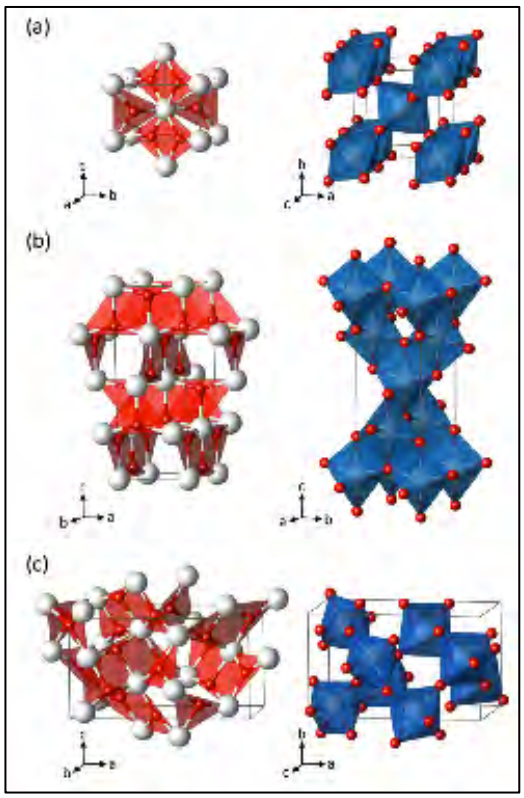

Figure 8: TiO_2 phases rutile (a), anatase (b) and brookite (c) (Ti (white); O (red)) [30].

Anatase shows a band gap of approximately 3.23 eV, corresponding to a UV wavelength adsorption of about 385 nm. One the other hand, rutile presents a band gap around 3.02 eV, with excitation wavelengths that extends into the visible light range, about 410 nm [21, 30].

Thermodynamic calculations based on calorimetry measurements, showed that rutile is the most stable form of this semiconductor at normal pressure and in all temperatures ranges up to its melting point. This phase also present a large crystallite size [33].

However, kinetically, the anatase is more stable because its conversion to rutile phase is very slow at room temperatures, making the occurrence of this transition practically never observed [34, 35]. This phase has a very small crystallite size, with the critical size of approximately 11nm in diameter, although smaller values have also been presented [36, 37]. However, at higher temperatures, anatase may be converted into rutile. The conversion of anatase to rutile is widely studied

because this is one of the most critical parameters in application of this semiconductor as a photocatalyst, in catalysis in general, and as powder ceramic material [38, 39].

There are few studies on the polymorphic surface of the brookite phase. In the past few years, the optical properties of brookite have been researched and were mainly focused on its absorption edge [40–42]. The electronic and optical properties ascribed to this crystalline phase were described, for the first time, by Landmann and his co-workers, in 2012. Anyway, a more detailed understanding of the surface structure, chemistry and photochemistry, is still required [30].

Anatase phase is also considered to be the most photochemically active phase of TiO_2. In other words, this phase presents a higher photocatalytic activity. This may be due to its high surface absorption capability and a high rate of hole trapping. Recently, researchers showed that the phase-mixed (anatase-rutile or brookite-anatase) has more activity than 100% anatase [43, 44].

2.3.2 – PHOTOCATALYTIC PROPERTIES

The TiO_2 is also the most used semiconductor for disinfection applications due to its strong photocatalysis mechanism. The photocatalytic activity process has its origins when TiO_2-surfaces are irradiated with sufficient photon energy, on aerobic conditions, to promote electrons from VB to the CB leading to the generation of (e^-/h^+) pairs (see Equation 1). As previously referred, the energy required to promote an electron to the CB in the case of anatase is about 3.2 eV, which means that, to occur a photocatalysis process it is necessary a wavelength of about 385nm (i.e., UVA).

Figure 9 shows the redox reactions after the formation of (e^-/h^+) pairs when irradiated by UV light.

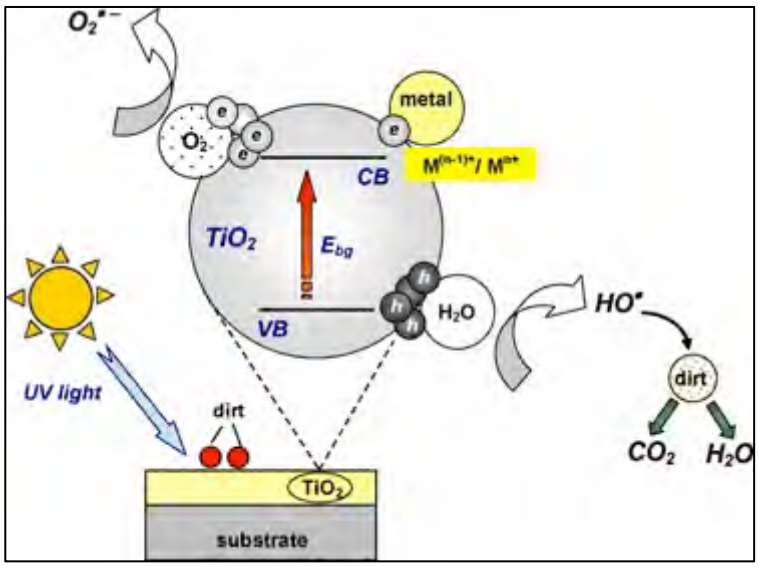

Figure 9: Image illustrating the photocatalytic mechanism of TiO_2 after UV light absorption [45].

The positively charged holes may be filled by migration of electrons from adjacent molecules, leaving these molecules with a hole. Thus, the holes may be mobile, and this process can be repeated. Electrons and holes can recombine with each other (bulk recombination) and the reaction is non-productive. When the electrons reach the surface they can migrate within the conduction band and react with oxygen molecules leading to the formation of superoxide radical (O_2^-) (Equation 2). This reaction, which competes with the fast electron-hole recombination, represents the initiation phase of a free-radical chain promoted by H_2O, leading to the formation of hydroxyl radical (•OH) (Equation 3). Therefore, there is the formation of reactive oxygen species (ROS). These ROS in solution can react to form hydrogen peroxide (H_2O_2) (Equation 4), promoting hydroxyl (•OH) (Equation 5) and hydroperoxyl (•OOH) (Equation 6) radicals. TiO_2 can also photodegrade organic compounds through oxidation reactions with free radicals leading to the formation of substances such as carbon dioxide (CO_2) and water (H_2O) (Equation 7). This process is called mineralization. These reactions can be extended to organic materials and/or microorganisms [46] and can be used in processes of sterilization, deodorization and disinfection [23].

$$TiO_2 + h\upsilon \rightarrow e_{cb^-} + h_{vb^+}$$ (Equation 1)

$$O_2 + e_{cb^-} \rightarrow O_2^-$$ (Equation 2)

$$h_{vb^+} + H_2O \rightarrow \bullet OH + H^+_{aq}$$ (Equation 3)

$$\bullet OH + \bullet OH \rightarrow H_2O_2$$ (Equation 4)

$$O_2^- + H_2O_2 \rightarrow \bullet OH + OH^- + O_2$$ (Equation 5)

$$O_2^- + H^+ \rightarrow \bullet OOH$$ (Equation 6)

$$\bullet OH + OrganicCompounds + O_2 \rightarrow CO_2 + H_2O$$ (Equation 7)

However, as the band gap energy ranges between 3.0 and 3.2 eV, one of the limitations in the photocatalysis process in a semiconductor is the relatively low value of the overall quantum efficiency due to the high recombination rate of the photo-induced (e^-/h^+) pairs in the semiconductor surface [24]. To address this disadvantage numerous studies have been made to increase the yield of visible photocatalysis such as: the use of nano-sized semiconductor crystallites instead of bulk materials [47, 48]; coupling TiO_2 to other oxides [49, 50]; modification of photocatalysts using doping elements [51, 52].

Photocatalytic activity of TiO_2 is strongly influenced by the presence of metallic species [23, 53]. A variety of attempts have been made to introduce different metals species into the TiO_2 matrix with the objective to enhance the photocatalytic activity or broaden the absorption of the solar spectrum [53]. The doping may include materials such as noble metals: gold (Au) and silver (Ag), magnetic particles: nickel (Ni) and ferrites, quantum dots, hydroxyapatites and various oxides: alumina (Al_2O_3), zirconia (ZrO_2), silica (SiO_2) and nickel oxide (NiO), metals such as: tin (Sn), palladium (Pd), copper (Cu), and iron (Fe), carbon (C) and neodymium (Nd) [22].

In the photocatalytic activity, it is very important to have in consideration the particle size. For larger particles, the (e^-/h^+) pair's volume recombination is the dominant process, while for small sized particles the distance covered by (e^-/h^+) pairs (during their trajectory from crystal interface to the surface) is shorter, increasing the migration rate to the surface in order to take part in the chemical redox reactions. The role of ion dopant is also very important because it can act as an electron trap in the semiconductor interface. The trap of charge carriers can decrease the volume recombination rate of (e^-/h^+) pairs and thus increasing the lifetime of charge carriers. The process of charge trapping can be described by equations 8, 9 and 10 [54]. In these equations M^{n+} is the metal ion dopant. The energy level of $M^{n+}/M^{(n-1)+}$ lies below the conduction band edge. Therefore, the energy level of transition metal ions thus affects trapping efficiency. Electron trapping makes it easy for holes to transfer onto the TiO_2 surface, reacting with OH^- to form active hydroxyl radicals (•OH) that will participate in the overall degradation of organic compounds [55].

$$M^{n+} + e_{cb^-} \rightarrow M^{(n-1)^+} \quad \text{(Equation 8)}$$

$$M^{n+} + h_{vb^+} \rightarrow M^{(n+1)^+} \quad \text{(Equation 9)}$$

$$OH^- + h_{vb^+} \rightarrow \bullet OH \quad \text{(Equation 10)}$$

As already mentioned previously, photocatalytic activity of the TiO_2 requires UV irradiation and this causes a limitation in this process. So the modification of the semiconductor by doping with metallic elements can, in general, reduce the band gap and promoting the absorption in the visible region of the electromagnetic spectrum [46].

Matsunaga and co-workers have demonstrated, for the first time, that antimicrobial activity of TiO_2 was activated by UV irradiation [56, 57] and since then this area became the subject of more research concerned with the reduction of bacteria, fungi, algae, protozoa and viruses as well as microbial toxins contaminations [58–60]. The ability to eliminate microorganisms on photocatalytic self-cleaning/self-disinfecting surfaces may provide a useful additional mechanism

in the control of diseases transmission, used for example in biomedical devices along with conventional disinfection methods.

2.3.3 – APPLICATIONS OF TIO_2 COATINGS

TiO_2 coatings present several applications, for example, self-cleaning windows, water/soil and air disinfection [61–62], purifying drinking water [63], treatment of wash waters from vegetable preparation [64], among others. Currently there are over 11,000 publications on photocatalysis (Figure 10). The effect of TiO_2 to eliminate microorganisms like bacteria, fungi, viruses have attracted great interest.

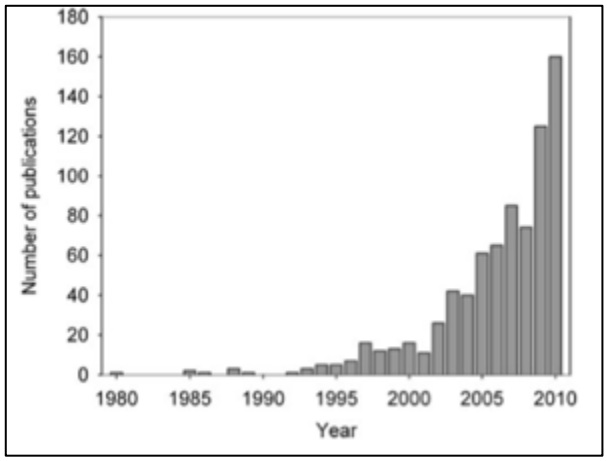

Figure 10: The graph shows increasing number of publications on photocatalytic disinfection over the years [46].

2.3.3.1 – ANTIMICROBIAL APPLICATIONS

Photocatalysis process has been shown to be able to degrade also a wide range of microorganisms such as bacteria, including endospores, fungi, algae, protozoa and viruses [65]. The major amount of studies performed in what concerns photocatalysis processes in microorganism's uses the *E. coli* bacteria. These bacteria (Figure 11) are common inhabitants of the gastrointestinal tract in humans [66]. *E. coli* is a Gram-negative bacilli that exist individually or in pairs, is facultative anaerobic with a type of metabolism that is both fermentative and respiratory [67].

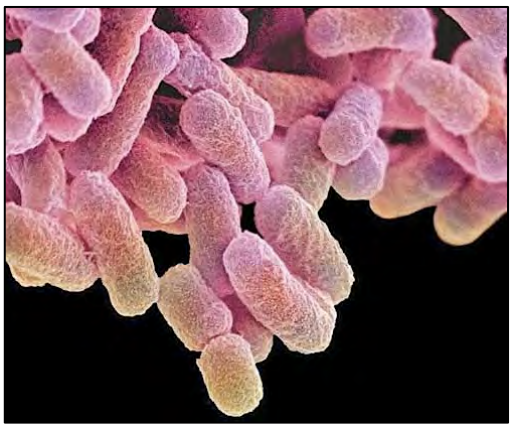

Figure 11: Electron microscopy photograph of *E. coli* cells [71].

TiO_2 photocatalytic process in Gram-positive bacteria was also studied and it was found that these bacteria were more resistant to the photocatalytic disinfection than Gram-negative bacteria [68–70]. This difference is generally attributed to cell wall differences between these two groups of bacteria. While Gram-negative bacteria have a thin peptidoglycan layer (PG), and an outer membrane (OM), Gram-positive bacteria have a thick peptidoglycan layer and show no outer membrane (see Figure 12).

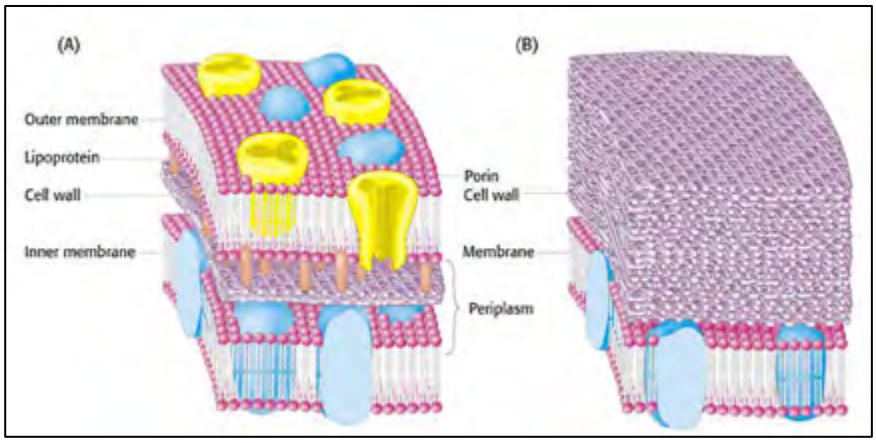

Figure 12: Cell walls of gram-negative (A) and gram-positive (B) bacteria [72].

However, some studies have shown that Gram-positive bacteria were more sensitive than Gram-negative ones [73–75]. These differences may be related with the different affinities for the TiO_2, that is, requires a close contact between the cells and TiO_2 so that there is a good antimicrobial activity. Although, more studies are needed in this area [75].

2.3.3.1.1 – Role of Reactive Oxygen Species (ROS) in the photocatalysis process

Many studies show that ROS, derived from the TiO_2 photocatalysis, are largely responsible for microorganisms cell death, such as *E. coli* bacterium [78–80], ·OH radicals are short-lived and probably would not diffuse far more than 1μm from the surface of TiO_2, especially in the presence of organic matter [81]. Some studies showed that both the ·OH and H_2O_2 radicals were responsible for killing microorganisms, but the ·OH kills closer to the TiO_2 surface, while H_2O_2 can diffuse more and kill at a higher in-depth distance [46] (see Figure 13).

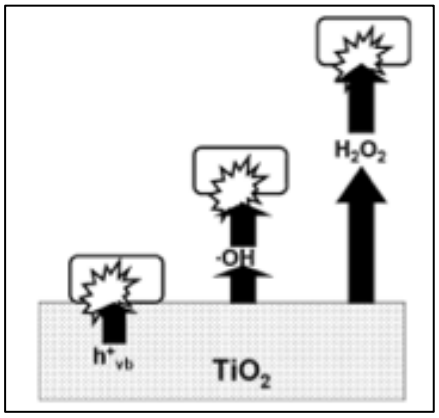

Figure 13: Role of ROS in photocatalytic killing of bacteria [46].

Many studies have shown the importance of TiO_2 contact with microorganisms. This contact will increase the oxidative damage since the TiO_2 particles and bacteria in suspension have a higher contact between them causing a larger surface area for ROS production and therefore a greater cell killing effect [82–84].

2.3.3.1.2 – Process of *E. coli* photo-killing on the surface of TiO_2 thin films.

As already explained earlier *E. coli* is a bacterium protected by an outer membrane, a thin layer of peptidoglycan and followed by an inner membrane (cytoplasmic membrane) (see Figure 14 (a)). When in contact with the TiO_2 coating, these bacteria adhere to the thin film surface and the outer membrane is attacked by the ROS produced by the photocatalytic effect of semiconductor (see Figure 14 (b)). During this process, cell viability is not lost very efficiently, but the damage in the

outer membrane affects the permeability of the membrane and makes easier the passage of ROS to the cytoplasmic membrane. Thus, this membrane is attacked by ROS leading to lipid peroxidation of the membrane (see Figure 14 (c)). With the damage occurring in the layers of the bacteria there is a leakage of small molecules such as ions, and higher molecular weight components, such as proteins. Finally, with the degradation of the cell internal components there is a loss in the cell viability and ultimately cell death [46, 76, 85].

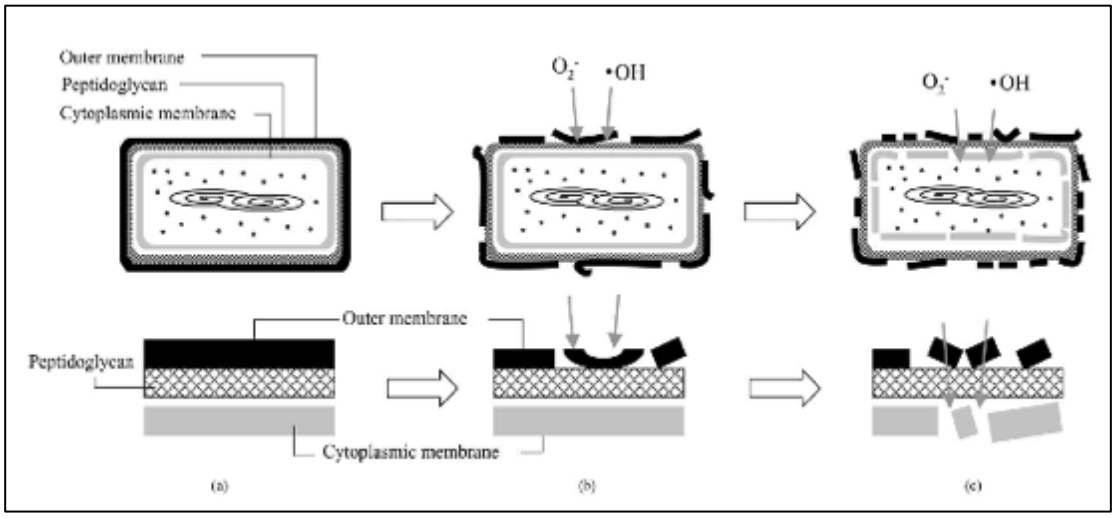

Figure 14: Scheme of the photocatalytic degradation process of *E. coli* representing the different steps in contact with TiO_2 thin films [85].

CHAPTER III

PRODUCTION TECHNIQUES

CHAPTER III – PRODUCTION TECHNIQUES

3.1 – INTRODUCTION

There are various techniques available to produce thin films. Techniques based on vacuum deposition can be divided in two categories: Chemical Vapor Deposition (CVD) and Physical Vapor Deposition (PVD). CVD technique consists in the introduction of gaseous molecules inside a reactor (deposition chamber). These reagents lead to chemical reactions occurring on the surface of the material (substrate), which will be coated in the form of a thin film. These chemical reactions are activated, for example, by heat, plasma or ultraviolet light. There are some limitations with this process, based on the maintenance to a minimum of the substrate temperature and we also have to take into account the types of possible occurring reactions. On the other hand in PVD processes the films are deposited from single atoms, or small clusters, from a target to a substrate that will be coated [86]. In the PVD techniques, we can highlight the Evaporation, Ion Plating and Sputtering processes. These processes are quite advantageous compared to other deposition processes because they are highly versatile, allow the deposition of any metal, alloy or compound or a combination of both, as well as some organic materials. Compared with the CVD processes, in PVD ones it is possible to control the temperature of the substrate, for example, from sub zero to high temperatures [87, 88].

In this study we used the sputtering process for the production of TiO_2 thin films to which was given full attention in this chapter.

3.2 – PHYSICAL VAPOR DEPOSITION (PVD)

PVD techniques are used in a wide range of applications, from decorative coatings, electrical contact coatings and even high temperature coatings [89]. In general, a PVD process consists of three steps:

1. Particle emissions from a condensed phase (solid or liquid) to the vapor phase, from a source;
2. Transportation of these particles to the substrate;
3. Condensation in the substrate and film nucleation and growth.

Typically, PVD depositions are performed in a vacuum chamber. The vacuum is needed to ensure minimal collision between the particles during transport to the substrate and to avoid involuntary reactions.

Generally, these techniques are atomic in nature since the films are deposited from single atoms or clusters and any reactions occur on the film surface, independently of the source parameters [90]. In this work the PVD process used was the Magnetron Sputtering technique. In this technique the source is in the solid state (target) and atoms are ejected by ion impact [91].

3.2.1 – SPUTTERING TECHNIQUE

The sputtering phenomenon was first observed by Groves in 1852, but it was Plücker, in 1858, that suggested that it could be used as a tool to produce metallic films [92]. Due to its increasing development in high-quality functional films in many diverse market sectors, this technique became the process of choice for the deposition of a wide range of important industrial coatings. Sputtering is commonly used for thin film deposition, as the extremes for melting or chemically reacting high melting point materials are not required, as with evaporation or an electrochemical process [93]. Nowadays, magnetron sputtering have a significant impact in application areas including hard, wear-resistant coatings, low friction coatings, corrosion-resistant coatings, decorative coatings and coatings with specific optical or electrical properties [94]. This technique is used due to the simplicity of the physical process, the versatility of the technique and flexibility for changes and standardization of deposition parameters. Very briefly this technique involves the condensation of compounds in the gaseous phase to form a solid material usually in the form of a thin film deposited on a substrate [93].

In the sputtering process, a target is bombarded by energetic particles, usually from an inert gas, e.g. argon ions, generated by glow discharge plasma, located in front of the target. The bombardment process causes the removal of the atoms on the target by physical processes, which will condense on a substrate (part to be coated) as a thin film (see Figure 15). With the sputtering technique we can obtain films with excellent uniformity (particularly in large areas) with smooth surfaces, where it is possible to acquire very similar properties of the volumetric material. These coatings exhibit good adhesion and the deposition rates are high, compared with the evaporation process [95].

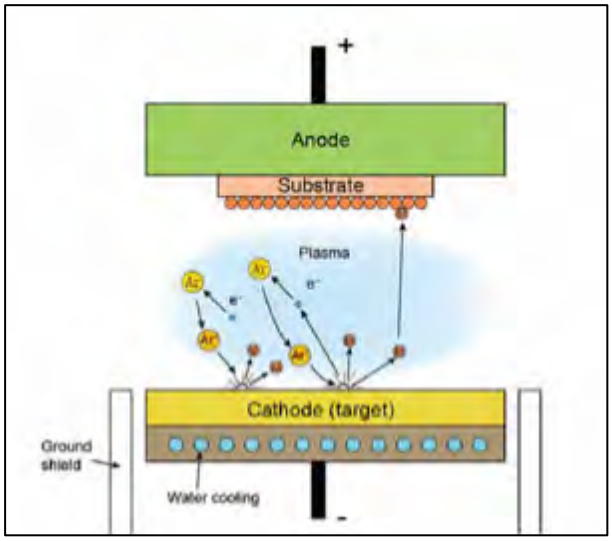

Figure 15: Schematic representation of a sputtering process [96].

Secondary electrons are also emitted from the target surface as a result of the ion bombardment (see Figure 16). These electrons play an important role in maintaining the plasma [95].

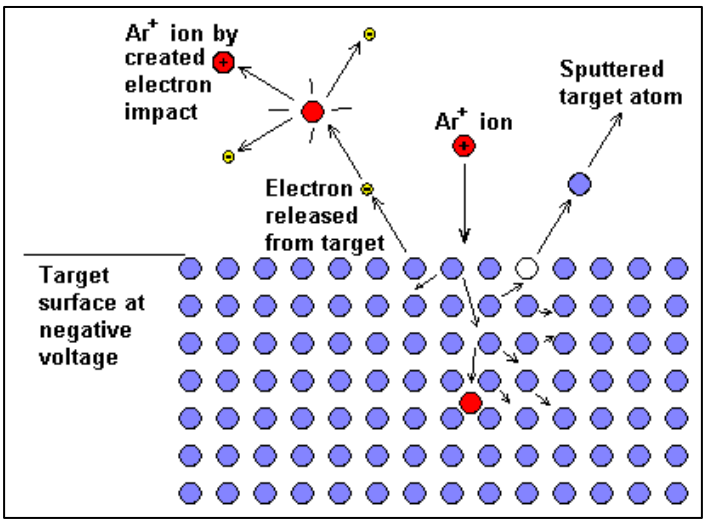

Figure 16: Bombarding of the argon atoms on the target surface and therefore electron emission [97].

3.2.1.1 – MAGNETRON SPUTTERING

Magnetrons are originally devices used for the generation, or amplification, of high frequency signals. These magnetrons are divided in, essentially, three types: cylindrical, circular and planar (see Figure 17) [98]. The planar magnetron is the one used in our study. Typical configurations of planar magnetrons (PM) are the rectangular and circular. The figure 18a shows a circular planar magnetron used in this work. In this type of magnetron there is a "looping" magnetic field that restricts the erosion of the target to a "racetrack" area (see Figure 18).

Figure 17: Different types of magnetrons: cylindrical, circular and planar [99].

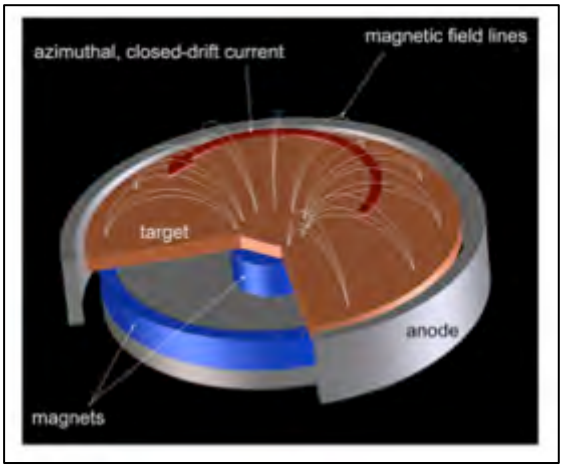

Figure 18: Illustration of a planar magnetron [100].

A magnetron system can be powered with direct current (DC) powered and radio frequency (RF). Under the impact of Ar ions on the target there is a increased heating of the target itself, so that the magnetrons are commonly cooled with water. A PM has an outer (N) and inner (S) magnet and all the magnetic field lines balance each other, to these magnetrons is given the name of conventional balanced magnetrons (CBM) (see Figure 19). With this arrangement, the discharge is confined, by the magnetic field, close to the cathode surface (target). Consequently the bombardment of the growing film at the opposing substrate by energetic particles (other than the deposition atoms) is minimal [101]. In addition to the CBM, there are also unbalanced magnetrons (UBM). In this case, the secondary electrons that escape from the cathode follow the magnetic field lines away from the target and undergo ionizing collisions with gas atoms. The plasma formed is not confined to the target area, and it expands away from the target surface (see Figure 19). The magnetic field confines the escaping electrons, which determine the number of formed ions [102].

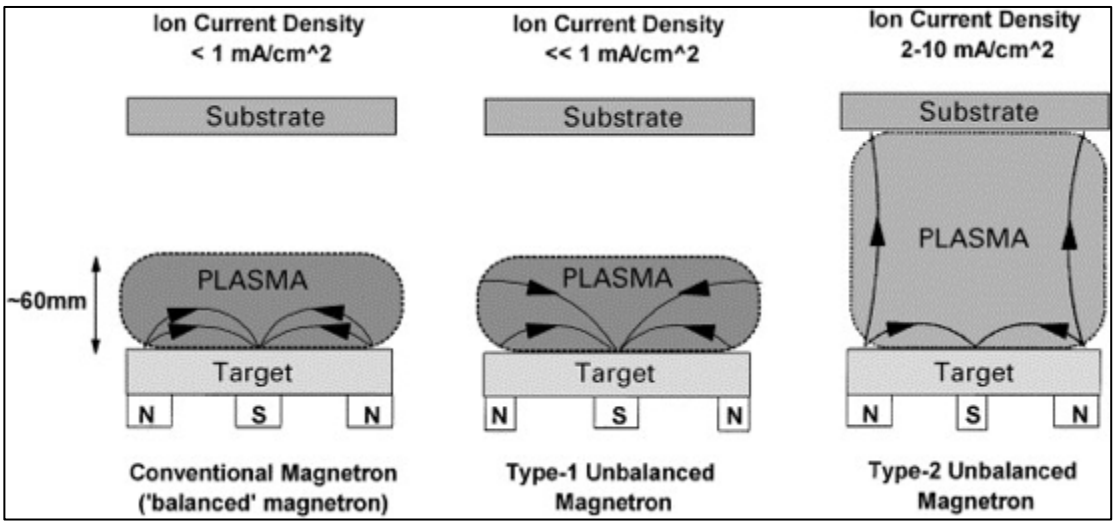

Figure 19: Schematic representation of the conventional and unbalanced magnetrons [103].

For the sputtering process to occur is required a working gas. If the sputtering atmosphere is an inert gas (e.g., argon) the process is described as unreactive. If used a reactive atmosphere (e.g., nitrogen), the process is called reactive.

3.2.1.2 – DC MAGNETRON SPUTTERING VS PULSED DC MAGNETRON SPUTTERING

In the process of DC (direct current) magnetron sputtering deposition of an oxide, from a metal target, in a mixture of oxygen and argon gas, the target is oxidized and an insulating layer is formed on its surface. This method is not the most suitable for thin films production, because of electrical breakdown in the insulating layer, in the form of an electrical arc, may occur. This phenomenon when the layer cannot withstand any longer the electric field strength. The formation of these arc lead to the ejection of droplets of material from the target surface that can cause defects and lack of stoichiometry in the growing film. This causes deterioration in the optical and electrical properties of the films produced [103].

On the other hand, with the process of Pulsed DC magnetron sputtering has been found that arc events can be prevented and the reactive sputtering process is stabilized. Arc events can be suppressed or significantly reduced by applying a

short positive pulse to the target. During the positive part of the pulsed period electrons are collected at the target surface, and due to the fact that they have lower mass compared to the ions, they have also much higher mobility. So, the discharge current (positive part) will be much higher than the charging current (negative part) and thus it will prevent the occurrence of arcs events. This process becomes more stable, repeatable and controllable [104].

3. 3 – FILM GROWTH

When a thin film is deposited on a substrate their final properties can be very different from their bulk counterparts. These properties vary with the structure that the coating can form, as well as the processes that occur during deposition. At the end of the deposition the substrate will have a different chemical nature than the coating material. When atoms reach the substrate, it is not observed immediately its condensation. These atoms, firstly, are adsorbed on the substrate and then are undergo condensation by the formation of small clusters through combination of various adsorbed atoms, which is given the name of nuclei and their forming process is called Nucleation. Then there is the enlargement of the nuclei to finally form a coherent film. This process is given the name of Growth. Usually the process of nucleation and growth occur simultaneously during thin film deposition [105].

In figure 20 we can observe the different steps of thin film formation. First there is the formation of adsorbed monomers. With the junction of these monomers there is the formation of nuclei (nucleation step). Then occurs the growth of nuclei of supercritical dimensions (growth step). The clusters formed earlier unite, forming a new island, occupying an area smaller than the sum of the original two (see Figure 21), thus exposing substrate surface, which will occur a "secondary" nucleation (coalescence step). The islands formed grow and increase their dimensions and there is the formation of channels and holes in the substrate (channels and holes step). Finally, through the "secondary" nucleation, channels and holes will form a continuous film [105].

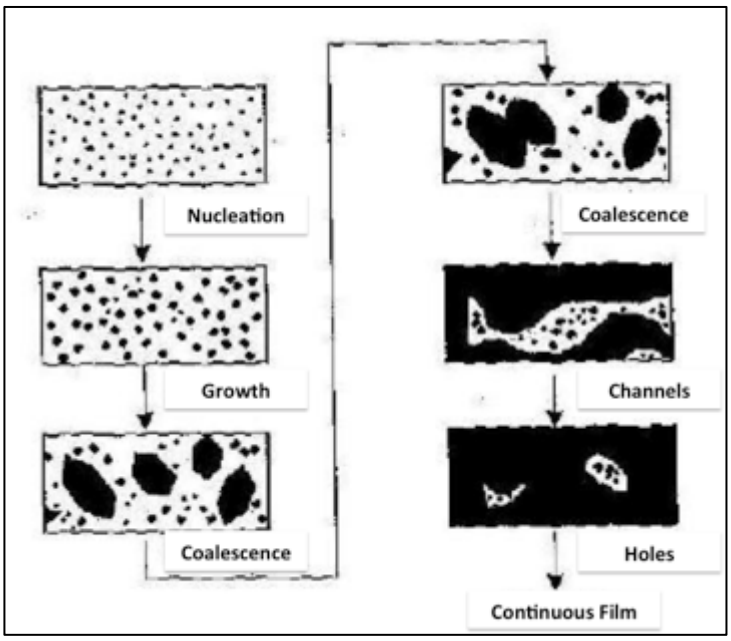

Figure 20: Steps of forming a continuous film.

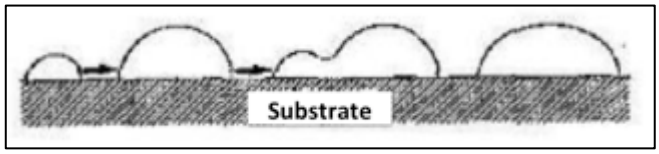

Figure 21: Schematization the formation of islands.

In the formation of a continuous film there are three types of growth that can occur (see Figure 22): (1) Island growth (Volmer-Weber), (2) layer growth (Frank-van der Merwe) and (3) a mixture of layer-island growth (Stranski-Krastanov) [106, 107]. These different types of growth are dependent on the affinity of the film material to the substrate, the activation energy of diffusion and the binding energies between film-film and film-substrate [107].

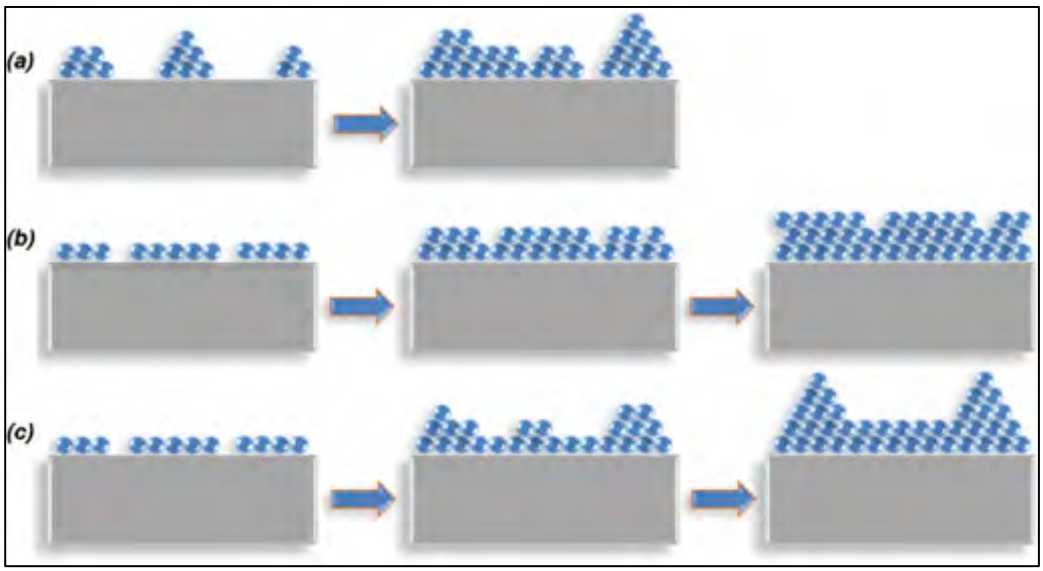

Figure 22: Illustrations of the three types of thin film growth including (a) Volmer-Weber (island growth), (b) Frank-van der Merwe (layer-by-layer growth), and (c) Stranski-Krastanov (mixed island-layer growth) growth [108].

The growth of a film depends on nucleation and/or growth kinetics to determine the coating structure. In the literature there are some theoretical models that try to correlate the structure of the coatings observed with the deposition parameters. These models are called structure zone models (SZM). Movchan and Demchisin, in 1969, defined three structure zones for very thick films made by evaporation (see Figure 23) [109]. In this case, the parameter studied was the homologous temperature (T_h). This parameter is defined as the film growth temperature normalized (T_s) by the melting temperature (T_m) of the deposited film material ($T_h = T_s/T_m$).

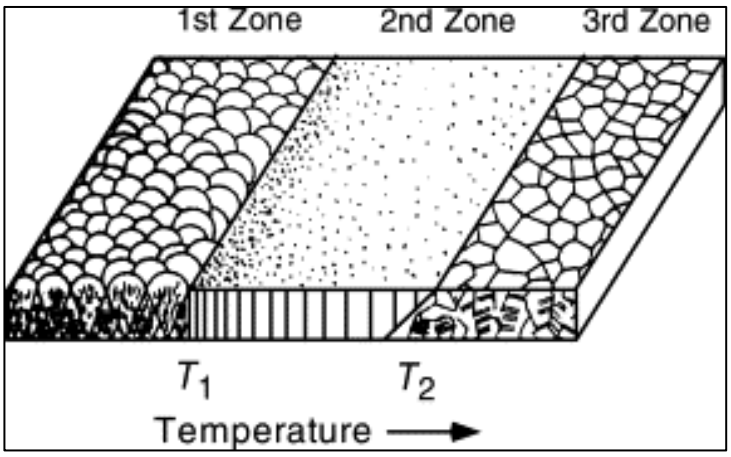

Figure 23: Schematic representation for the structure zone model proposed by Movchan and Demchishin. The micro-structure of the metal film is divided into three structure zones by the melting temperatures T_1 = 0.3 and T_2 = 0.5 [109].

Thornton, in 1997, [110] published an SZM showing the film structure as the effect of two important parameters: the homologous temperature and the argon pressure (see Figure 24). With increasing inert gas pressure there is a shift of the structure zones to higher temperatures. Thornton's model was modified by Messier [111], where the pressure axis is replaced by an ion energy axis, and "T" refers to a transition zone that is unique when ion assistance is present (see Figure 24). Zone T is widened to lower temperatures at the expense of Zone I. This is caused by an ion bombardment induced mobility of the surface atoms.

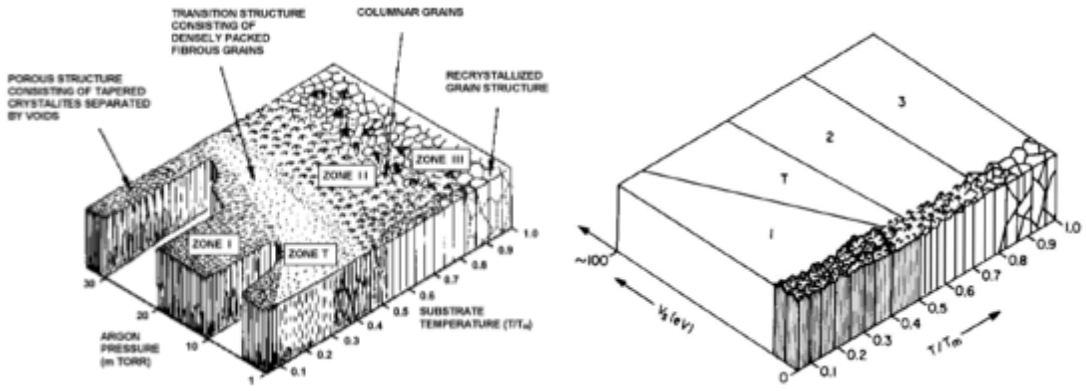

Figure 24: Schematic representation of Thornton's Model (left) and its modification by Messier (right).

Na Zone 1 (T_h<0.3) the adatom mobility is low, leading to continued nucleation of grains. In Zone T (between Zone 1 and Zone 2) there is a dense array of poorly

defined fibrous grains without voided boundaries. In Zone 2 ($0.3<T_h<0.5$) there is the formation of uniform columnar grains separated by distinct, dense, inter-crystalline boundaries. With the increase of T_h increases the size of grains and may extend all the way throughout the film thickness. In the last zone, Zone 3 ($T_h>0.5$), there is the formation of dense films with large grains, with a bright surface (recrystallized grain structure) [110, 111].

CHAPTER IV

CHARACTERIZATION TECHNIQUES

CHAPTER IV – CHARACTERIZATION TECHNIQUES

4.1 – INTRODUCTION

For a detailed knowledge of thin films and their photocatalytic and antimicrobial properties, it is essential to study their characteristics. There are different techniques to characterize these nanostructures, such as, crystalline structure properties (X-ray diffraction), surface properties (scanning electron Microscopy and Atomic Force Microscopy) and optical properties (UV-Vis-Nir Spectroscopy).

4.2 – STRUCTURAL PROPERTIES

4.2.1 – X-RAY DIFFRACTION (XRD)

X-Ray Diffraction (XRD) is a technique that is used to evaluate the crystalline structure, preferential orientation and grain size of thin films.

For the structural analysis of thin films, it is typically used the x-ray diffraction method with incidence angle. For this work, the grazing incidence method was used to minimize the influence of the film-substrate interface, since the x-ray beam crosses the film longitudinally instead of transversally.

The XRD technique is based on the diffraction of X-ray radiation interacting with the atoms, of the material, that are in different crystallographic planes. The angle of incidence is decoupled from the angle traveled by the detector and remains fixed at small values. This ensures a low penetration depth and a large volume irradiated [89].

X-ray wavelength is in the same order of the distance between atoms in a lattice; with this parameter it is possible to observe the diffraction phenomenon, obtaining information about the material that diffracts the radiation.

The positions and the intensities of the peaks (which characterize crystalline planes) are used for identifying the underlying structure (or phase) of the material [112]. In Figure 25 it is possible to observe an example of a XRD result where it is presented three diffractograms showing the peaks of the TiO_2 anatase phase.

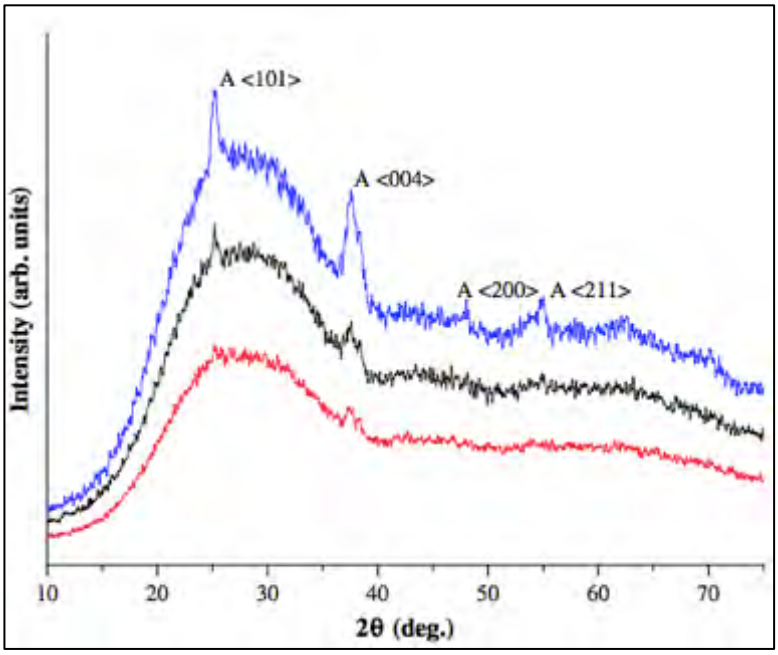

Figure 25: Diffractograms of a XRD result of a TiO_2 sample [45].

The diffraction peak formation in a characteristic spectrum follows Bragg's Law, which mathematically expresses the condition that should exist between incident angle, θ, and the distance between adjacent atomic planes, d, in order to have constructive interference between diffracted waves [120]:

$$n\lambda = 2d\text{sen}\theta \qquad \text{(Equation 11)}$$

Where λ is the wavelength of X-ray incident radiation and n is an integer or half-integer.

The beam intensity depends on the type of atoms or ions present in the crystal and also on its position in the unity cell. Diffraction planes, distance between them and electronic density of atoms along each crystalline plane, are

specific and unique characteristics of each crystalline structure which make possible the determination of inter-planar spacing and Miller indices (hkl), lattice parameters and the lattice type on the sample (see Figure 26) [89].

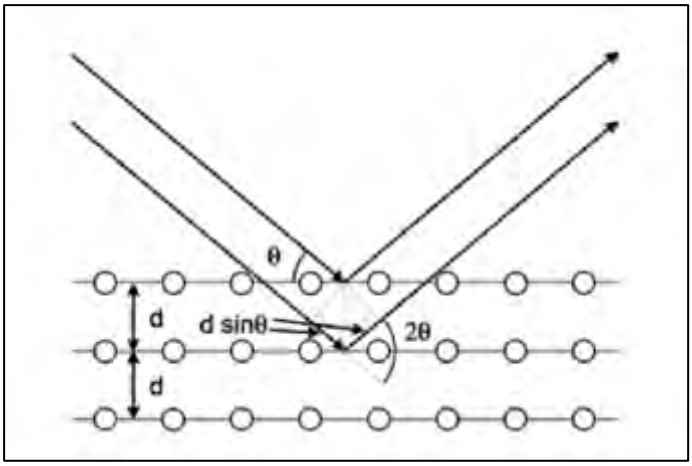

Figure 26: Schematic of diffraction according to Bragg's law.

In this project, X-ray diffraction analysis was performed to investigate the TiO_2 thin films in a Philips PW 1710 X-ray Diffractometer. Through this technique, it was possible analyze the crystal structure of TiO_2 thin films such as, anatase, rutile and brookite.

4. 3 – SURFACE PROPERTIES

4.3.1 – SCANNING ELECTRON MICROSCOPY (SEM)

Scanning Electron Microscopy (SEM) was first developed in the 1930s and eventually commercialized in 1965. This technique uses a focused beam, of high energy, to produce a variety of signals from the surface of the samples. These signals reveal information about the sample as in its external morphology, chemical composition, crystal structure and the orientation of the materials that constitute the sample [121].

SEM has many advantages compared to traditional microscopes. This technique presents a very high resolution, so closely spaced specimens can be magnified at much higher levels; also presents a large depth of field, which allows focusing more than one specimen at a time. Once the SEM technique uses electromagnets instead of lenses, the user has much more control of the degree of magnification. All these advantages make the SEM one of the most useful and used techniques in the research of various materials, as for example, in thin films [121].

In the SEM technique the image is produced using an electron beam instead of visible light. This electron beam is formed on top of the microscope, which is given the name of electron gun, and travel vertically in the microscope. This process is kept under vacuum. The electron beam passes through different electromagnetic fields and lenses that are focusing the electron beam toward the sample. When the electron beam hits the sample, electrons and X-rays are ejected and then are collected in the detectors, which convert the information received into electrical signals generated, and this information is then sent to a computer screen, so we can see the final image [122] (see Figure 27).

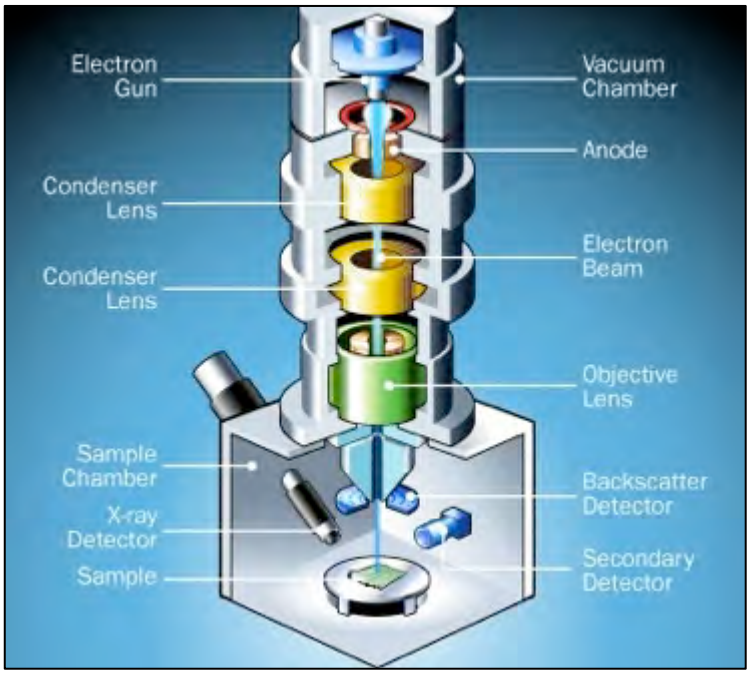

Figure 27: Image showing the Scanning Electron Microscopy equipment.

Signals formed when the electron beam hits the sample are: the secondary electrons (SE), backscattered electrons (BSE), diffracted backscattered electrons (EBSD that are used to determine crystal structures and orientations of samples), X-rays, visible light, and heat. These signals are represented in figure 28. To obtain the SEM image is usually used the secondary electrons and backscattered electrons. The SE are used to show the morphology and topography of the sample, on the other hand the BSE are used to illustrate contrasts of the composition in multiphase samples [123].

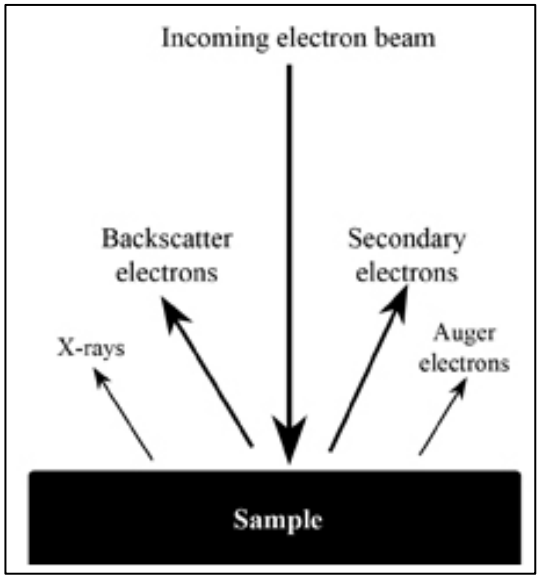

Figure 28: Signals generated by the incidence of the electron beam on the sample surface.

The X-rays formed by incidence of the electron beam on the sample will give information on the elemental composition of the material. This analysis has the name of Energy Dispersive X-ray (EDX), or EDS or EDAX. The data generated by this analysis consist in a spectrum showing peaks corresponding to the chemical elements constituting the composition of the sample. Figure 29 shows a typical EDS spectrum of a sample of TiO_2. The X-rays generated by interaction of the electrons on the sample surface do not lead to volume loss of the sample this makes the SEM a "non-destructive" technique. Thus, it is possible to analyze samples more than once [124].

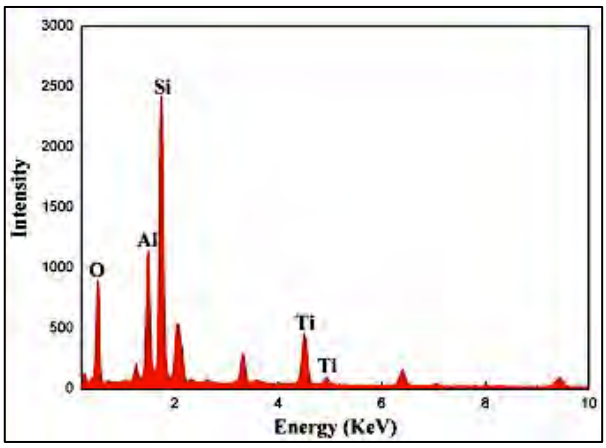

Figure 29: Typical EDX spectrum of a sample of TiO_2. When are present the respective peaks of Titanium (Ti) and oxygen (O). The Carbon (C), Gold (Au) and palladium (Pd) peaks may also be observed [113].

4.3.2 – ATOMIC FORCE MICROSCOPY (AFM)

Scanning probe microscopes (SPM) is defined as a group of techniques used to image and measure properties of material, in chemical and biological surfaces. Scanning Tunneling Microscopy (STM) and Atomic Force Microscopy (AFM) are the two primary techniques of SPM. The development of STM in Zurich by Binnig et al [125], in 1982, received the Nobel Prize in Physics in 1986. This technique allowed the detection of atomic scale features on a wide range of insulating surfaces that include ceramic materials, biological samples, and polymers.

The operation mode of AFM is through a scanning, with a sharp tip (see figure 30), across the sample. This tip may be made of Si or Si_3N_4, and is connected to a low spring constant cantilever. An extremely low force (approximately 10^{-9} N) is applied in the cantilever and the tip is pushed against the sample as it raster's. Thus, there is a repulsive force between the tip and the sample or the actual tip deflection, obtaining an analogue image of the sample surface [126].

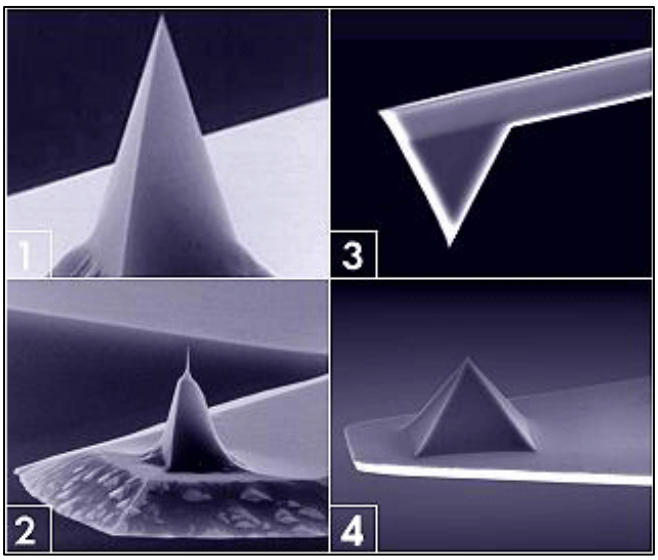

Figure 30: Different types of tips of the AFM technique.

The principle of this technique is illustrated in Figure 31. Firstly, the tip of the cantilever is displaced (manually) near the surface of the sample and then, the scanner makes a final adjustment in the distance between the tip and the sample that is based on a set-point determined by the user. Then, the tip, in contact with the sample surface, starts to scan the sample by action of a piezoelectric actuator, by moving either the sample or the tip relative to the other. A laser beam, located at the back of the cantilever-tip set is projected on the surface of the cantilever and reflected to a photodiode, which will detect the small deflections of the cantilever. The separation between the sample and the tip is maintained constant and there is movement of the scanner in the z direction to maintain the set-point deflection. If this doesn't happen the tip would be trapped in the sample, even with small topographical features. By Hooke's law (Equation 12) and maintaining a constant separation between the tip and the sample is possible to calculate the force between the sample and the tip [126, 127]:

$$F = -K.x \qquad \text{(Equation 12)}$$

Where F is the force, K is the spring constant and x is the cantilever deflection. Finally, the information, regarding the spatial variation of the x-y plane and forms a topographic image of the sample surface, is stored in the computer.

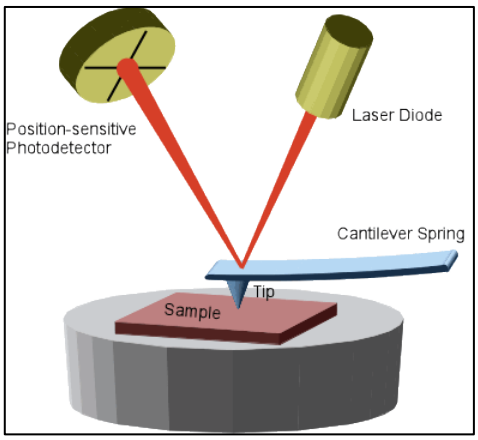

Figure 31: Principle of operation of an AFM

With this technique it is possible to make measurements in three dimensions (x, y and z) and thus display three-dimensional images of the sample surface (see Figure 32). In good samples (clean, without excessively large surface features), the resolution of the x-y plane varies between 0.1 and 1.0 nm and z direction is 0.01 nm (atomic resolution). The AFM technique does not require a vacuum environment or any special sample preparation and they can be used in any environment. This makes the AFM technique very advantageous and for these reasons has a significant impact in the fields of materials science, chemistry, biology, physics, and the specialized field of semiconductors [125–127].

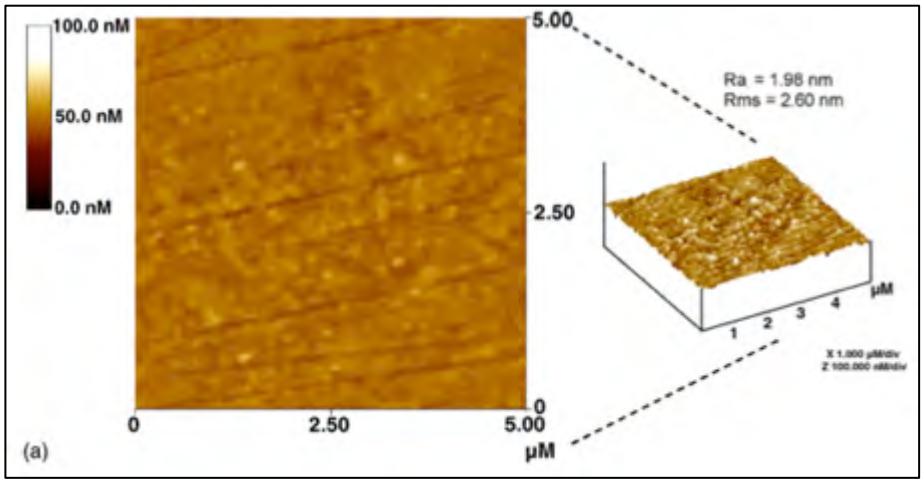

Figure 32: Example of a result obtained after analysis by AFM technique [45].

4.3.3 – CONTACT ANGLE

The contact angle can be defined in several ways. Qualitatively, a contact angle is the macroscopic representation of microscopic phenomena. Microscopic characteristics such as surface roughness, surface energies of the materials involved, and surface coatings play a role in the wettability of a material for a given fluid. Quantitatively, a contact angle is the interior angle formed by the substrate being used and the tangent to the drop interface at the apparent intersection of all three interfaces. This intersection is called the contact line. In Figure 33 it is possible to see the tangent line and the contact angle of a liquid droplet on a surface.

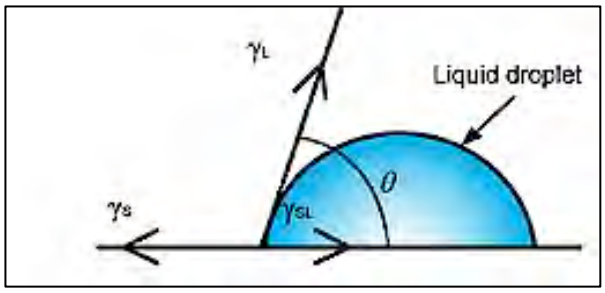

Figure 33: The angle between the tangent line at the contact point and the horizontal line of the solid surface.

A static contact angle on a at surface may be defined by the Young Equation, using interfacial surface tensions between solid and liquid, γ_{SL} , solid and vapor, γ_{SV} , and liquid and vapor, γ_{LV} (Equation 13). Young's equation is essentially a balance of forces in the horizontal direction. The contact angle may also be directly measured to calculate the ratio of interfacial surface tensions if the interfacial surface tensions are unknown.

$$\gamma_{LV}\cos\theta = \gamma_{SV} - \gamma_{SL} \qquad \text{(Equation 13)}$$

Through the measurement of this angle it is possible to obtain information of: (1) the affinity of the liquid to the solid surface, that is, when the angle is less than 90 degrees the surface is hydrophilic and when the angle is greater than 90

degrees the surface is hydrophobic (figure 34); (2) surface energy, if used different liquids; (3) non-homogeneity of the surface (roughness, contamination, etc.), by of the measurement of the hysteresis between the initial and final angle.

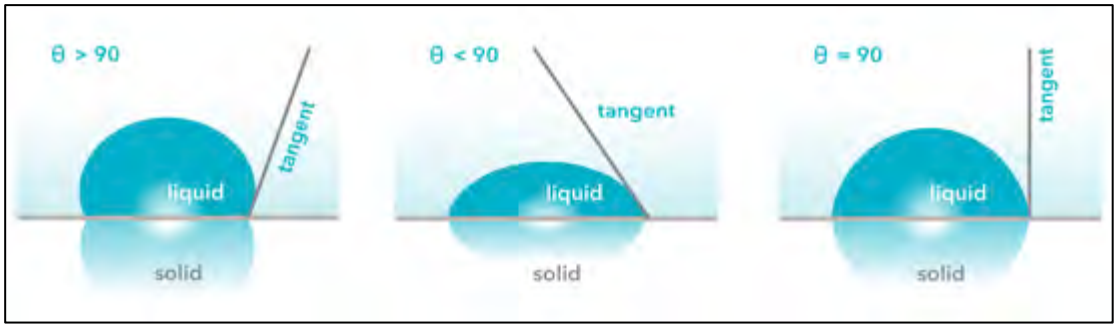

Figure 34: Formation of the angle through the contact between the sample surface and a liquid at the three phase boundary: (a) high values of the 90º (θ>90º), (b) low values of the 90º (θ<90º) and (c) when the angle θ=90º.

4. 4 – OPTICAL PROPERTIES

4.4.1 – UV-VIS SPECTROSCOPY

Spectrophotometers were originally developed for the absorption measurement of liquid samples. However, in recent years, spectrophotometers have been used to measure the reflection, absorption and transmission of solid samples, such as semiconductors, thin films, glasses and adsorbent materials [128]. The optical properties of the materials depend on the interaction phenomena between light and the material. Visible light is a very small component of the electromagnetic spectrum and is the part that can be seen by the human eye. The electromagnetic radiation wavelengths for the different spectral regions are: Ultra-Violet (UV) radiation – 100 to 390nm, Visible (Vis) radiation – 390nm to 780nm and Near Infra-Red (NIR) radiation - 780nm to 3200nm (Figure 35). The UV radiation of the spectrum is divided into three regions: UV-A (315 – 400 nm); UV-B (280 – 315 nm) and UV-C (100 – 280 nm) [129, 130].

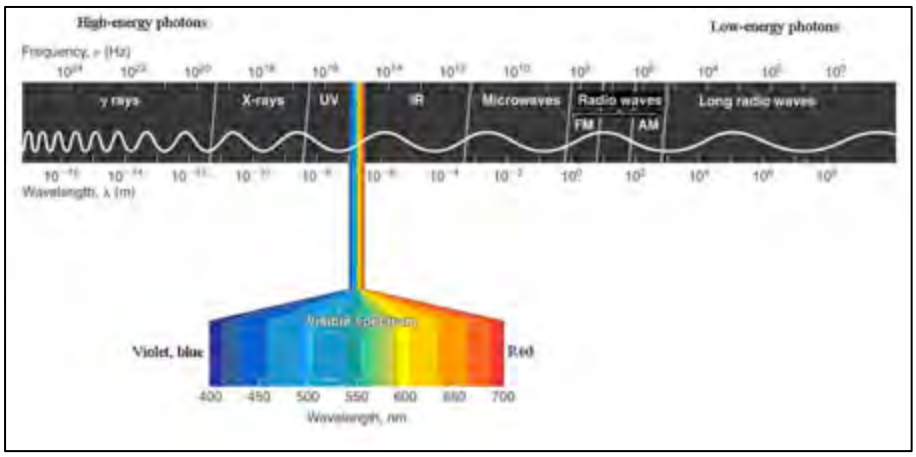

Figure 35: Electromagnetic spectrum. [130].

UV-Vis-Nir spectroscopy equipment has a light source that generates light at a specific wavelength or wavelength ranges. Normally the UV/Vis spectrophotometers use two light sources: a tungsten-halogen lamp and a deuterium arc lamp. This light is directed to a dispersion device (prisms) causing dispersion of wavelengths in different angles. After passing in the dispersion device and have reached the sample of interest, it is received by the detector. In a conventional spectrophotometer, polychromatic light from the monochromator is transmitted through the sample, and the sample absorbance is determined by comparing the intensity of the light hitting the detector with just a sample blank with the intensity of light hitting the detector with the sample in place [131].

The intensity of the reference beam, which should have suffered little or no light absorption, is defined as I_0. The intensity of the sample beam is defined as **I**. If a sample does not absorbs light at a given wavelength, $\mathbf{I = I_0}$. However, if the sample absorbs light, the intensity **I** is less than $\mathbf{I_0}$, and this difference may be represented on a graph versus wavelength. Absorption may be presented as transmittance (Equation 14) or absorbance (Equation 15) [132]. An example of a transmittance spectrum is shown in Figure 36.

$$T = \frac{I}{I_0} \qquad \text{(Equation 14)}$$

$$A = -\log_{10} T \qquad \text{(Equation 15)}$$

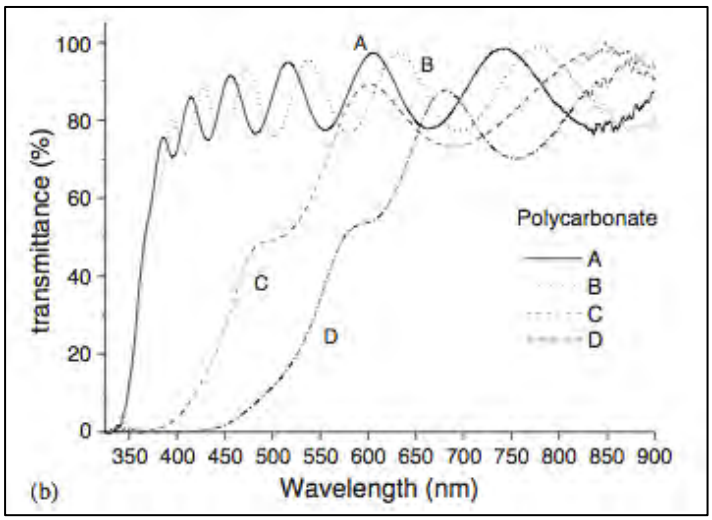

Figure 36: Transmittance spectrum of TiO2 and Fe-TiO2 samples [55].

The principal characteristic of the transmittance spectrum is the presence of interference fringes that result from multiple reflections in the inside of the thin film (see Figure 37). Through the position of the maxima and minima, obtained by oscillations in the graph, it is possible to calculate approximately the thin film thickness using the following equation [133].

$$d = \frac{\lambda_1 \lambda_2}{2n(\lambda_2 - \lambda_1)} \qquad \text{(Equation 16)}$$

where λ_1, λ_2 are two maxima or two minima consecutive and n is the refractive index of the thin film. In the case of the TiO_2 thin film it was used the refractive index of the 2.40 (pure TiO_2) [134].

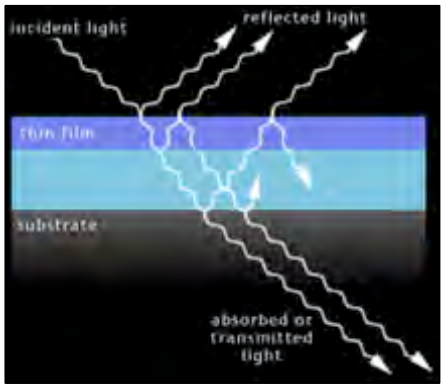

Figure 37: Schematic representation showing the incidence of light on a sample. When light meets an interface, a portion of it will be reflected, and the rest will pass into the incident medium and get refracted.

CHAPTER V

MATERIALS AND METHODS

CHAPTER V – MATERIALS AND METHODS

5. 1 – THIN FILMS PRODUCTION

TiO_2 thin films, pure or doped with iron and silver, were deposited by DC reactive magnetron sputtering on cotton and glass substrates by using a deposition system designed in the Department of Physics, at the University of Minho.

Five main parts compose the deposition system: deposition chamber, a vacuum system, a gas flow control system, an electrical system and a control unit (Figure 38). The deposition chamber is composed of a stainless steel reservoir and its base is made of the same material. The top of this reservoir is removable and inside it there is a circular magnetron, which allows the fixing of a target (in this case, a pure titanium target). The magnetron is cooled by water flow during the sputtering process (see figure 38). In the chamber there is also a shutter that allows the performing of pre-sputtering processes.

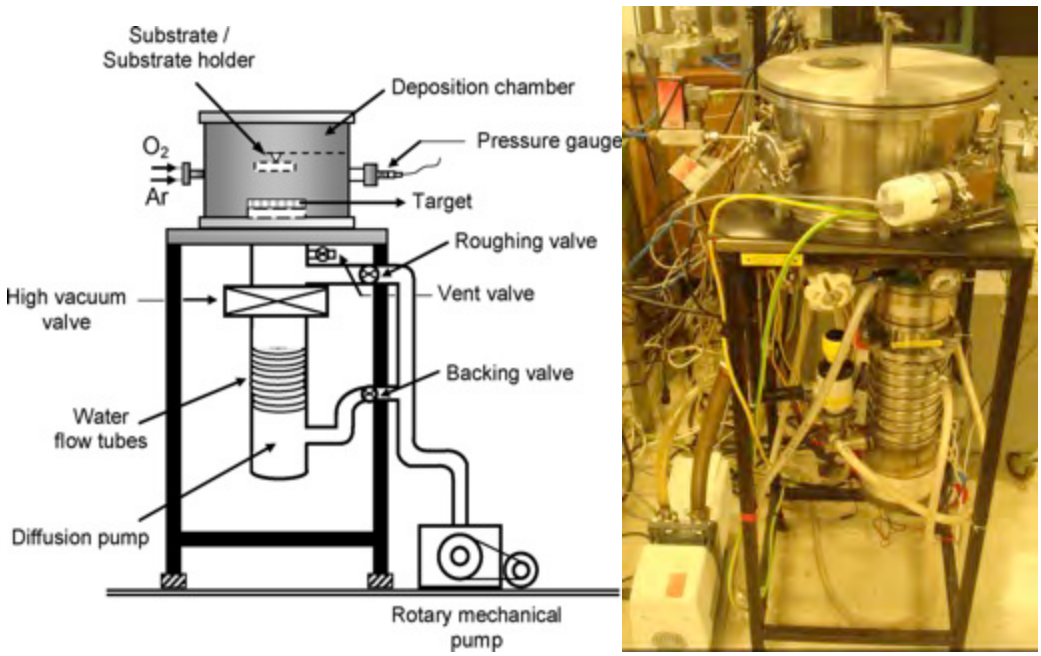

Figure 38: Representative scheme of the reactive magnetron sputtering system used to produce TiO_2 based thin films (left) [45]. Photographic image of the system (right).

The deposition chamber has several gases inlets that allow the entry of the working gas (argon), reactive gas (oxygen), among others. The power supply used in this work is a Huttinger's PFG 2500DC, the pressure regulator is a Bronkhorst Hi-Tec Type E-FA-55M and the temperature controller is a Shimaden SR53 (see Figure 39).

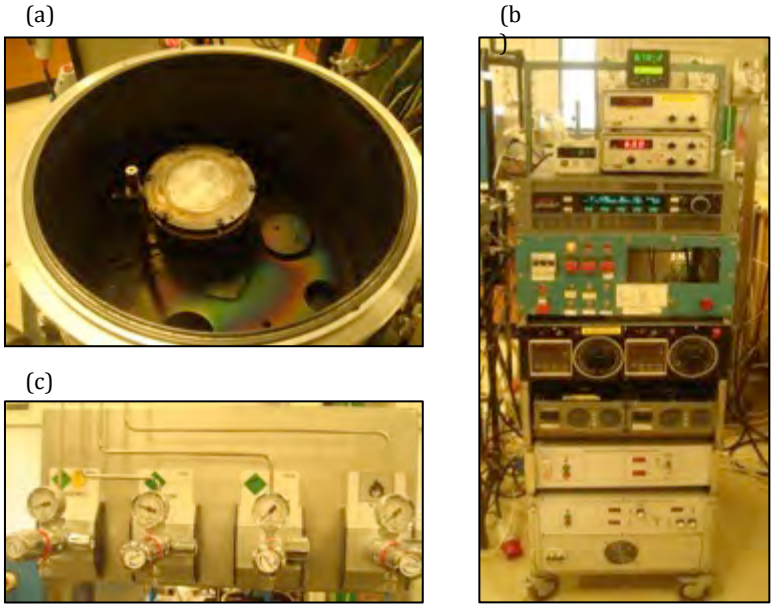

Figure 39: (a) Image of the inside of the deposition chamber; (b) Electrical system and a control unit; (c) Deposition gases.

The target used was titanium with a purity of 99.9% and a total surface area (TA) of 7854 mm^2. Thin iron and silver pieces (5mm/3mm) with purity of 99.9%, were placed on the titanium target (diameter = 7,5 cm), in order to promote the film doping effect.

First the chamber needs to achieve a primary pressure of 1 x 10^{-2} mbar. Then it reaches a base pressure lower than 3 x 10^{-5} mbar. After that base pressure is achieved, a 99.9% pure argon and 99.5% pure oxygen gas sputtering, was introduced into the chamber with a constant current of 1.00 A or 0,45 A. For different thicknesses of thin films were made changes in the deposition time.

The deposition parameters used for the production of TiO_2 thin films, Fe- and Ag-doped TiO_2 thin films are listed in Table 1, 2 and 3, respectively (1ª part of this work). In the Table 4 is represented the deposition parameters for the production of TiO_2 thin films used for the 2ª part of this work.

Table 1: Sputtering deposition parameters for the TiO_2 thin films samples.

PARAMETER	VALUES		
Base Pressure (mbar)		$3{,}1x10^{-5}$	
Working Pressure (mbar)		$1{,}5x10^{-2}$	
Deposition time (min)	60	120	180
Oxygen flow (sccm)		7	
Argon flow (sccm)		20	
Target Current (A)		1,00	
Voltage (V)		490	
Potency (W)		490	
Reverse time (μs)		5	
Frequency (kHz)		25	
Designation	TiO_2 1h	TiO_2 2h	TiO_2 3h

Table 2: Sputtering deposition parameters for the Fe-TiO_2 thin films samples.

PARAMETER	VALUES		
Base Pressure (mbar)		$3{,}1x10^{-5}$	
Working Pressure (mbar)		$1{,}5x10^{-2}$	
Deposition time (min)	60	120	180
Oxygen flow (sccm)		7	
Argon flow (sccm)		20	
Target Current (A)		1,00	
Voltage (V)		456	
Power (W)		456	
Reverse time (μs)		5	
Frequency (kHz)		25	
Designation	Fe-TiO_2 1h	Fe-TiO_2 2h	Fe-TiO_2 3h

Table 3: Sputtering deposition parameters for the Ag-TiO_2 thin films samples.

PARAMETER	VALUES		
Base Pressure (mbar)	$3{,}1x10^{-5}$		
Working Pressure (mbar)	$1{,}4x10^{-2}$		
Deposition time (min)	60	120	180
Oxygen flow (sccm)	7		
Argon flow (sccm)	20		
Target Current (A)	1,00		
Voltage (V)	486		
Power (W)	486		
Reverse time (μs)	5		
Frequency (kHz)	25		
Designation	Ag-TiO_2 1h	Ag-TiO_2 2h	Ag-TiO_2 3h

Table 4: Sputtering deposition parameters for the TiO_2 thin films samples.

PARAMETER	VALUES			
Base Pressure (mbar)	$5x10^{-5}$			
Working Pressure (mbar)	$2.3x10^{-3}$	$3.7x10^{-2}$	$2.3x10^{-3}$	$2.4x10^{-2}$
Deposition time (min)	30		120	
Oxygen flow (sccm)	2			
Argon flow (sccm)	5	30	5	30
Target Current (A)	0,45			
Voltage (V)	526	400	529	433
Power (W)	237	180	238	194
Reverse time (μs)	2			
Frequency (kHz)	100			
Designation	A11	A14	A15	A17

5. 2 – THIN FILMS CHARACTERIZATION

The crystal structure of the films was determined using X-ray diffraction (XRD) with a CuKα radiation source in a Philips PW 1710 BASED diffractometer (Figure 40).

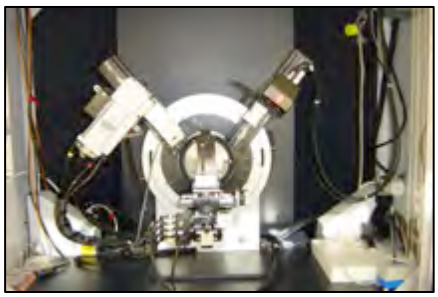

Figure 40: Diffraction system used to determine the structural properties of the produced TiO_2 thin films.

The surface morphology of the thin films was studied by using a Scanning Electron Microscopy: NanoSEM - FEI Nova 200 (FEG/SEM); EDAX - Pegasus X4M (EDS/EBSD) (Figure 41).

Figure 41: Scanning Electron Microscopy used to study surface properties of thin films.

The surface roughness of the samples was studied by using an Atomic Force Microscope (AFM): Veeco Metrology Multimode / Nanoscope IVA (see Figure 42).

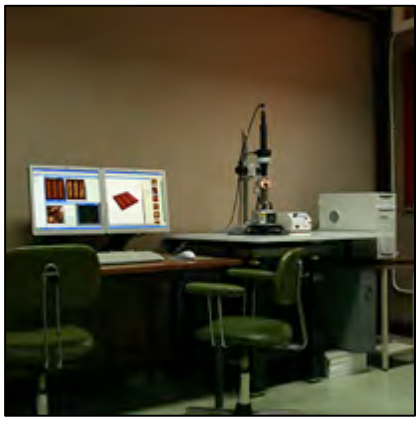

Figure 42: Atomic Force Microscopy used to study roughness of thin films.

The optical transmission spectra of the thin films were measured with a Shimadzu UV-310PC Scanning Spectrophotometer.

The photocatalytic activity of TiO_2 thin films, Fe- and Ag-doped TiO_2 thin films was evaluated by measuring the absorption spectra of methylene blue ($C_{16}H_{18}ClN_3S$) aqueous solution in function of time irradiation of UV light. The reaction product, which results from the photocatalytic degradation of methylene blue (MB), are mainly composed by carbon dioxide (CO_2), nitrates, sulfates and water. The reaction can be described as follows:

$$C_{16}H_{18}N_3S^+ + 25.5O_2 \rightarrow 16CO_2 + 3N_3^- + SO^{2-} + 6H^+ + 6H_2O \quad \text{(Equation 17)}$$

Since methylene blue presents an initial strong blue color, when it undergoes degradation by the action of the semiconductor material will lose its color over time. The initial concentration of MB solution used in this study was 5 mg/L. TiO_2 coated specimens were placed in a container filled with 50 mL MB solution and irradiated in a perpendicular direction with a lamp of the UV light (with a power of $12W/m^2$). To measure the absorbance over time, MB aliquots of about 3mL were removed and introduced into quartz cells for the absorbance measurements. The absorbance of the solution was measured at intervals of 30 min up to 240 min by UV-visible spectrophotometer for a range of wavelength between 350 and 700nm. A decrease in absorbance of the solution indicates the decomposition of MB by TiO_2 photocatalysis effect.

5.3 – ANTIMICROBIAL ACTIVITY

Our main goal was the production of thin films that exhibit the capability to inhibit the growth or eliminate microorganisms, due to their high photocatalytic effect, thereby presenting antimicrobial characteristics.

The microorganism used in this study was *Escherichia coli* HB 101, which was tested under different conditions of thin films, such as, TiO_2, Fe-TiO_2 and Ag-TiO_2

thin films, all at different deposition times, 1hour, 2hours and 3hours. To study the effect of these thin films on bacterial growth, experiments were performed in liquid medium (LB) and growth curves over time were obtained, which are presented in the 1st part of the results. The behavior of *E. coli* HB 101 was also studied in solid medium in contact with ultra-thin TiO_2 films by counting colony-forming units (CFUs). This study can be seen in the 2nd part of the results.

5.3. 1 – Test in liquid medium

To obtain the pre-inoculum the *E. coli* HB 101 strain was grown in sterile conditions in an 500mL Erlenmeyer flask containing 50 mL of LB culture medium (1% w/v bactotriptona, 0.5% w/v Yeast Extract and 1% w/v NaCl), at pH 7. The culture was incubated at 37 ºC with agitation of 180 rpm for 24h.

The TiO_2, Fe-TiO_2 and Ag-TiO_2 coatings were sterilized in 70% ethanol for 1 hour. Then the whole procedure was performed in a laminar flow hood to keep all the material sterile. After sterilization, the coatings were four times washed with deionized H_20 and with the aid of forceps they were passed through the flame. Afterwards, the samples were placed in 250mL Erlernmayer flasks duly marked, and with 50 mL of LB culture medium. *E. coli* was inoculated into each flask [Optical Density (OD) = 0,295] and the flasks were incubated at 37°C with agitation of 80 rpm. Aliquots of 1 mL were taken every hour for quartz cells and the absorbance was measured at a wavelength of 640nm. This procedure went on during approximately 24hours. A flask with *E. coli* only without any coating was used as a control. The percentage of growth inhibition in the different conditions was calculated against the growth obtained in the control culture.

5. 3. 2 – Test in solid medium

For this test the strain *E. coli* HB 101 was also used. The preparation of the bacteria pre-inoculum was performed as described above. The TiO_2 coatings were sterilized with 70% ethanol during 1h. Then, in a laminar flow hood, the thin films were washed with deionized H_2O (4 washes) and placed in sterile petri dishes with the

TiO_2 coating facing upwards. After successive decimal dilutions, 1 mL of the *E. coli* culture was inoculated on top of the coatings and the petri dishes were placed under UV irradiation for 2 and 4 hours. Then, 40uL of the *E. coli* culture were removed and plated on petri dishes with solid LB medium. All the plates were sealed, duly identified and incubated at 37ºC overnight. After 24 hours of incubation the plates were photographed.

CHAPTER VI

RESULTS AND DISCUSSION

CHAPTER VI – RESULTS AND DISCUSSION

In this chapter the results will be divided into two parts. The first part aimed the study of TiO_2 thin films and it's doping with Fe and Ag. The second part corresponds to the optimization of deposition conditions by varying some process parameters in order to produce thinner thin films with enhanced crystalline properties. These characteristics are very important since it is anticipated that the TiO_2 based thin films will be applied to textile substrates and it is fundamental that the fabric malleability, and thus its intrinsic comfort conditions, should be guaranteed.

1st Part – Preliminary Tests

6. 1 – X-RAY DIFFRACTION (XRD)

The analysis by XRD allows the evaluation of the TiO_2 crystalline structures. The diffractograms of some samples are shown in the following figure.

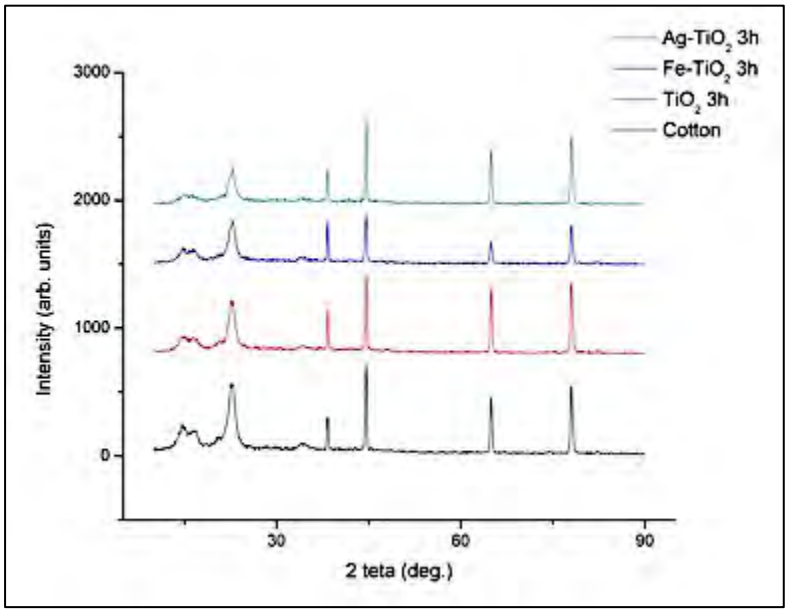

Figure 43: X-Ray Diffraction Spectra of TiO_2 thin films and Fe – and Ag – doped TiO_2 thin films by the Bragg Brentano method.

When comparing the XRD results of the TiO_2 based thin films deposited during 3 hours and the bare cotton substrate (obtained by using the Bragg Brentano method), it is clear that non-additional crystalline peaks were detected. None of the characterized samples shows crystalline structure; therefore, the samples are amorphous.

6. 2 – MORPHOLOGICAL CHARACTERIZATION OF THE THIN FILMS

The Scanning Electron Microscope (SEM) was used in order to study the morphology of the TiO_2 thin films. By using this technique it was not only possible to evaluate the surface morphology of the thin film but also its thickness through the observation of the cross section micrographs. Figure 44 shows the surface SEM micrographs and EDX spectrum of TiO_2 thin films deposited during 1 and 3 hours.

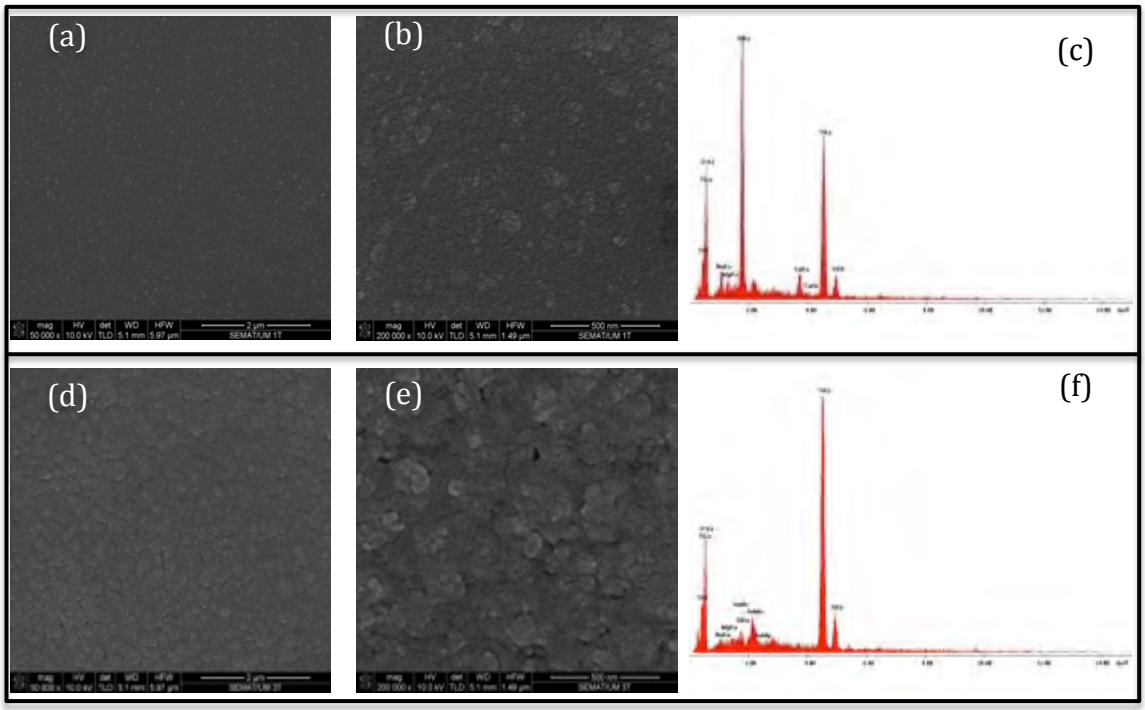

Figure 44: Surface SEM micrographs of TiO_2 thin films deposited with different deposition times: 1 hour (a) magnification of 50 000x, (b) magnification of 200 000x and (c) EDX spectrum; 3 hour (d) magnification of 50 000x, (e) magnification of 200 000x and (f) EDX spectrum.

The SEM micrograph corresponds to a magnification of 50.000x and 200.000x for the all samples. To evaluate the chemical composition of the samples, it was

performed an EDX analysis. Both samples, produced by using different times, present a similar surface morphology. However, some differences can be highlighted: the sample obtained by using a higher deposition time (3 hours) apparently seems to have a more heterogeneous surface. In addition, when comparing the EDX spectra it is clearly observed the presence of Ti but the peaks intensities are different. In fact, the most intense Ti peak is observed for the sample produced during 3 hours (Fig. 44f), which anticipates that, this sample as a higher thickness. The presence of a high intensity Si peak in Figure 44 (c) (TiO_2 thin oxide thin film deposited during 1hour) may arises from the contribution of the substrate since this sample corresponds to the thinner thin film.

The AFM technique was used to analyze the surface topography of the produced samples. Figure 45 shows the AFM images of the samples produced by using two different deposition times.

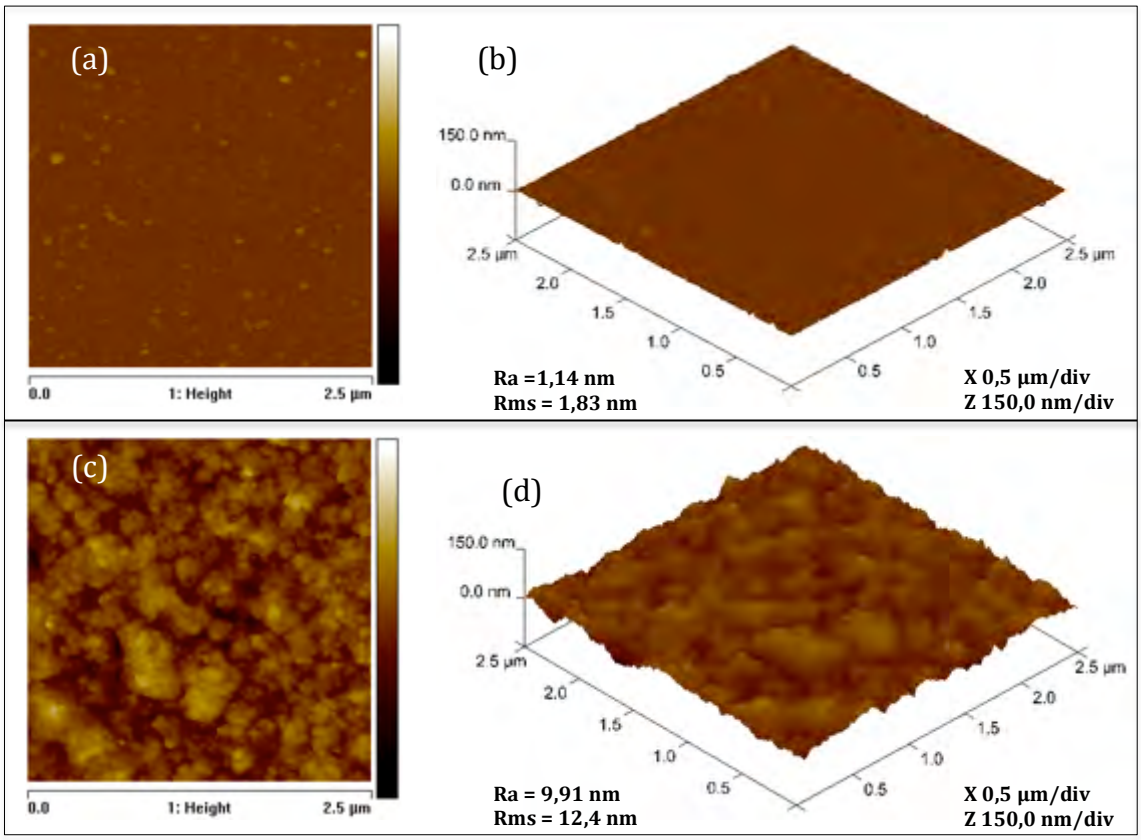

Figure 45: AFM images of the TiO2 thin films produced by using different deposition times: 1hour (a) 2D; (b) 3D and 3hours (c) 2D; (d) 3D.

It is possible to observe that the both samples present homogeneous surfaces with typical characteristics of amorphous structures. By another hand, it is possible to infer that the sample deposited during 3 hours presents a higher surface roughness (9.91nm) in comparison with the one obtained by using 1 hour (1.14 nm). In fact it is expectable that the surface roughness should increase as the random-like heterogeneous structures growth larger.

As explained during the experimental procedure section, the same deposition times were used to deposit Fe- and Ag- doped TiO_2 thin films. Figure 46 shows the surface SEM micrographs and EDX spectrum of Fe- doped TiO_2 thin films.

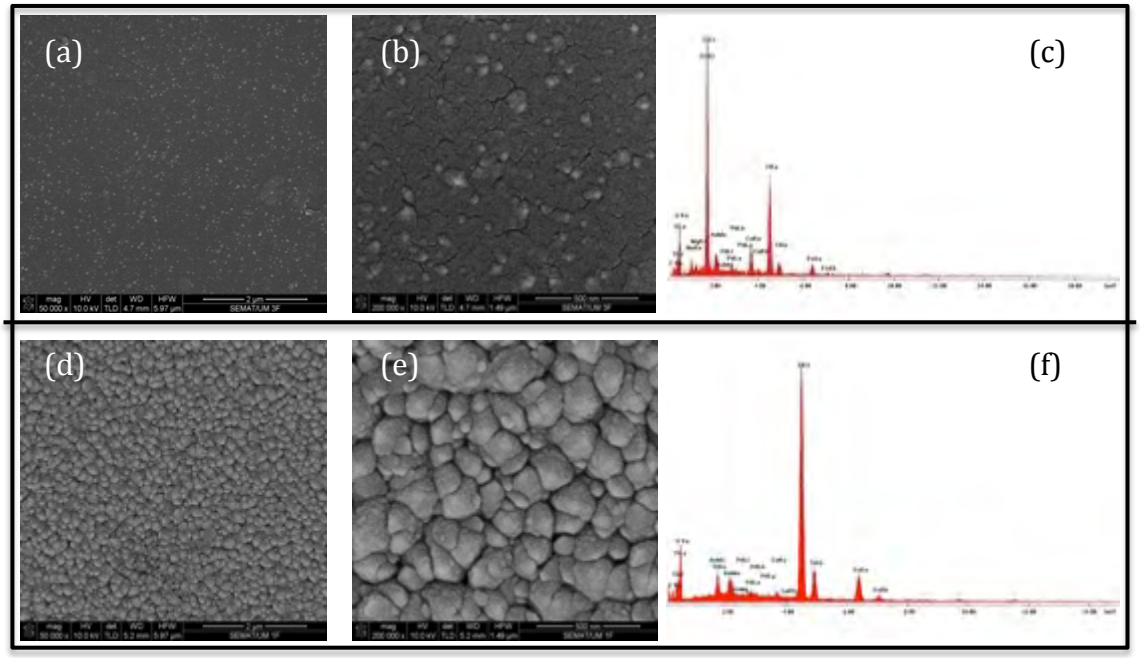

Figure 46: SEM micrograph and EDX spectrum of Fe- doped TiO_2 thin films produced with different deposition times: 1 hour (a) magnification of 50 000x, (b) magnification of 200 000x and (c) EDX spectrum; 3 hour (d) magnification of 50 000x, (e) magnification of 200 000x and (f) EDX spectrum.

In what concerns the Fe-doped TiO_2 thin films (see Figure 46), it is possible to observe that when using a deposition time of 1 hour, the sample presents a non-homogeneous surface. In fact, there is a variation of the particles size and the presence of some cracks on the surface (see figure 46 (b)). With increasing the deposition time (3hours), the surface has changed drastically; becoming more uniform but still presenting a random-like structure with different size particles. It seems that there is also the presence of clusters formation (see figure 46 (e)).

By EDX analysis, it was possible to verify the presence of oxygen and titanium as well as iron, as already expected (see Figure 46 (c) and (f)). The oxygen quantity in both samples is very similar (27.36% and 27.62% for samples produced during 1 and 3 hours, respectively). Moreover, the amount of Ti element almost doubled (24.86% and 47.19% for samples produced during 1 and 3 hours, respectively). In addition, the differences in iron amount are also obvious: for the sample produced with the shortest deposition time (Figure 46 (c)) it presents a Fe quantity of about 5.90%, while the sample obtained with higher deposition time (Figure 46 (f)) has a Fe quantity of 10.85%.

Figure 47 shows the AFM images of the Fe- doped TiO_2 thin films produced by using two different deposition times.

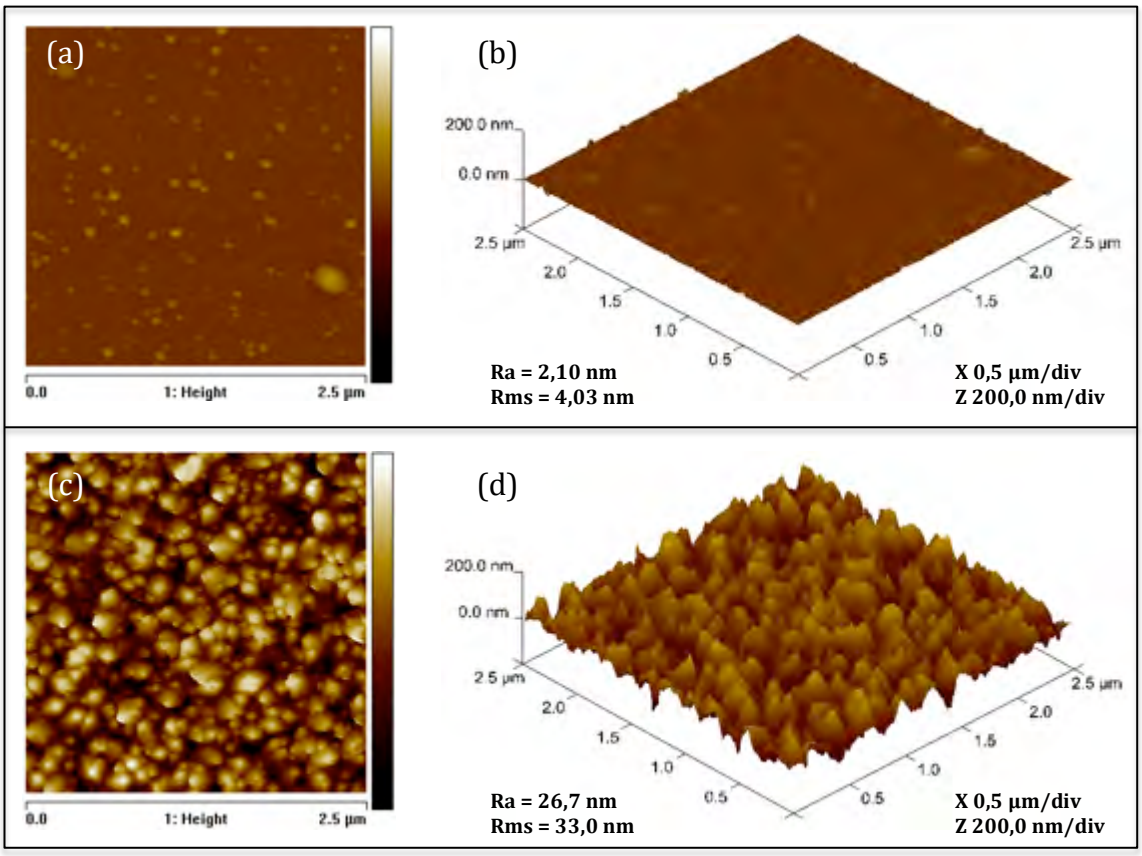

Figure 47: AFM images of the Fe-doped TiO2 thin films produced by using different deposition times: 1hour (a) 2D; (b) 3D and 3hours (c) 2D; (d) 3D.

As can be observed from the results presented in the last figure, the TiO_2 thin film seem to become rougher with the increase of the deposition times (see Figure 47 (a) and (c). In fact, by increasing the deposition time it seems that there exists

agglomerate-like structures with higher dimensions. The unorganized structures have a random size distribution.

As the deposition occurs, it is expected that the iron ions substitute the ions forming the crystal structure of TiO_2. The ionic radius determines the position of the dopant in relation to the host Ti^{4+}. The radius of Fe^{3+} ions is 0.645A while the ionic radius of Ti^{4+} is 0.605A. Thus, it is energetically favorable than the Fe^{3+} ions occupy the sites of Ti^{4+}, due to its ionic radius being so close [45]. However there may be formation of an iron oxide surface, since iron concentrations can be much greater than its solubility in TiO_2, and so there is the formation of bigger particles and particle clusters, increasing the samples surfaces roughness.

In what concerns samples produced by doping TiO_2 thin films with Ag, in Figure 48 are presented their SEM micrographs.

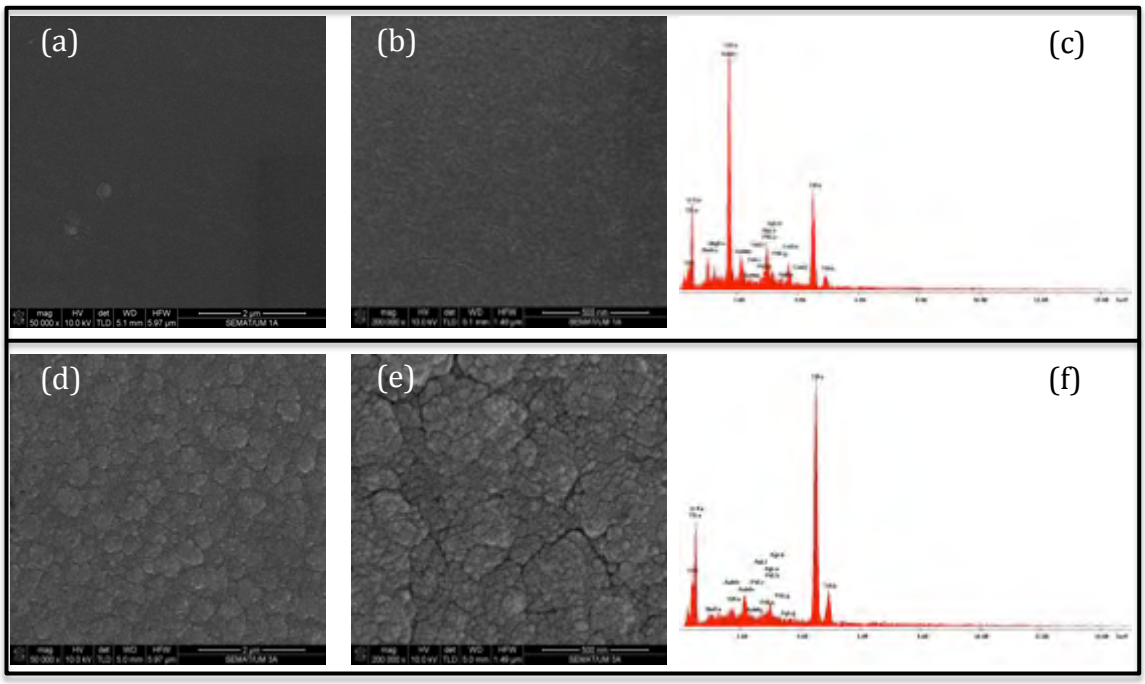

Figure 48: SEM micrograph and EDX spectrum of Ag- doped TiO_2 thin films produced with different deposition times: 1 hour (a) magnification of 50 000x, (b) magnification of 200 000x and (c) EDX spectrum; 3 hour (d) magnification of 50 000x, (e) magnification of 200 000x and (f) EDX spectrum.

As can be inferred from the last figure, the samples doped with Ag and with a deposition time of 1hour showed a best uniformity and homogeneity when compared with the remaining samples. As one can see in Figure 48 (a), the sample

surface is very smooth and regular, but it is possible to observe some cracks when the sample is observed with a magnification of 200 000x. With increasing the deposition time it can be seen that the sample surface presents some changes. In Figure 48 (c) it is possible to visualize the presence of random-like structures with a larger size and became rougher with the formation of particles agglomerates.

By observing EDX spectra it is possible to detect the presence of oxygen and titanium peaks in both samples, which indicates the formation of TiO_2. In the sample of Ag- doped TiO_2 thin films produced during 1h it was obtained a quantity of 28.90% of oxygen and 27.29% of titanium. One the other hand, in the samples of Ag-TiO_2 3h there was an increased quantity of oxygen and titanium, 36.23% and 57.91% respectively (see figure 48 (c)). Regarding the Ag amount there was a reduction with increasing deposition time: in the sample produced during 1 hour the quantity of Ag was 12.89% while in the sample produced during 3 hours was 4.01%. This decrease in Ag can be related to the amount of silver present in the titanium target, in the deposition chamber. As deposition occurs over time, the Ag pieces will be exhausted and after a deposition of 3 hours, the amount of Ag may have been spent before completing the deposition.

Figure 49 shows the AFM images of the Ag- doped TiO_2 thin films produced by using two different deposition times.

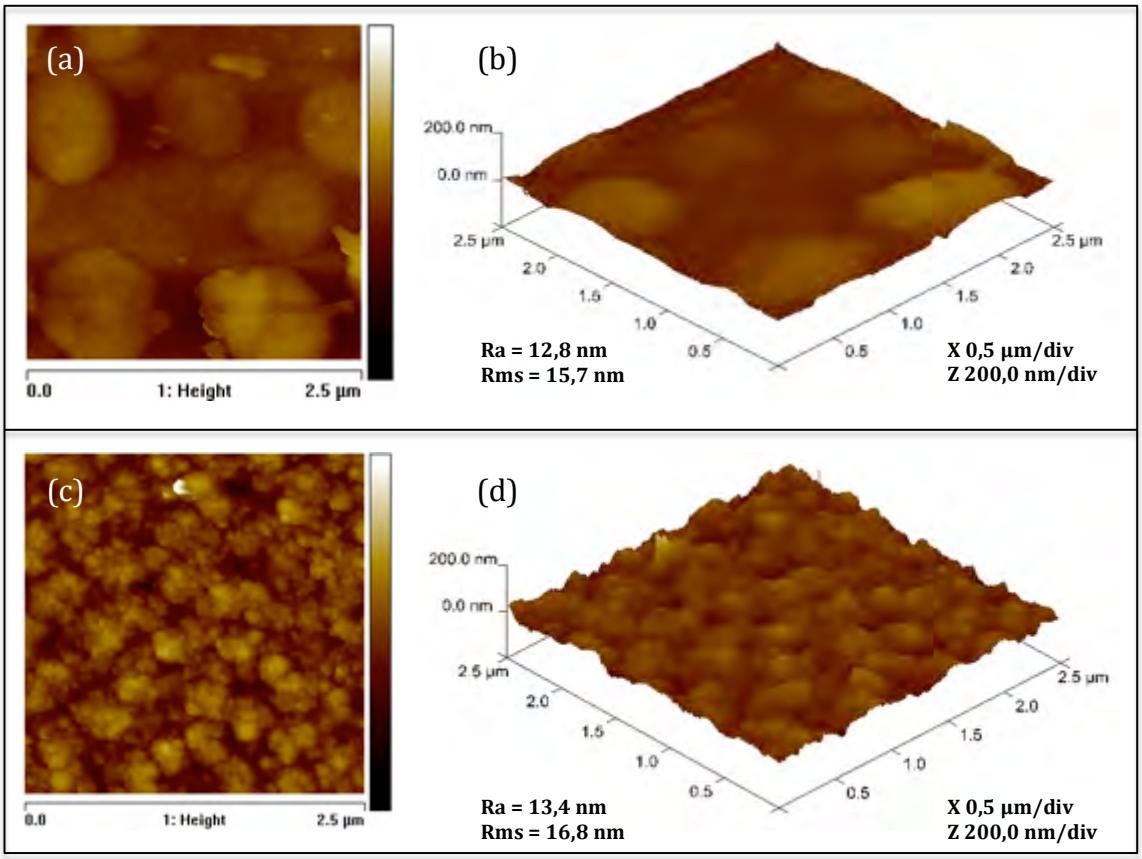

Figure 49: AFM images for samples Ag- doped TiO_2 thin films produced by using different deposition times: 1hour (a) 2D; (b) 3D and 3hours (c) 2D; (d) 3D.

On the contrary of what occurred to the TiO_2 thin films and TiO_2 thin films doped with iron, for the Ag- doped TiO_2 thin films the roughness has not increased significantly with the increase of deposition time. This fact can be related with the fact that the Ag pieces have been spent during the deposition.

In table 5 is presented a summary of the roughness values for all the produced samples.

Table 5: Roughness values for all the produced samples.

Thin Films		Roughness (nm)
TiO_2	**1h**	1.14
	3h	9.91
Fe-TiO_2	**1h**	2.10
	3h	26.7
Ag-TiO_2	**1h**	12.8
	3h	13.4

It is important to mention that the high roughness value of the Ag- doped TiO_2 thin films produced during 1 hour (when compared with the samples deposited during the same time) can be related with an incorrect experimental procedure with which was not possible to avoid the occurrence of some arcs discharge that may contribute for a higher degree of metallic sputtering Ag particles.

From the cross-section SEM micrographs of the TiO_2 thin films deposited during 1 hour (Figure 50) it is possible to observe that the sample has a thickness of about 395 nm. Moreover, these results are in agreement with the ones presented in Figure 44 (surface micrographs) where no organized structures were detected.

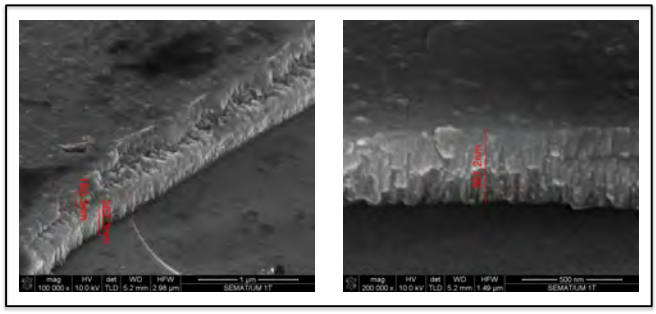

Figure 50: Cross-section SEM micrograph of TiO_2 thin films produced during 1h.

Figure 51 shows the cross-section SEM micrographs of the Fe- doped TiO_2 thin films produced for the different deposition times.

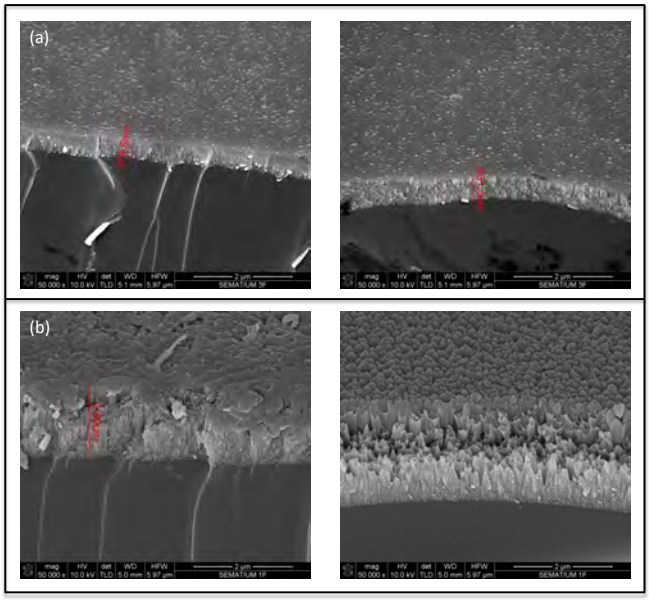

Figure 51: Cross-section SEM micrographs of Fe- doped TiO_2 thin films deposited during (a) 1 hour and (b) 3 hours.

Figure 52 presents the cross-section SEM micrographs of the Ag- doped TiO_2 thin films produced during 3 hours.

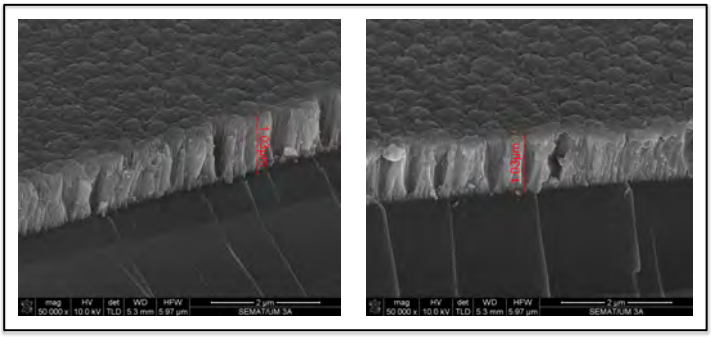

Figure 52: Cross-section SEM micrographs of Ag- doped TiO_2 thin films deposited during 3 hours.

From the cross-section SEM micrographs of Fe- and Ag- doped TiO_2 thin films (Figure 51 and 52, respectively) it can be concluded the samples do not present a well-defined columnar structures, thus evidencing an amorphous structure. Moreover, it is important to state that the obtained deposition rate were similar for all the produced samples (about 7nm/min).

6. 3 – OPTICAL SPECTROPHOTOMETRY

The optical properties of TiO_2 based thin films were studied by measuring the transmittance spectra in a wavelength range from 300 to 850 nm. In Figure 53 are presented the transmittance spectra of the TiO_2 thin films, Fe- and Ag-doped TiO_2 thin films produced with different deposition times (1, 2 and 3 hours).

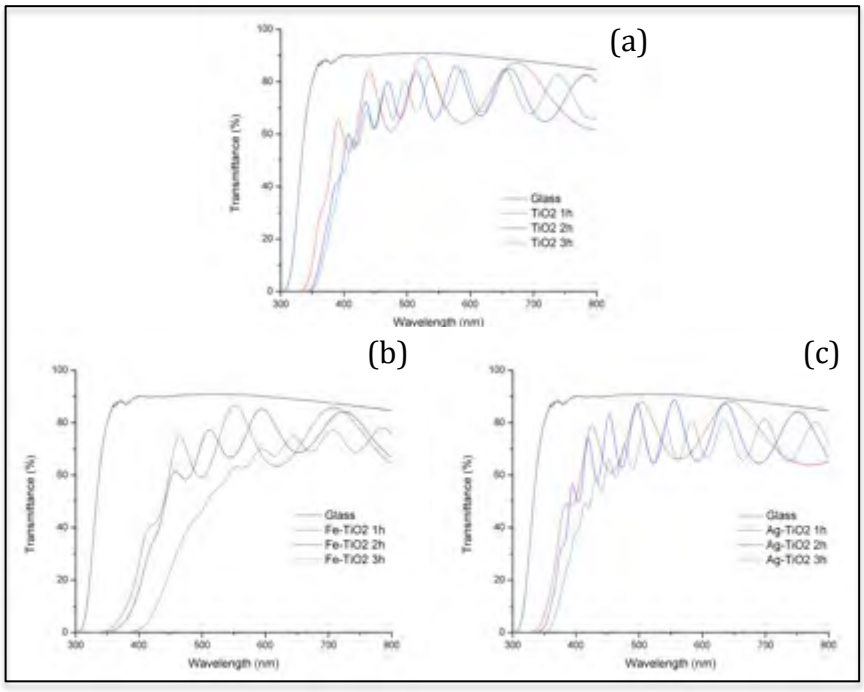

Figure 53: UV–Vis transmittance spectra of: (a) TiO_2 thin films, (b) Fe-doped TiO2 thin films and (c) Ag-doped TiO_2 thin films produced with different deposition times.

The TiO_2 based thin films are transparent in the visible region of the electromagnetic spectrum and its transmittance spectra present a sharp decrease in the UV region (thus indicating that the thin films may have a high absorbance in this region). In addition, in the visible region it is possible to observe the characteristic waveforms from the light interference [55]. From all the transmittance spectrum of the samples is possible to observe that the number of waveforms increases with increasing of the deposition time, making the spectrum with bands closer to each other. This was already expected since the amount of waveforms from light interference is directly related with the films thickness.

Through the maxima and minima of the waveforms is possible to obtain the thickness of the thin films. Using the Equation 16 it was possible to determine the thicknesses for all the samples. In Table 6 is presented a summary of the obtained results.

Table 6 – Summary of the calculated thicknesses for all the produced samples.

THIN FILMS	THICKNESS (nm)
TiO_2 1h	~498

TiO_2 2h	~1105
TiO_2 3h	~1586
Fe-TiO_2 1h	~525
Fe-TiO_2 2h	~927
Fe-TiO_2 3h	~1565
Ag-TiO_2 1h	~562
Ag-TiO_2 2h	~1048
Ag-TiO_2 3h	~1513

When comparing the transmittance spectrum of TiO_2 thin films with the doped ones, it is possible to observe a more pronounced change for the samples deposited during 3 hours (see Figure 54).

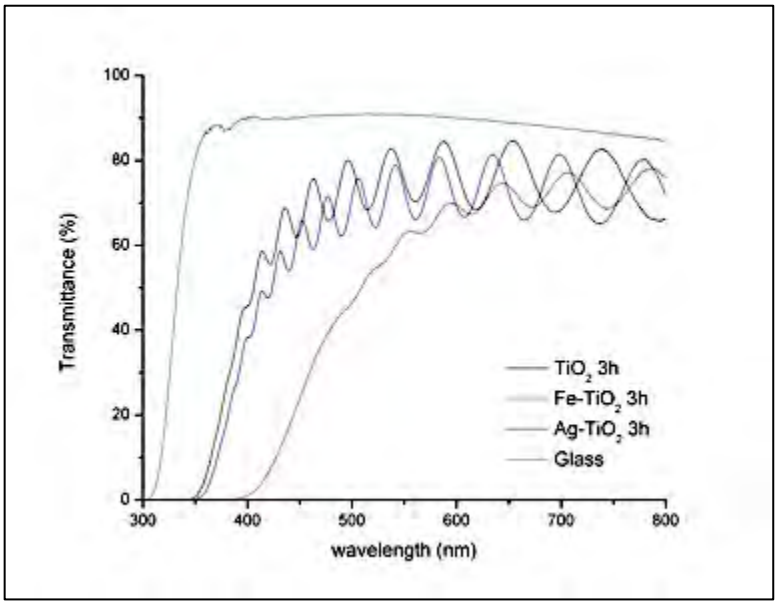

Figure 54: UV-Vis transmittance spectra of TiO_2 thin films, Fe- and Ag- doped thin films deposited during 3 hours.

There are significant changes in comparison to the transmittance spectra of TiO_2 and the Fe-doped TiO_2. These changes are more pronounced for thin films where the deposition time was higher (3hours). The observed changes are not very relevant when TiO_2 is doped with silver. It may be necessary a higher concentration of Ag-ions for the dopant effect could be manifested, since it should not be forgotten that the amount of Ag content in the sample deposited during 3hours was lower than the one measured for the sample produced during 1hour (see EDX spectra in the figure 48). However, it was expected an increase of the

radiation absorption in the visible range when TiO_2 is doped with silver. In fact, Ag particles can act as electron traps, aiding electron-hole separation and inducing a local electric field capable of easing the electron excitation [114]. On the other hand, in the Fe-doped TiO_2 samples, it is possible to observe that the absorption edge presents a pronounced shift for higher wavelengths. This red shift has been attributed to the excitation of 3d electrons of Fe^{3+} to the conduction band. This is a great advantage of TiO_2 doping with iron because the main purpose of this doping is to extend the light absorption edge for the visible spectrum region so it can be possible to use the an higher amount of the visible light spectrum [115].

6. 4 – PHOTOCATALYTIC ACTIVITY

The photocatalytic effect of TiO_2, Fe-and Ag-doped TiO_2 thin films was evaluated by measuring the absorbance spectra of an methylene blue (MB) aqueous solution over time since it is expected a in the absorption maxima as a consequence of the photodegration of the dye. In figure 55 is presented the typical absorption spectrum of MB being photodegraded by the action of the Ag-doped TiO_2 photocatalyst under UV irradiation.

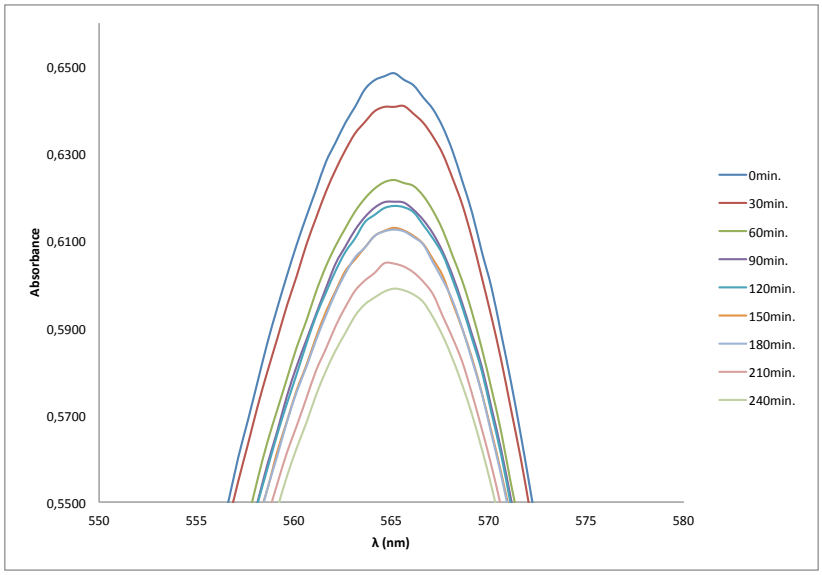

Figure 55: Absorption spectra of the MB aqueous solution over time under UV irradiation the photocatalytic action of Ag- doped TiO_2 thin films deposited during 1 hour.

The methylene blue has, as the name indicates a blue color, and over time it becomes colorless, thus indicating the occurrence of chemical redox reactions on the surface of the photocatalyst.

The analysis of the absorption spectra for the different irradiation times allowed the determination of the yield (η) and photodegradation rate (k). The photodegradation yield can be determined by using the next equation:

$$\eta = \frac{(A_0 - A_i)}{A_0} \quad \text{(Equation 18)}$$

where A_0 is the maximum absorbance at time zero (t = 0) and A_i is the maximum absorbance on the absorption spectra of the methylene blue solution, over time (i = 30, 60, 90, 120, 150, 180 , 210 and 240 minutes). By analyzing the absorption spectra is it also possible to determine the photodegradation rate constant (k). It is known that, for low concentrations, the absorbance (A) can be related to the solution concentration by the Beer-Lambert law (Equation 19):

$$A = \varepsilon l c \quad \text{(Equation 19)}$$

where ε is the molar extinction coefficient, *l* is the light path length through the quartz cell, and c is the concentration of the absorbing compound in the solution. The parameters, ε and l are constant, then:

$$\frac{A}{A_0} = \frac{C}{C_0} \quad \text{(Equation 20)}$$

where $A_0 = C_0$ is the maximum absorbance at the time zero (t = 0). Through the linear equation of the type y = mx + b, we have:

$$\ln\left(\frac{C}{C_0}\right) = -kt \quad \text{(Equation 21)}$$

The photodegradation rate constant (k) can be calculated from the slope of the linear fit of the experimental values [116].

In Figure 56 are presented the results of the photodegration yield and the corresponding photodegradation rate constant for all the produced samples.

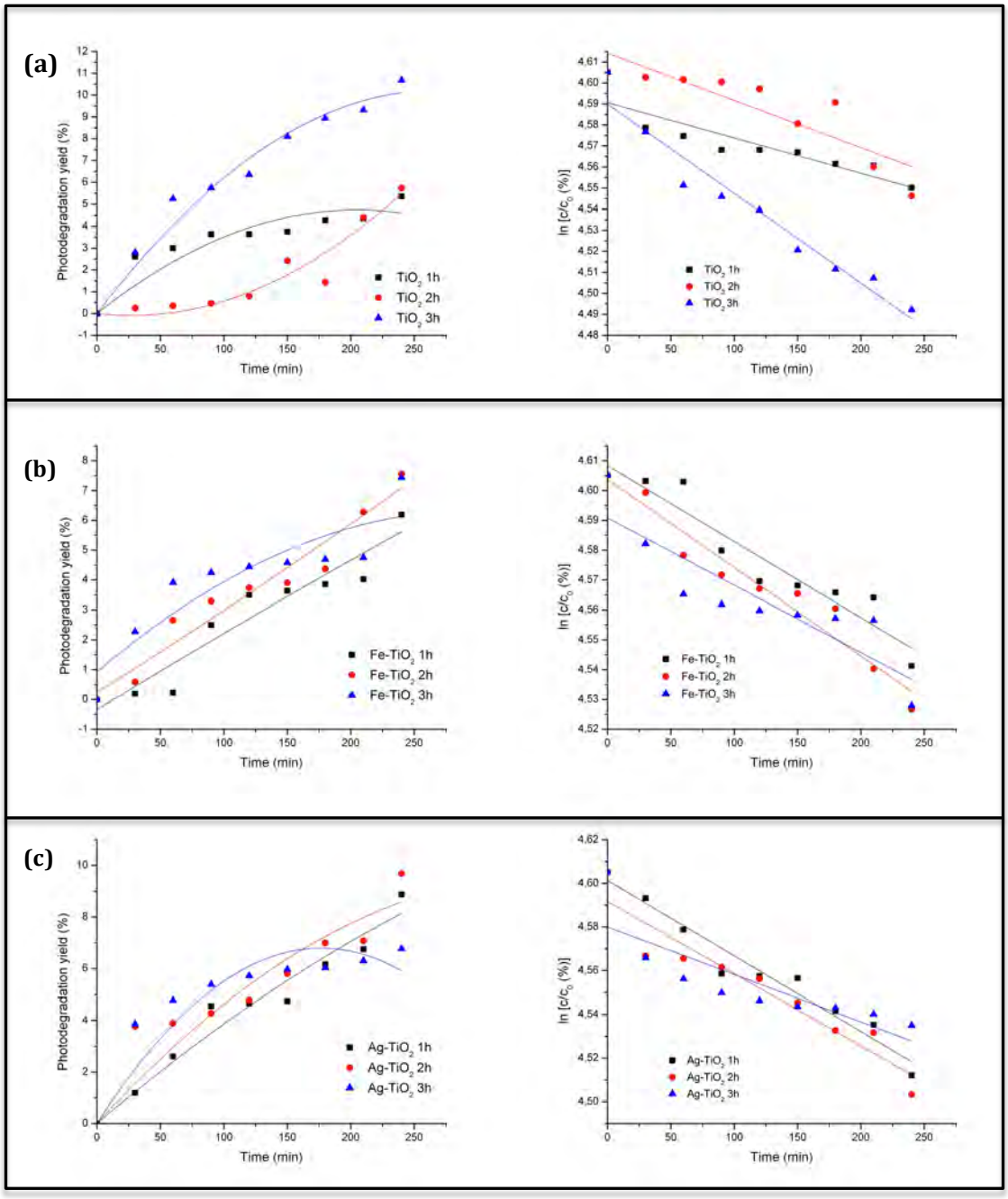

Figure 56: MB photodegradation yield and k values under UV irradiation and the action of (a) TiO_2, (b) Fe- doped TiO2 and (c) Ag-doped thin films.

Additionally, in table 7 are summarized the calculated k values and photodegradation yield for all the produced samples.

Table 7: Values obtained of the yield (%) and the rate constant of photodegradation in different coatings.

Thin Films	Photodegradation yield (%)	k (min^{-1})
TiO_2 1h	5.36	$1.68x10^{-4}$
TiO_2 2h	5.73	$2.25x10^{-4}$
TiO_2 3h	10.69	$4.25x10^{-4}$
Fe-TiO_2 1h	6.19	$2.55x10^{-4}$
Fe-TiO_2 2h	7.55	$2.96x10^{-4}$
Fe-TiO_2 3h	7.44	$2.25x10^{-4}$
Ag-TiO_2 1h	8.88	$3.45x10^{-4}$
Ag-TiO_2 2h	9.69	$3.30x10^{-4}$
Ag-TiO_2 3h	6.77	$2.17x10^{-4}$

As can be inferred from the presented results, the photocatalytic activity of the TiO_2 based thin films is quite low (not higher than 11%). This behavior is undoubtedly due to the fact that all the samples do not have any crystalline nature. Due to equipment limitations, during the execution period of the experimental work it was not possible to add the contribution of a visible lamp in order to study the effect of visible irradiation on the photocatalytic yield and k values. In this sense, both the photocatalytic yield and k values are the same order of magnitude for the Fe- and Ag- doped TiO_2 thin films.

Nevertheless, for the TiO_2 thin films doped with iron it can be perceived a slightly increase of the photocatalytic activity compared to un-doped TiO_2 thin films. This small increase may be due to the transmittance red shift into the visible region (see Figure 54). Thus, this photocatalytic effect occurs due to the fact that the equipment box was not completely sealed and some of the ambient light could enter and may be slightly absorbed by the photocatalyst material.

6. 5 – ANTIMICROBIAL ACTIVITY

The antimicrobial activity of the TiO_2 based thin films deposited on cotton substrates was tested by growing *E. coli* HB 101 in the presence of the produced thin film samples that had been previously UV irradiated. The growth curves obtained in the absence and in the presence of TiO_2 and Fe-doped thin films are presented in Figure 57.

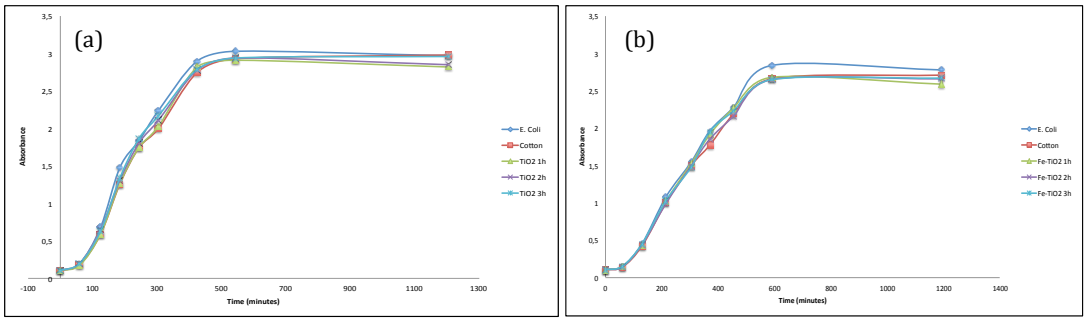

Figure 57: *E. coli* HB 101 growth curves obtained in the presence of (a) TiO_2 thin films and (b) in the presence of Fe-doped thin films.

From the results presented in the figure, it is possible to conclude that the curves are very similar in all the experimental conditions. These observations indicate that the presence of the different thin films do not have a direct effect on the growth of this *E. coli* strain in the conditions tested.

This absence of antimicrobial activity might have happened because these thin films were not continuously irradiated with UV light. As it is known, when TiO_2 is irradiated with UV light, the electrons of the valence band absorb the UV energy and are promoted to the conduction band, forming (e^-/h^+) pairs. These forming (e^-/h^+) pairs are responsible for the redox chemical reactions and react with H_20 and O_2^- leading to the formation of ROS species. These ROS can cause bacteria death [76]. However, the aforementioned process did not fully occurred and, it can also be concluded that TiO_2 itself is not toxic to the bacteria under our experimental conditions.

Doping with Fe caused a shift of the absorption edge for visible region of the electromagnetic spectrum and, consequently, the majority of visible light spectrum can be used for the photocatalysis and antimicrobials processes.

The growth curves of *E. coli* HB 101 when incubated with Ag-doped thin films are presented in Figure 58.

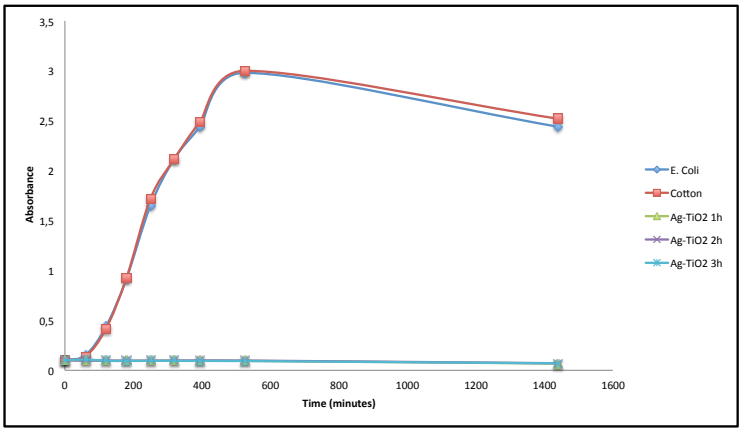

Figure 58: *E. coli* HB 101 growth curves obtained in the presence and in the absence of Ag-doped thin films.

Contrarily to what was observed in the above-referred experiments, the TiO_2 thin films doped with Ag showed a strong antimicrobial effect. With these samples the inhibition of bacterial growth is clearly evident. As it can be seen in Figure 58, for all the samples, a complete growth inhibition is observed. Over the time it was observed that the bacteria maintained its initial concentration (A~0.1), that is, Ag^+ ions only did not allow the bacteria division. The bacteria, which remained alive over time, may have used nutrients and energy available not to divide but to stay alive against the Ag^+ ions.

Several studies were done to explain the inhibitory effect of silver on bacteria growth [8, 22]. Silver has a well-known bactericidal capability *per se*. The antibacterial activity of silver is known to be due to Ag^+ ions, which strongly bind the tiol groups present in the bacteria cell membrane, leading to the inactivation of the proteins, destroying the cell by rupturing the wall. Moreover, silver ions can interact with the bacteria's DNA preventing cell reproduction [117–119]. In silver nanoparticles exist the release of Ag^0 atoms and the chemical species, Ag^+ ions and Ag^0 atoms, increase the generation of ROS (Equations 22, 23 and 24), causing the rapid death of the microorganisms [46, 117]. The silver present in TiO_2 thin films also plays an important role in the oxide surface. This metal strongly influences charge separation upon light absorption and Ag^+ ions can change the characteristics of the TiO_2 surface locally, which can cause measurable variations

in the point of zero charge (PZC), altering in this way the adhesion of the microorganism in the surface of the oxide [117].

$$Ag^{+} + O_2^{-} \rightarrow Ag^{0} + O_2 \quad \text{(Equation 22)}$$

$$Ag^{0} + O_2^{-} \rightarrow Ag^{+} + O_2^{2-} \quad \text{(Equation 23)}$$

$$H_2O_2 + Ag^{0} \rightarrow HO^{-} + {\bullet}OH + Ag^{+} \quad \text{(Equation 24)}$$

Firstly, the Ag loading amount and the TiO_2 active sites are the two essential parts for the photocatalytic activity of Ag/TiO_2. The higher electron-hole recombination inhibition is achieved at higher Ag loading rate according to Schottky barrier formation. And the increasing of Ag loading will increase the O_2 adsorption to produce more reactive oxygen species (ROS) for photooxidation. However, on the contrary, the excess of Ag loading on TiO_2 surface could reduce the active sites, which could reduce the photocatalytic activity of Ag/TiO_2. Therefore, it is important to load Ag on TiO_2 surface while maintaining sufficient active sites [135].

2nd Part – Optimization of DC Magnetron Sputtering Process Parameters: Production of ultra-thin TiO_2 thin films

In this section we used the nomenclature of A11, A14, A15 and A17 to identify the developed TiO_2 thin films so that the results can be better understandable. Although the deposition parameters were previously presented in the table 4 of Chapter V in table 8 it is emphasized the main sputtering conditions that were used in this optimization step.

Table 8: Sputtering deposition parameters for the TiO_2 thin films samples.

Samples	Argon Flow (sccm)	Deposition time (min)	Working Pressure (mbar)
A11	5	30	2.3×10^{-3}
A14	30	30	3.7×10^{-2}
A15	5	120	2.3×10^{-3}
A17	30	120	2.4×10^{-2}

6. 6 – METALIC TO OXIDE MODE

In DC reactive magnetron sputtering there are three oxidation modes as a function of the reactive gas flow (O_2): at a low gas flow there is the sputtering of metallic mode, compound mode at high gas flow and the transition mode in which the target changes from metallic to compound mode. The degree of oxide coverage on the target is represented by these different modes. Figure 59 shows the discharge voltage achieved as a function of oxygen flow during reactive magnetron sputtering for different argon flow rates (5sccm, 15sccm and 30sccm).

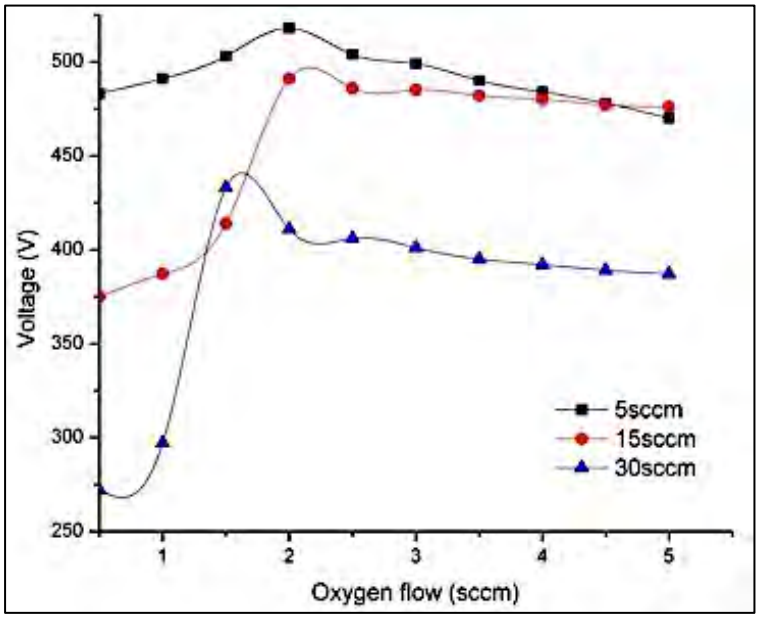

Figure 59: Discharge voltage at different oxygen flow for three different argon flow rates (5sccm, 15sccm and 30sccm) during DC reactive magnetron sputtering (discharge current was 0,45 A, reverse time was 2µs and frequency was 100kHz).

Working at a constant current (0.45 A), the discharge voltage increased as the oxygen flow increased from zero up to the threshold. For the processing conditions using argon flow rate of 5sccm, 15sccm or 30sccm, the threshold occurs at 2sccm, 2sccm and 1.5sccm of oxygen flow, respectively. This demonstrates a reduction of the metal area being sputtered due to the coverage of oxide on the metallic target [45]. After that, the target voltage decreased to a stable value corresponding to the compound-sputtering mode in which a transparent TiO_2 film is expected to form on substrate surface. For 0.5sccm oxygen flow, the discharge voltage varied from 272 V (for an argon flow of 30sccm), to 375 V (for an argon flow of 15sccm), and to 483 V (for an argon flow of 5sccm). It should be noted that, under an argon flow of

30sccm, the oxide formation should occur sooner for smaller values oxygen flow (1.5sccm), when compared with an argon flow of 5sccm and 15sccm. When the argon atoms are injected into the chamber and the Ar^+ impinges the target surface, titanium atoms are ejected. These atoms, when in contact with the oxygen ones can lead to the formation of titanium oxide and then condense on the substrate to form the TiO_2 thin film.

6. 7 – XRD – X-Ray Diffraction

Figure 60 shows the X-ray diffraction (XRD) spectrum of the TiO_2 thin films produced in this second part of the work.

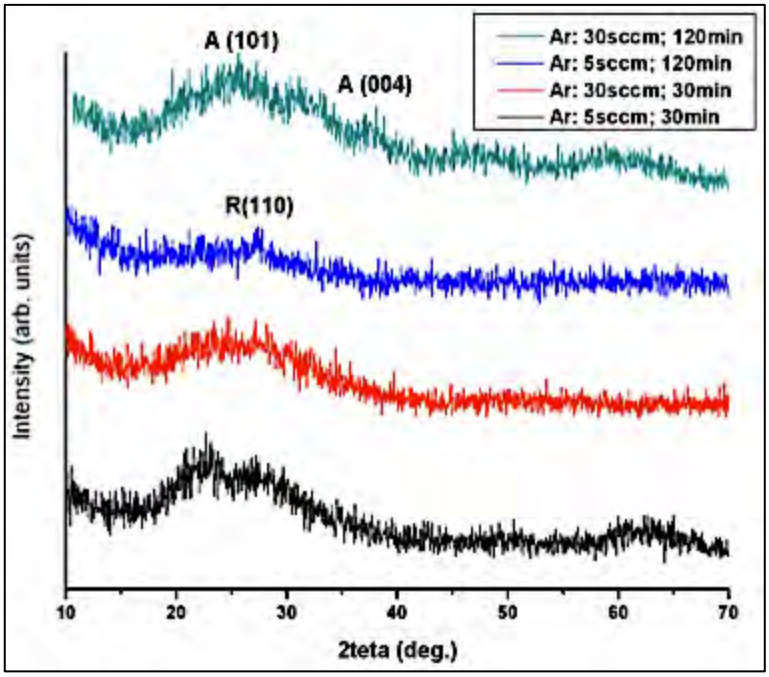

Figure 60: XRD Diffraction of TiO_2 thin films by the Bragg Brentano method.

The crystalline phases can be confirmed by the presence of (101), (004) diffraction peaks, in the case of anatase phase and (110) for the rutile crystalline phase. It should be pointed out that the process parameters have an important influence in the crystalline nature of the produced TiO_2 thin films. In fact, when comparing these results with the ones obtained in the first part we can conclude that strategy was successfully performed. However, more efforts should be make in future

works to increase the crystallinity of the samples. Nevertheless, a conclusion may be drawn: the working pressure as well as deposition time has a significant influence on the attained crystal polymorph.

6. 8 – MORPHOLOGICAL CHARACTERIZATION

The TiO_2 coatings have been analyzed by SEM and AFM techniques in order to observe and study the surface structure, morphology, thickness and roughness. Figure 61 shows the surface and the cross-section SEM micrographs of the samples A11 and A14 produced with an argon flow rate of 5 and 30 sccm during 30 minutes, respectively.

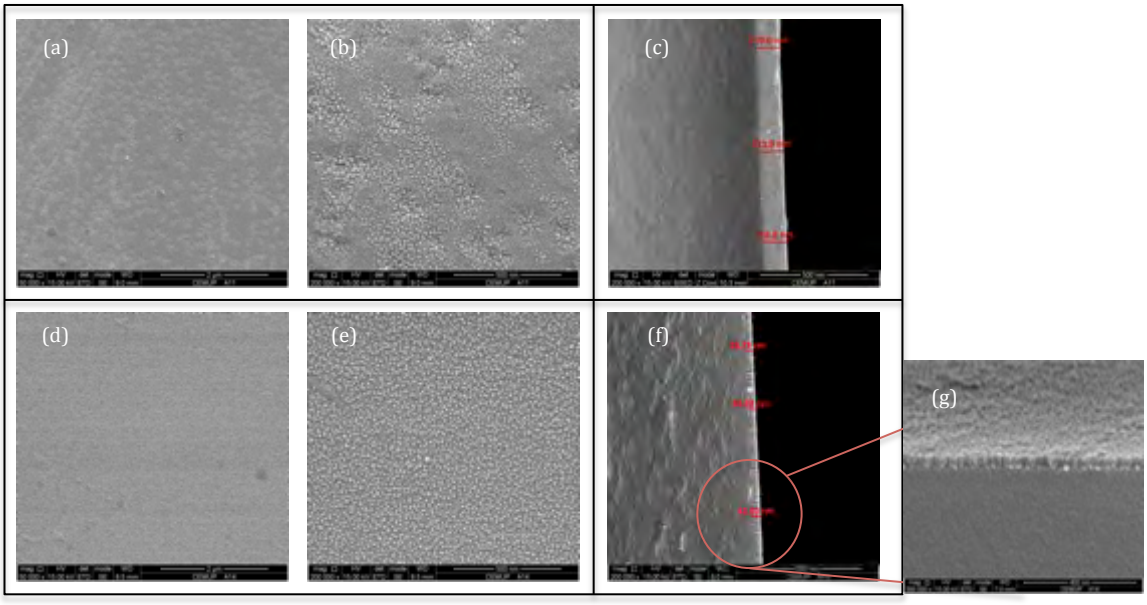

Figure 61: SEM micrograph for TiO_2 samples with 30minutes of the deposition time in different argon flow: A11 – 5sccm (a) magnification of 50 000x, (b) magnification of 200 000x and (c) cross section; A14 – 30 sccm (d) magnification of 50 000x, (e) magnification of 200 000x, (f) cross section and (g) detail of the thin film morphology – A14. Red numbers indicate the thickness of the film.

As can be observed the surfaces of the thin films exhibited a certain degree of roughness and, apparently, the thin film became rougher when argon flow is decreased and the working pressure decreased. It can be also observed that the TiO_2 thin films are composed of small spherical particles. Moreover, through the

cross section SEM micrographs it can be seen that, increasing the argon flow rate the thin films have a very small thickness (42nm). With a deposition time of 30min is almost impossible to see where the substrate ends and where the thin film begin (A14). On the other hand in the sample A11, is clearly visible the presence of the thin film, with a thickness of about 114nm. The thin layer of the sample A14 can be seen in the inset (Figure 61g), which is formed by small spherical organized particles.

Figure 62 shows the AFM images of the TiO_2 thin films of the samples mentioned previously (A11 and A14).

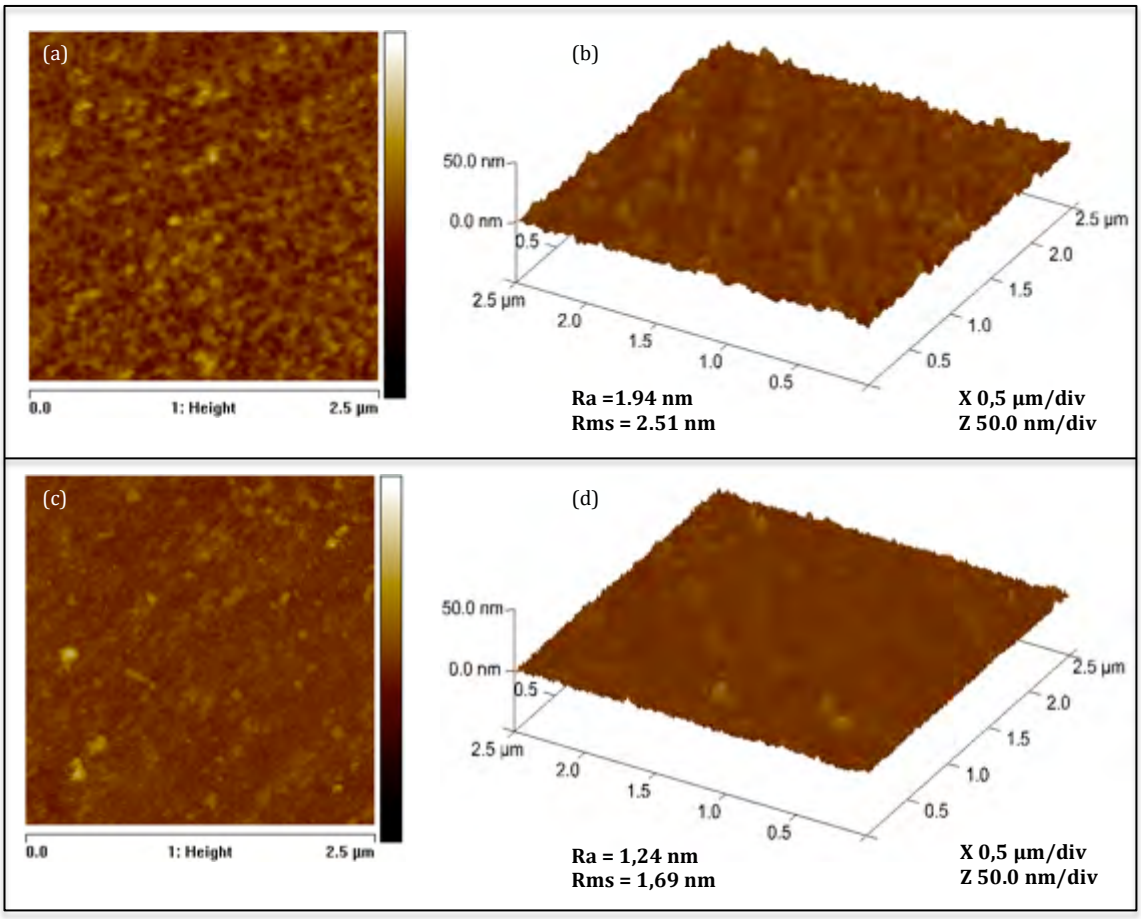

Figure 62: AFM images for samples TiO_2 thin films produced by using 30min of the deposition time and different argon flows: A11 – 5sccm (a) 2D; (b) 3D and A14 – 30sccm (c) 2D; (d) 3D.

As can be inferred from the presented results, the produced samples have a very smooth surface (with an average roughness below 2 nm). Nevertheless, it is

important to emphasize that, as already observed in the SEM micrographs; the increase in the argon flow rate contributes to a decrease in the Ra from 1.94 to 1.24 nm.

In order to understand what happens with increasing deposition time under the same conditions of the previous samples (A11 and A14), the deposition time was changed from 30 min to 120min. Figure 63 presents the SEM micrographs of the samples A15 and A17.

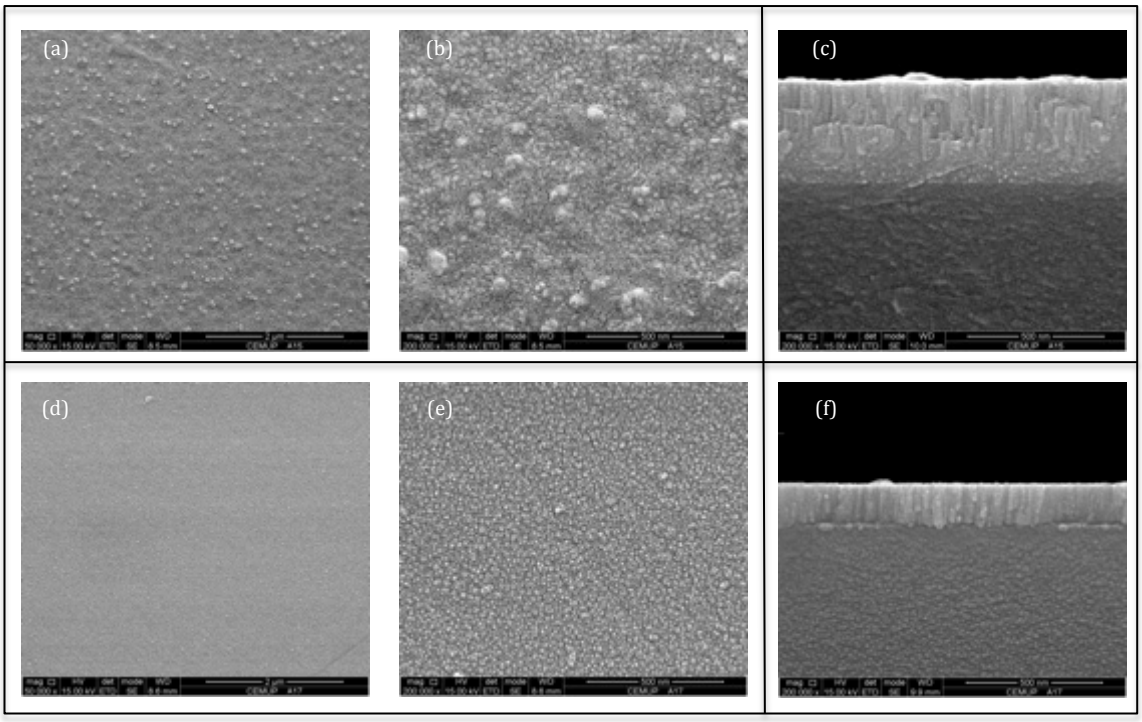

Figure 63: SEM micrograph for TiO_2 samples with 120minutes of the deposition time in different argon flow: A15 – 5sccm (a) magnification of 50 000x, (b) magnification of 200 000x and (c) cross section; A17 – 30 sccm (d) magnification of 50 000x, (e) magnification of 200 000x, (f) cross section

In these two cases there are significant differences in the morphology of the thin films. In sample A17, its morphology is similar to the previous two (A11 and A14), also presenting small spherical particles and an apparent uniform and smooth surface. Meanwhile, the sample A15 presents larger particles, which indicates that the sample may possesses a certain degree of roughness in comparison with the previous ones. Through the cross section images it can be observed that, with increasing deposition time there is a change in the oxide growth. While in the

sample A14 there are small spherical-like particles deposited on the substrate, in these samples the oxide appears to have a columnar growth (see Figure 61f and Figure 63). Moreover, it should also be pointed out that, as occurred for samples A11 and A14, the thin films thickness is strongly influenced by the argon flow rate. For the sample produced with higher flow rate, the obtained thickness is lower (130 nm) than the one obtained by using a smaller argon rate (380 nm).

In Figure 64 are presented the EDX results corresponding to the samples A15 and A17.

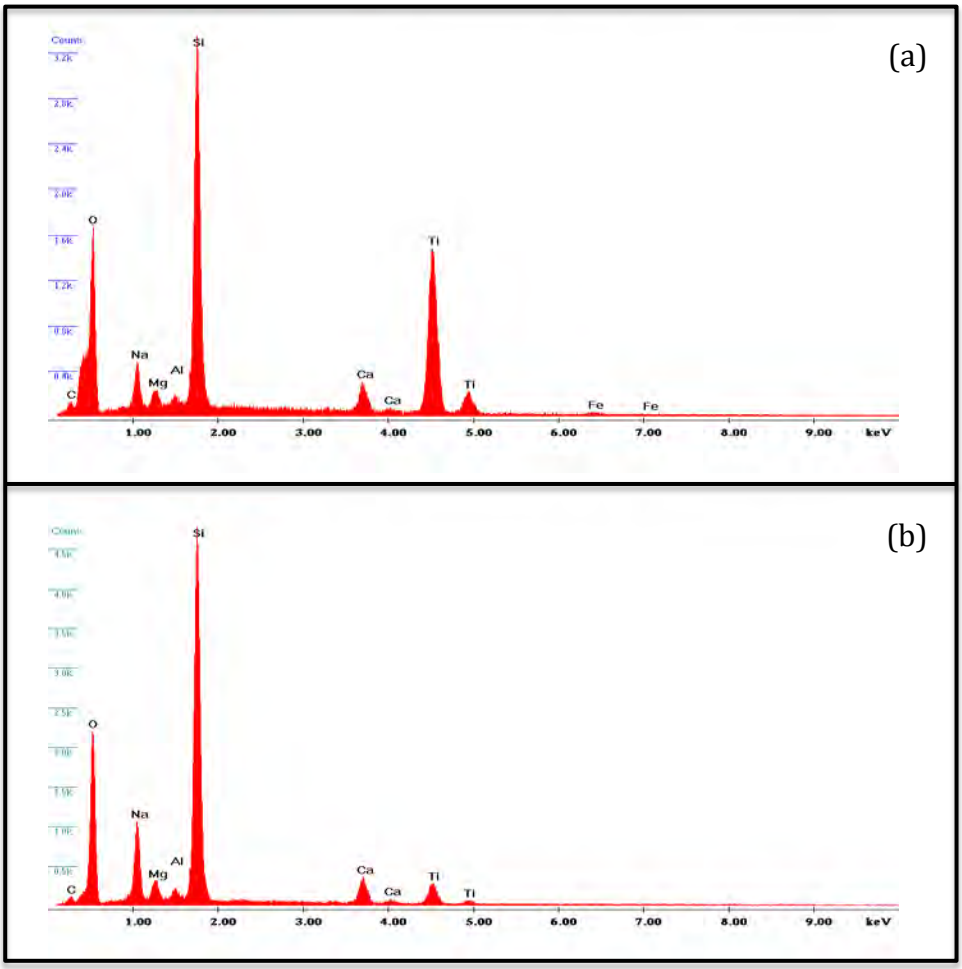

Figure 64: EDX spectrum for TiO_2 samples in the different argon flows (a) 5 sccm (A15) and (b) 30 sccm (A17).

Through of the EDX results is possible to detect the presence of TiO_2 in the A15 and A17 samples. Both presented peaks of the Ti and O_2, thus proving the presence of TiO_2.

Figure 65 shows the AFM images of the TiO_2 thin films of the samples mentioned previously (A15 and A17).

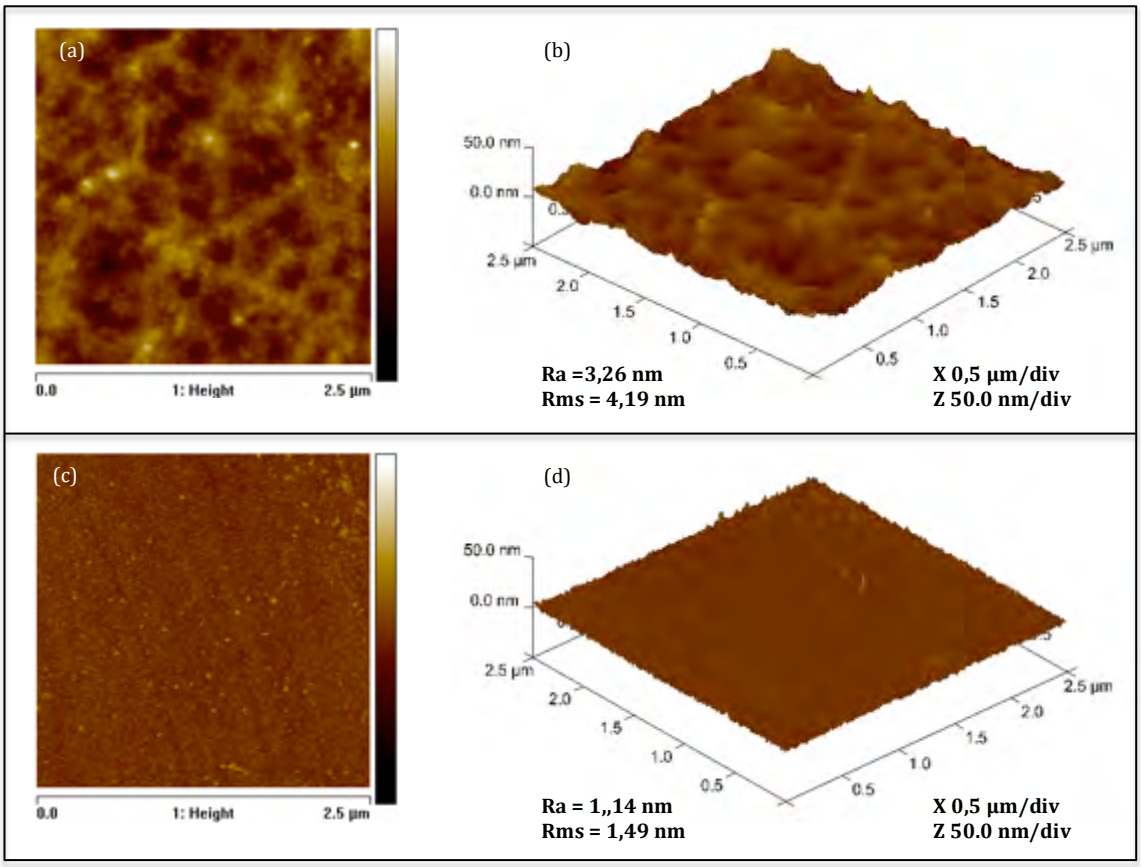

Figure 65: AFM images for TiO_2 thin films produced by using a deposition time of 120min at different argon flow rates: A15 – 5sccm (a) 2D; (b) 3D and A17 – 30sccm (c) 2D; (d) 3D.

In this case and because the samples have a very distinct thickness, the effect of argon flow rate is very perceptible. The sample produced by using the argon flow rate becomes rougher (3.26 nm in comparison with 1.14 nm). These results are expected since the working pressure strongly imparts the obtained morphology of the thin films as previously explained in the Thornton Model (presented in Figure 24).

6. 9 – OPTICAL SPECTROPHOTOMETRY

The optical properties of thin films were studied by recording the transmittance spectra in a wavelength range from 250 to 2500nm. In Figure 66 are presented the

obtained results for all the produced samples. In Figure 66a are presented the samples with a deposition time of the 30min, while that, in Figure 66b the samples have a deposition time of the 120 min.

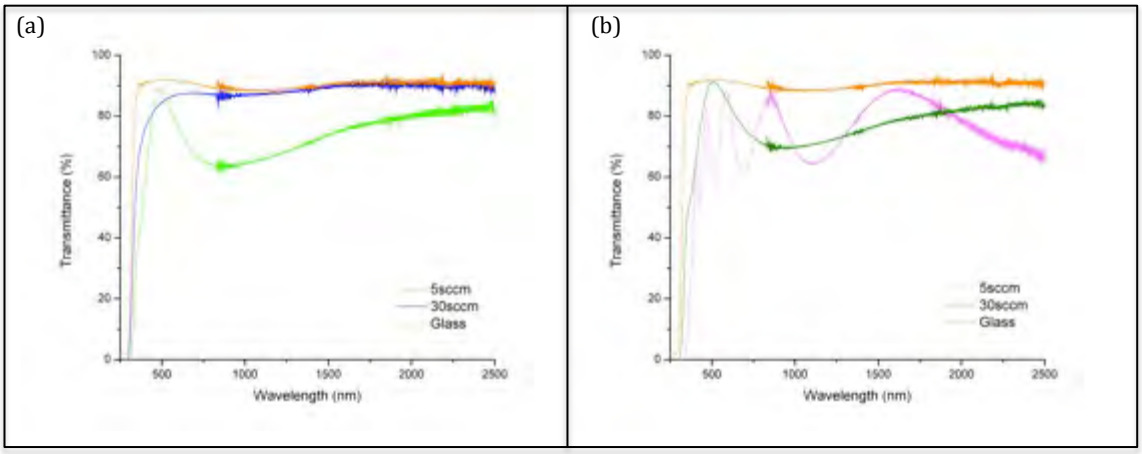

Figure 66: UV-Vis-NIR transmittance spectra of samples with argon flow 5sccm and 30sccm for 30min (a) and 120min (b).

If transmittance spectra of Figure 66 are observed individually it is possible to conclude that, increasing argon flow and working pressure causes a decrease in the thickness of the thin film. These data are in agreement with the results obtained in SEM. By analyzing the transmittance spectra for different deposition times, we can conclude that with the increase of the deposition time there is an increased of the thickness of the thin film. This can be clearly observed by the increase in the number of the recorded waveforms.

Using equation 16, it was possible to determine the thickness of the samples through at least two maximum or minimum of the waveforms. As can be seen from the spectra, three samples (A11, A14 and A17) do not present more than one waveform, so it becomes impossible to determine the thickness by this method. Table 9 summarizes the thickness obtained by SEM and from the ones determined by using the transmittance spectrum values.

Table 9: Thicknesses of the samples A11, A14, A15 and A17.

SAMPLES	THICKNESS (NM)
A11	~114
A14	~40
A15	~380
A17	~130

6. 10 – CONTACT ANGLE

For the purpose of understanding surface properties of the TiO_2 samples, the contact angle between a deionized water droplet (5µL) and the samples surface (at room temperature) was measured by using the equipment Dataphysics - Contact Angle System OCA.

In figure 67 is presented the lateral image of the water droplet on the surface for the different samples (A11, A14, A15 and A17). The behavior of the water droplet was observed during 90s. The images were obtained for the initial time (immediately after the drop touches the sample surface: t=0s), for t = 30s, t = 60s and t = 90s.

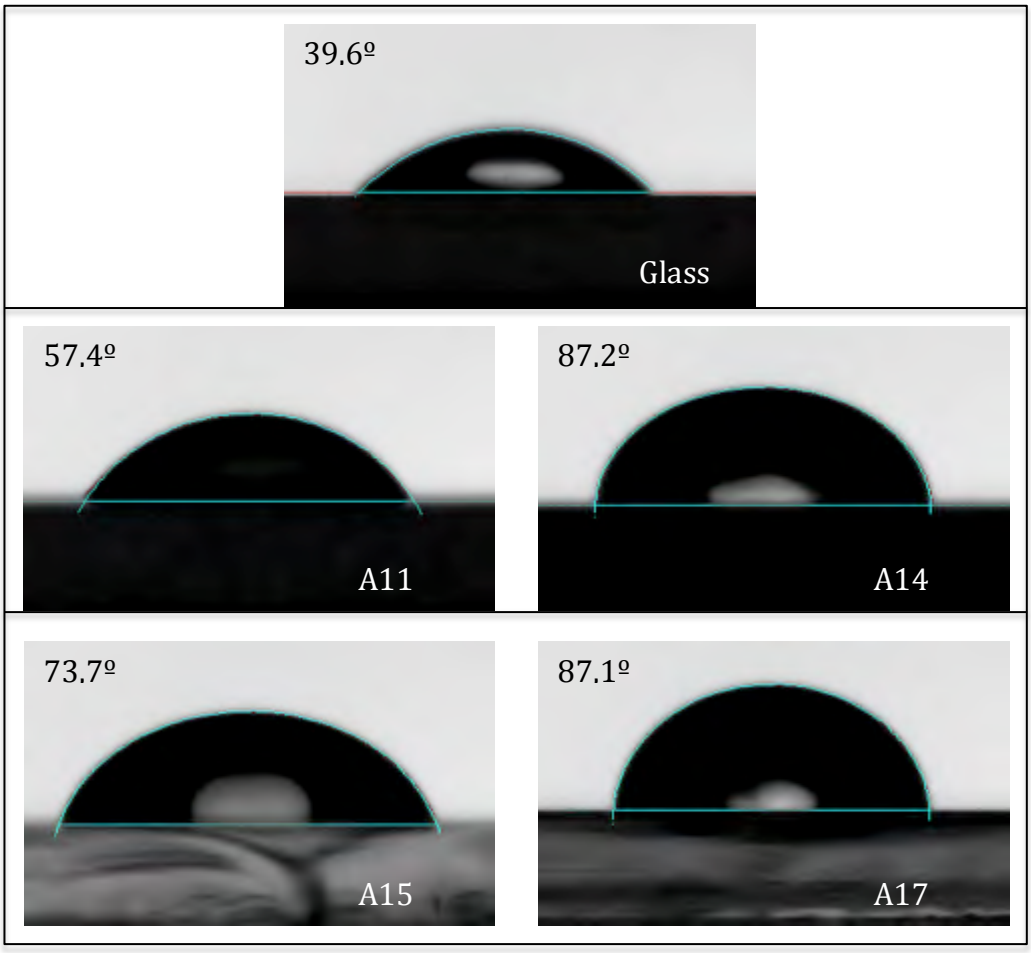

Figure 67: Images of the water droplet form deposited on the sample surface after 90s.

The obtained results show that the glass substrate has a hydrophilic behavior (since it presents a contact angle of 39.6 °). The TiO_2 samples also present a hydrophilic behavior, but are more hydrophobic in comparison with the glass substrate. Figure 68 shows the contact angle variation over time.

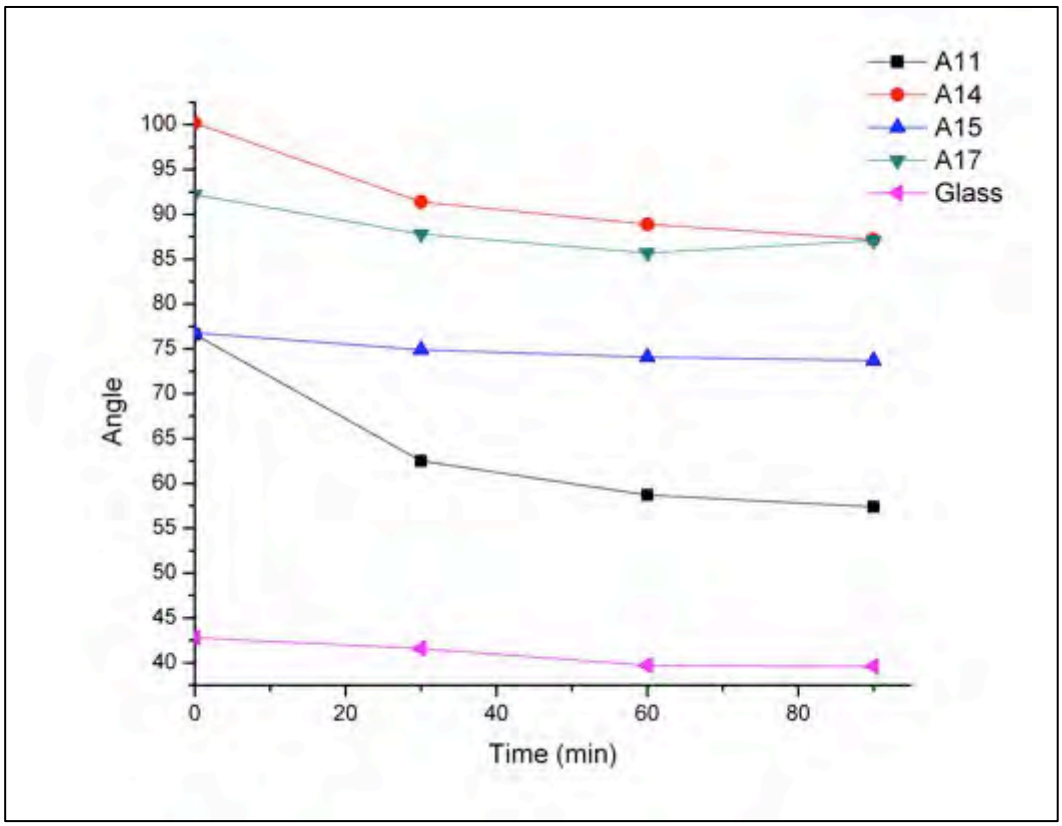

Figure 68: Contact angle variation over time.

6.11 – PHOTOCATALYTIC ACTIVITY

To evaluate the photocatalytic effect of the TiO_2 thin films was used the same method mentioned in the 1st part of the results, by measuring the absorbance spectra of a methylene blue (MB) aqueous solution over time.

In Figure 69 are presented the results of the photodegration yield and the corresponding photodegradation rate constant for all the TiO_2 produced samples.

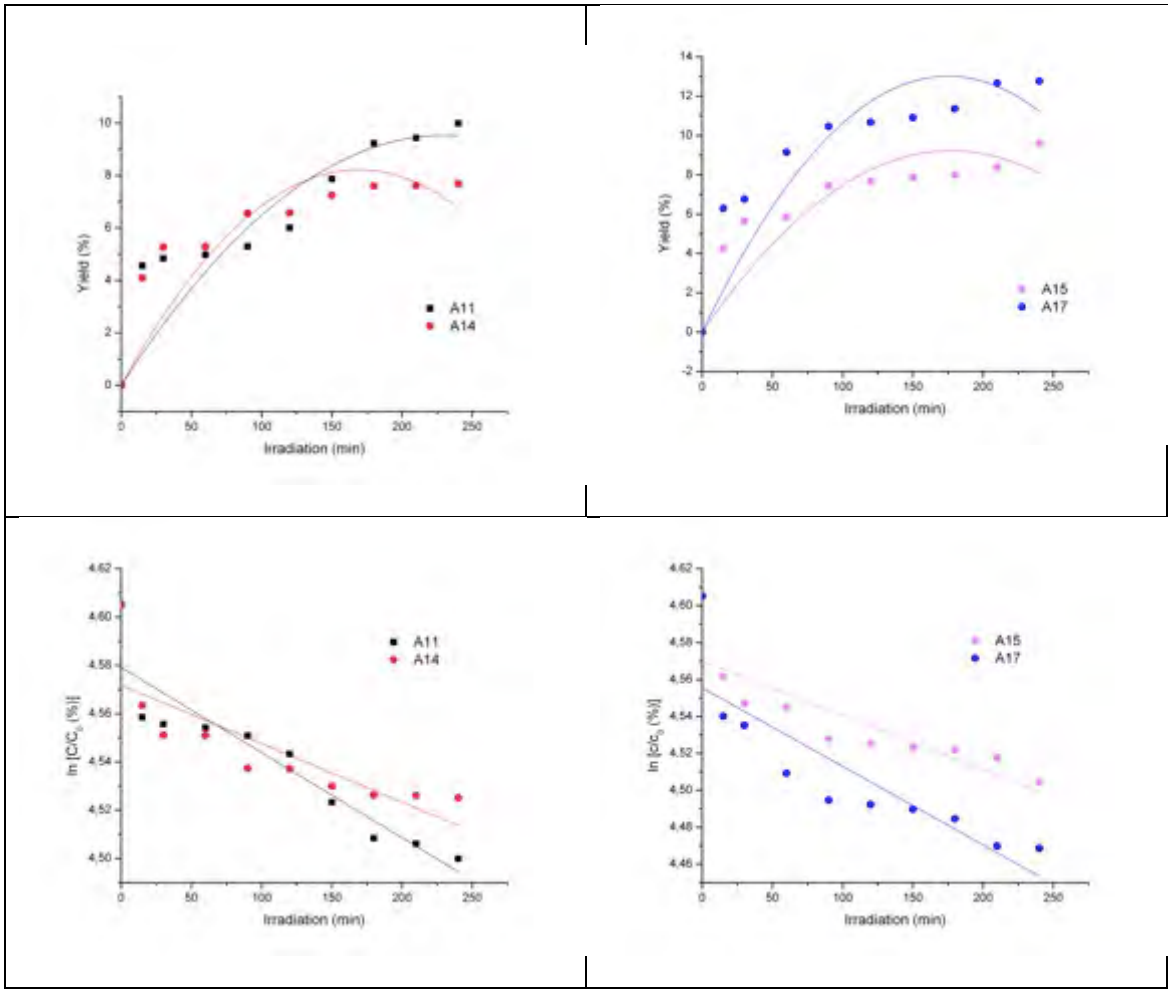

Figure 69: Photocatalytic degradation of methylene blue aqueous solution on A11, A14, A15 and A17 samples under UV light source (C_0 is the initial aqueous *RhB* concentration, 0,5 mg/l and C is the aqueous *RhB* concentration after 15, 30, 60, 90, 120, 150, 180, 210 and 240 min irradiation time).

Additionally, in table 10 are summarized the calculated k values and photodegradation yield for the TiO_2 samples.

Table 10: Values obtained of the yield (%) and the rate constant of photodegradation in different coatings.

Thin Films	Photodegradation yield (%)	k (Photodegradation Rate)
A11 (5sccm; 30 min)	~10	$3,5x10^{-4}$
A14 (30 sccm; 30 min)	~7,7	$2,4x10^{-4}$

A15 (5sccm; 120min)	~9,6	$2,9x10^{-4}$
A17 (30 sccm; 120 min)	~12,8	$4,3x10^{-4}$

The thicker samples are those with higher photocatalytic yield. However, it is also noted that the sample with a higher degree of crystallinity (mainly by anatase) is the one that presents the highest photocatalytic yield. It is noteworthy that these performances are of the same order of magnitude as those obtained in the 1st part of the results. Nevertheless, it should be mentioned that these yields were achieved with much lower thicknesses. Although it has not been possible to deposit thin films with processing conditions in this second part, we anticipate that these will lead to a more efficient superficial finishing of the textile fibers in terms of comfort and malleability.

6. 12 – ANTIMICROBIAL ACTIVITY

Antimicrobial activity was studied by counting the number of colony forming units in petri dishes. Figures 70 and 71 represent photographs of the bacterium *E. coli* growth in petri dishes, subsequently subjected to the A15 (Ar=5sccm; t=120min.) and A17 (Ar=30sccm; t=120min.) samples, respectively.

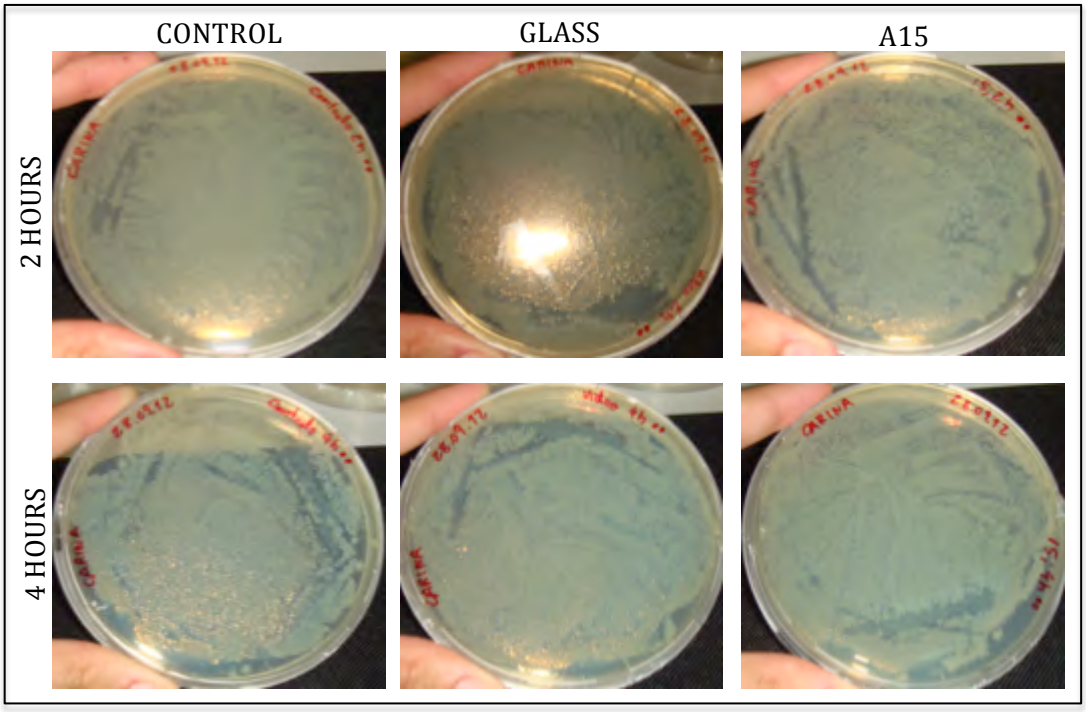

Figure 70: Photographs of the petri dishes showing *E. coli* growth under different conditions: in the control, in contact with the glass and A15, after 2hours and 4 hours of UV irradiation.

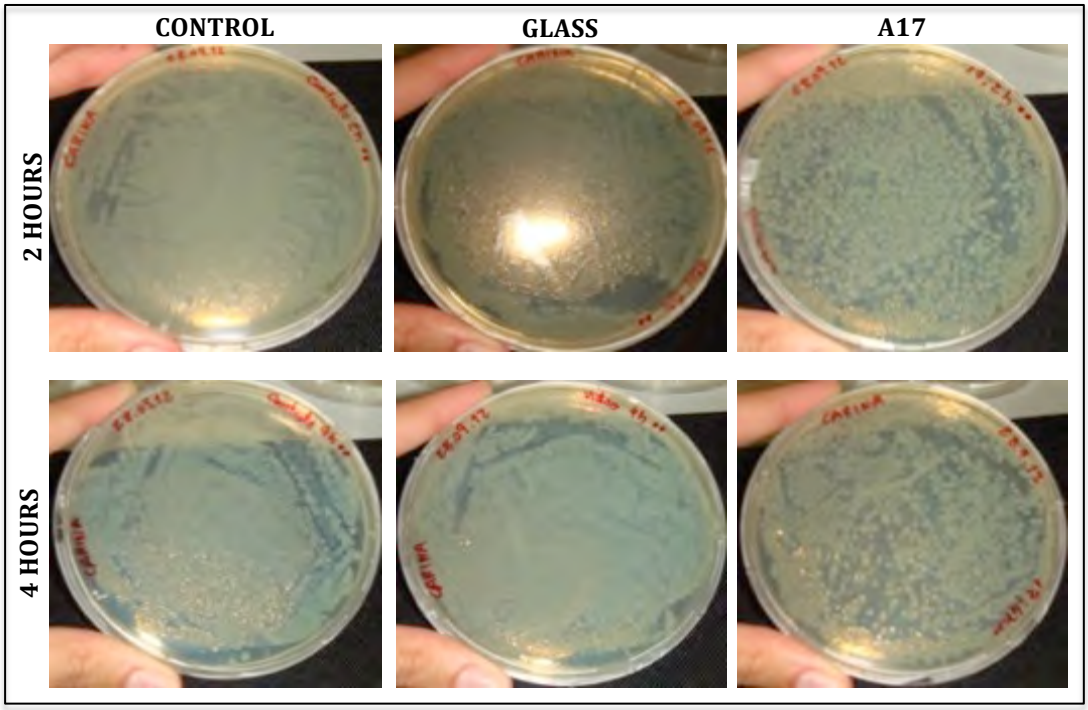

Figure 71: Photographs of the petri dishes showing *E. coli* growth under different conditions: in the control, in contact with the glass and A17, after 2hours and 4 hours of the UV irradiation.

These are preliminary results that have to be repeated using a smaller inoculum because the initial number of cells is to high to allow CFU counting. Although it is not possible to count the number of colonies present in every plate, it is noteworthy that in the photographs of the sample A17, the number of colonies decreased after 4 hours of UV exposure, when compared with the control. This sample shows more crystalline phases and a higher photocatalytic effect and, apparently, presents some effect in inhibiting bacteria growth.

CHAPTER VII

CONCLUSIONS

CHAPTER VII – CONCLUSIONS

In order to produce TiO_2 thin films that present antimicrobial activity, we studied these thin films by processes of structural characterization, by XRD technique, its surface morphology characterization by SEM and AFM techniques, optical characterization by UV-Vis spectroscopy, hydrophobicity by Angle Contact and the study of photocatalytic activity of this semiconductor.

In the 1st part of this work concluded that:

- The results of XRD showed that all samples were amorphous, since none diffractogram showed peaks characteristic of TiO_2 crystalline forms: anatase and rutile, which are the most studied;
- The deposition time increases the roughness and thickness of the sample;
- Fe-doped TiO_2 samples, it is possible to observe that the absorption edge presents a pronounced shift for higher wavelengths;
- Photocatalytic activity of the TiO_2 based thin films is quite low (not higher than 11%);
- The TiO_2 thin films doped with Ag show a strong antimicrobial effect.

In the 2nd part of this work concluded that:

- The results of XRD showed that the samples are crystalline (A15 and A17);
- TiO_2 thin films are composed of small spherical particles;
- Increasing argon flow and working pressure causes a decrease in the thickness and roughness of the thin film;
- The TiO_2 samples also present a hydrophilic behavior;
- The sample with a higher degree of crystallinity (mainly by anatase) is the one that presents the highest photocatalytic yield and antimicrobial effect.

CHAPTER VIII

FUTURES PERSPECTIVES

CHAPTER VIII – FUTURE PERSPECTIVES

After this work we intend to pursue the study of the second part, so that such solutions can be applied to textile and/or polymer materials. With the aim of endowing increased very important features, such as self-cleaning effect and anti-microbial capacity. Moreover, optimizing the process parameters leading to improve of the crystalline nature must optimize the photocatalytic performance of the process. It is emphasized the importance of, introducing dopants metallic elements in the produced TiO_2 thin films, using the process parameters presented in 2nd part of the results, in order to use a significant part of the electromagnetic spectrum.

Another interesting possibility for a future work could consist in comparing the photocatalytic yield obtained through the vapor phase deposition techniques (used in this study), with those that could be obtained by impregnation of TiO_2 nanoparticles in textile fibers.

REFERENCES

(1) OECD. Opportunities and risks of Nanotechnologies. Report in co-operation with the OECD International Futures Programme.

(2) Cândice Felippi. Esmaltes e Nanotecnologia: Produtos cosméticos inovadores (November 2012).

(3) West J. and Halas Naomi. **2003**. Engineered Nanomaterials for Biophotonics Applications: Improving Sensing, Imaging, and Therapeutics. *Annu. Rev. Biomed. Eng.* 5: 285-92.

(4) http://fgamedia.org/faculty/rdcormia/NANO/nanostructures/thinfilms.htm (Online) November 2012.

(5) www.chemistryland.com(Online) November 2012.

(6) Gao, J. and Xu, B. **2009**. Applications of nanomaterials inside cells. *Nano Today.* 4 (1) 37 – 51.

(7) Caruthers, S. D., Wickline, S. A., Lanza, G. M. **2007**. Nanotechnological applications in medicine. *Current Opinion in Biotechnology*. 18 (1) 26-30.

(8) Flores, C. Y., Diaz, C., Rubert, A., Benítez, G. A., Moreno, M. S., Fernández, M.A., Salvarezza, R. C., Schilardi, P. L., Vericat, C. **2010**. Spontaneous adsorption of silver nanoparticles on Ti/TiO2 surfaces. Antibacterial effect on Pseudomonas aeruginosa. *Journal of Colloid and Interface Science*. 350, 402–408.

(9) Suni I. **2008**. Impedance methods for electrochemical sensors using nanomaterials. *TrAC Trends in Analytical Chemistry*. 27 (7). 604-611.

(10) Saji V., Thomas J. **2009**. Nanomaterials for corrosion control. *Current Science.* 92 (1).

(11) Rapoport L., Billk Y., Feldman Y., Homyonfer M., Cohen S., Tenne R. **1997**. Hollow nanoparticles of WS2 as potential solid-state lubricants. *Nature*. 387.

(12) Silvestre C., Duraccio D., Cimmino S. **2011**. Food packaging based on polymer nanomaterials. *Progress in Polymer Science*. 36 (12). 1766-1782.

(13) Adrievski R. **2009**. Brittle Nanomaterials: Hardness and Superplasticity. Bulletin of the Russian Academy of Sciences: Physics. 73 (9). 1222-1226.

(14) Kamat P. **2007**. Meeting the Clean Energy Demand: Nanostructure Architectures for Solar Energy Conversion. *J. Phys. Chem. C.* 111(7). 2834-2860.

(15) Wasa K.; Kitabatake M.; Adachi H. **2004**. Thin Film Materials Technology. Sputtering of Compound Materials.

(16) Rao C. N. R., Muller A., Cheetham A. K. The Chemistry of Nanomaterials. Synthesis, Properties and Applications. Volume 1.

(17) Sahoo S. K., Parveen S., Panda J. J. **2007**. The present and future of nanotechnology in human health care. *Nanomedicine: Nanotechnology, Biology and Medicine.* 3 (1). 20-31.

(18) Vasilev K., Cook J., Griesser H. **2009**. Antibacterial surfaces for biomedical devices. Expert Rev. Med. Devices 6(5), 553-567.

(19) Costorton J., Stewart P., Greenberg E. **1999**. Bacterial Biofilms: A common Cause of Persistent Infections. Science, New Series. Vol. 284 No. 5418, 1318-1322.

(20) Costerton J., Lewandowski Z., Caldwell D., Korber D., Lappin-Scott H. **1995**. Microbial Biofilms. *Journals Microbiology*. 49. 711-745.

(21) Visai L., Nardo L., Punta C., Melone L., Cigada A., Imbriani M., Arclola C. **2011**. Titanium oxide antibacterial surfaces in biomedical devices. Int. J. Artif. Organs. 34 (9): 929-946.

(22) Bala, T., Armstrong, G., Laffir, F., Thornton, R. **2011**. Titania–silver and alumina–silver composite nanoparticles: Novel, versatile synthesis, reaction mechanism and potential antimicrobial application. *Journal of Colloid and Interface Science*. 356, 395–403.

(23) Yuan, Y., Ding, J., Xu J., Deng J., and Guo J. **2010**. TiO2 Nanoparticles Co-Doped with Silver and Nitrogen for Antibacterial Application. *Journal of Nanoscience and Nanotechnology.* Vol. 10, 1–7.

(24) Liqiang J., Yichun Q., Baiqi W., Shudan L., Baojiang J., Libin Y., Wei F., Honggang F., Jiazhong S. **2006**. Review of photoluminescence performance of nano-sized semiconductos materials and its relationships with photocatalytic activity. Solar Energy Materials e Solar Cells 90. 1773-1787.

(25) Goenland.blogspot. Photocatalytic what? (Online) Dezember 2012.

(26) Henderson M. A. **2011**. A surface science perspective on TiO2 photocatalysis. Surface Science Reports. 66. 185-297.

(27) Caronna T, Gambarotti C, Palmisano L, Punta C, Recupero F. **2005**. Sunlight-induced reactions of some heterocyclic bases with ethers in the presence of TiO2: A green route for the synthesis of heterocyclic aldehydes. J Photochem Photobiol A. 171(3):237-242.

(28) Caronna T, Gambarotti C, Palmisano L, Punta C, Pierini M, Recupero F. **2007.** Sunlight-induced functionalisation reactions of heteroaromatic bases with aldehydes in the presence of TiO_2: A hypothesis on the mechanism. J Photochem

Photobiol A. 189(2-3):322-328.

(29) Gambarotti C, Punta C, Recupero F, Caronna T, Palmi- sano L. **2010**. TiO_2 in organic photosynthesis: Sunlight induced functionalization of heterocyclic bases. Curr Org Chem. 14(11):1153-1169.

(30) Landmann M., Rauls E., Schmidt W. G. **2012**. The electronic structure and optical response of rutile, anatase and brookite TiO_2. J. Phys.: Condens. Matter 24. 195503 (6pp).

(31) Dambournet D., Belharouak I., Amine K. **2010**. Chem. *Mater.* 22 1173.

(32) Qyourzal S., Tamimi M., Assabbane A., Ait-Ichou Y. **2005**. J. of Colloid and Interface Sci. 186:261.

(33) Norotsky A., Jamicson J. C. Kleppa O. J. **1967**. 158-338.

(34) Kuman P. N., Keizer K., Burggraff A. J., Okubo T., Nagomato H., Morooka S. Nature. **1992**. 358-48.

(35) Garvie R. C. J. Phys. Chem. **1978**. 82, 218.

(36) Zhang, H., and Banfield, J. F. **2000**. Understanding polymorphic phase transformation behavior during growth of nanocrystalline aggregates: insight from TiO2. *Journal Physical Chemistry B*, Vol. 104, pp. 3481.3487.

(37) Gopal, M., Moberly Chan, W. J., De Jonghe, L. C. **1997**. Room temperature synthesis of crystalline metal oxides. *Journal of Materials Science*, Vol. 32, pp. 6001.6008.

(38) Tanaka K., Capule M. F. V., Hisanaga T. **1991**. Chem. Phys. Lett. 187, 73.

(39) Kuman K. N. P., Keizer K., Burrgraaf A. J. **1993**. J. Mater. Chem. 3, 1141.

(40) Zallen R., Moret M. P. **2006**. Solid State Commun. 137-154.

(41) Li J. G., Isshigaki T. Sun X. **2007**. J. Phys. C. 111, 4969.

(42) Wanbiao H., Liping L., Guangshe L., Ghanglin T., Lang S. **2009**. Cryst. Growth Des. 9, 3676.

(43) Shah RR, Kaewgun S, Lee BI, Tzeng TRJ. **2008**. The Antibacterial Effects of Biphasic Brookite-Anatase Titanium Dioxide Nanoparticles on Multiple-Drug-Resistant Staphylococcus aureus. J Biomed Nanotechnol. 4(3):339-348.

(44) Miyagi T, Kamei M, Mitsuhashi T, Ishigaki T, Yamazaki A. **2004**. Charge separation at the rutile/anatase interface: a dominant factor of photocatalytic activity. Chem Phys Lett. 3. 390(4-6):399-402.

(45) Carneiro J. O., Teixeira V., Portinha A., Magalhães A., Coutinho P., Tavares C. J., Newton R. **2007**. Iron-doped photocatalytic TiO2 sputtered coatings on plastics for self-cleaning applications. *Materials Science Engineering B*. 138: 144-150.

(46) Foster H., Ditta I., Varghese S., Steele A. **2011**. Photocatalytic disinfection using titanium dioxide: spectrum and mechanism of antimicrobial activity. Appl Microbiol Biotechnol. 90. 1847-1868.

(47) Maira A. .J., Yeung K.L., Lee C.Y., Yue P.L., Chan C.K., **2000**. *J. Catal.* 192. 185.

(48) Xu Z.L., Shang J., Liu C.M., Kang C., Guo H.C., Du Y.G. **1999.** *Mater. Sci. Eng. B.* 63, 211.

(49) Vinodgopal K., Kamat P.V. **1995**. *Environ. Sci. Technol.* 29, 841.

(50) Do Y.R., Lee K., Dwight K., Wold A. **1994**. *J. Solid State Chem*. 108, 198.

(51) Shah RR, Kaewgun S, Lee BI, Tzeng TRJ. **2008**. The Antibacterial Effects of Biphasic Brookite-Anatase Titanium Dioxide Nanoparticles on Multiple-Drug-Resistant Staphylococ- cus aureus. J Biomed Nanotechnol. 4(3):339-348.

(52) Miyagi T, Kamei M, Mitsuhashi T, Ishigaki T, Yamazaki A. **2004**. Charge separation at the rutile/anatase interface: a dominant factor of photocatalytic activity. Chem Phys Lett. 3. 390(4-6):399-402.

(53) Mai L, Wang D, Xie Y, Huang C, Zhang Z. **2010**. Synthesis and bactericidal ability of Ag/TiO_2 composite films deposited on titanium plate. Applied Surface Science 277. 974-978.

(54) Carneiro J. O., Teixeira V., João A., Magalhães A., Tavares C. J. **2008**. Study of Nd-doping effect mechanical cracking on photoreactivity of TiO2 thin films. *Vacuum.* 82: 1475-1481.

(55) Carneiro J. O., Teixeira V., Portinha A., Dupák L., Magalhães A., Coutinho P. **2005**. Study of the deposition parameters and Fe-dopant effect in the photocatalytic of TiO_2 films prepared by dc reactive magnetron sputtering. Vacuum 78. 37-46.

(56) Matusunga T. **1985**. Sterilization with particulate photosemiconductor. Journal of Antibacterial Antifungal Agents. 13:211–220.

(57) Matsunaga T., Tomoda R., Nakajima T., Wake H. **1985**. Photo-electrochemical sterilization of microbial cells by semiconductor powders. FEMS Microbiol Lett 29(1–2):211–214.

(58) Brook L.A., Evans P., Foster H.A., Pemble M.E., Steele A., Sheel D.W., Yates H.M. **2007**. Highly bioactive silver and silver/titania composite films grown by chemical vapour deposition. Journal of Photochemistry and Photobiology 187(1):53–63.

(59) Yates H.M., Brook L.A., Sheel D.W., Ditta I.B., Steele A., Foster H.A. **2008**. The growth of copper oxides on glass by flame assisted chemical vapour deposition. Thin Solid Films 517(2):517–521.

(60) Ditta I.B., Steele A., Liptrot C., Tobin J., Tyler H., Yates H.M., Sheel D.W., Foster H.A. **2008**. Photocatalytic antimicrobial activity of thin surface films of TiO_2, CuO and TiO_2/CuO dual layers on Escherichia coli and bacteriophage T4. Applied Microbiology Biotechnology 79(1):127–133.

(61) Chan D.W.T., Law K.C., Kwan C.H.S., Chiu W.Y. 2005. Application of an air purification system to control air-borne bacterial contamination in a university clinic. Trans. Hong Kong Inst. Eng. 12(1):17–21.

(62) Chong M.N., Jin B., Chow C.W.K., Saint C. **2010**. Recent developments in photocatalytic water treatment technology: a review. Water Research 44(10):2997–3027.

(63) Makowski A., Wardas W. **2001**. Photocatalytic degradation of toxins secreted to water by cyanobacteria and unicellular algae and photocatalytic degradation of the cells of selected microorganisms. Curr. Top. Biophys. 251:19–25.

(64) Selma M.V., Allende A., Lopez-Galvez F., Conesa M.A., Gil M.I. **2008**. Heterogeneous photocatalytic disinfection of wash waters from the fresh-cut vegetable industry. Journal of Food Protection 71(2):286–292.

(65) Paspaltsis I., Kotta K., Lagoudaki R., Grigoriadis N., Poulios I., Sklaviadis T. **2006**. Titanium dioxide photocatalytic inactivation of prions. Journal General Virology 87(10):3125–3130.

(66) Giraud A., Radman M., Matic I., Taddei F. **2001**. The rise and fall of mutator bacteria. *Current Opinion in Microbiology.* 4 (5): 582-585.

(67) Jhttp://www.cdc.gov/ecoli/.

(68) Hu C., Guo J., Qu J., Hu X. **2007**. Photocatalytic degradation of pathogenic bacteria with AgI/TiO_2 under visible light irradiation. Langmuir 23(9):4982–4987.

(69) Sheel D.W., Brook L.A., Ditta I.B., Evans P., Foster H.A., Steele A., Yates H.M. **2008**. Biocidal silver and silver/titania composite films grown by chemical vapour deposition. International Journal of Photoenergy. Article ID 168185, 11 pp.

(70) Skorb E.V., Antonouskaya L.I., Belyasova N.A., Shchukin D.G., Möhwald H., Sviridov D.V. **2008**. Antibacterial activity of thin-film photocatalysts based on metal-modified TiO_2 and TiO_2:In_2O_3 nano-composite. Appl. Catal. B 84(1–2):94–99.

(71) Matthew Banks. Earth Spared: The Small Scale. **2012**.

(72) Utakokikutani-en.blogspot.pt (Online) Dezember **2012**.

(73) Dunlop P.S.M., Sheeran C.P., Byrne J.A., McMahon M.A.S., Boyle M.A., McGuigan K.G.

2010. Inactivation of clinically relevant pathogens by photocatalytic coatings. J. Photochem. Photobiol. A 216:303–310.

(74) Grieken R., Marugan J., Pablos C., Lopez A. **2010**. Comparison between the photocatalytic inactivation of Gram-positive E. faecalis and Gram-negative E. coli faecal contamination indicator microorganisms. *Appl Catal B.* 100:212–220.

(75) Kangwansupamonkon W., Lauruengtana V., Surassmo S., Ruktanonchai U. **2009**. Antibacterial effect of apatite-coated titanium dioxide for textiles applications. Nanomed Nanotechnol Biol Med 5:240– 249.

(76) Arellano U., Asomoza M., Ramírez F. **2011**. Antimicrobial activity of Fe-TiO_2 thin films photocatalysts. J. Photochem. Photobiol. A 222: 159-165.

(77) www.genetic-testings.com (Online) Dezember 2012.

(78) Cho M., Chung H., Choi W,. Yoon J. **2004**. Linear correlation between inactivation of E. coli and OH radical concentration in TiO_2 photocatalytic disinfection. Water Research 38(4):1069–1077.

(79) Cho M., Chung H., Choi W., Yoon J**. 2005**. Different inactivation behaviors of ms-2 phage and Escherichia coli in TiO2 photo- catalytic disinfection. Appl. Environ. Microbiol. 71(1):270–275.

(80) Cho M., Yoon J. **2008**. Measurement of OH radical ct for inactivating Cryptosporidium parvum using photo/ferrioxalate and photo/ TiO_2 systems. J. Appl. Microbiol. 104(3):759–766.

(81) Kikuchi Y., Sunada K., Iyoda T., Hashimoto K., Fujishima A. **1997**. Photocatalytic bactericidal effect of TiO_2 thin films: dynamic view of the active oxygen species responsible for the effect. J. Photochem. Photobiol. A 106(1–3):51–56.

(82) Pratap Reddy M., Phil H.H., Subrahmanyam M. **2008**. Photocatalytic disinfection of Escherichia coli over titanium (IV) oxide supported on Zeolite. Catal. Lett. 123(1–2):56–64.

(83) Caballero L., Whitehead K.A., Allen N.S., Verran J. **2009**. Inactivation of Escherichia coli on immobilized TiO_2 using fluorescent light. J. Photochem. Photobiol. A 202(2–3):92–98.

(84) Cheng C.L., Sun D.S., Chu W.C., Tseng Y.H., Ho H.C., Wang J.B., Chung P.H., Chen J.H., Tsai P.J., Lin N.T., Yu M.S., Chang H.H. **2009**. The effects of the bacterial interaction with visible-light responsive titania photocatalyst on the bactericidal performance. J. Biomed. Sci. 16(7):10.

(85) Sunada K., Watanabe T., Hashimoto K. **2003**. Bactericidal activity of copper-deposited TiO_2 thin film under weak UV light illumination. Environ. Sci. Technol. 37(20):4785–4789.

(86) Rossnagel S. M. in Aputter Deposition, Sproul W. D., lEGG k.o., EDITORD. 1995. Opportunities for Innovation: Advanced Surface Engineering. Switzerland: Technomic Publishing Co.

(87) Mathews A., 1996. Surface Engineering Casebook, Woodhead Publishing Ltd. J. S. Burnell-Gray, P. K. Datta (Eds.). Cambridge 23.

(88) Hocking M. G., Vasantasree P. S. **1989**. Sidky, Metallic and Ceramic coatings, Longman Scientific Technical. Essex.

(89) T Powell, C. F.; Oxley, J. H. and Blocher Jr. **1967**. *J. M. Vapor Deposition*; Wiley, New York.

(90) Tese Mattox, D. M. Handbook of Physical Vapor Deposition (PVD) Processing: Film Formation, Adhesion, Surface Preparation and Contamination Control; Noyes Publications, *New Jersey*. **1998**.

(91) Westwood, W. D. Sputter Deposition; AVS Education Committee book series, v. 2. New York: Education Committee, **2003**.

(92) http://www.globalspec.com/reference/82036/203279/chapter-3-sputtering-phenomena

(93) Granqvist C. **2012**. Oxide electrochromics: An introduction to devices and materials. Solar Energy Materials & Solar Cells. 99:1-13.

(94) Kouznetsov V., Macák K., Schneider J., Helmersson U., Petrov I. **1999**. A novel pulsed magnetron sputter technique utilizing very high target power densities. *Surface and Coatings Technology*. 122(2-3): 290-293.

(95) Anders A. **2008**. Self-sputtering runaway in high power impulse magnetron sputtering: The role of secondary electrons and multiply charged metal ions. *Applied Physics Letters*. 92(20).

(96) Micro Magnetics. Magnetron Sputtering Technology. Sensible Solutions.

(97) www.alacritas-consulting.com (Online) Dezember **2012**.

(98) Chapman B. N. **1980**. Glow Discharge Processes, John Wiley & Sons Inc. New York.

(99) www.tfe-thinfilmequipment.com (Online) Dezember **2012**.

(100) Anders A. **2011**. Discharge physics of high power impulse magnetron sputtering. Surface & Coatings Technology 205. S1-S9.

(101) Window B., Savvides N., **1986**. J. Vac. Sci. Technol. A, 4 (3) 453.

(102) Sproul W. D., **1991**. Surf. Coat. Technol. 49-284.

(103) yKelly P. J. and Arnell R. D. **2000**. Magnetron sputtering: a review of recent developments and applications. *Vaccum*. 56(3): 159-172.

(104) Carneiro J. O., Teixeira V., Nascimento J. H. O., Neves J., Tavares P. B. **2011**. Photocatalytic activity and UV-protection of TiO**2** nanocoatings on poly(lactic acid)

fibres deposited by pulsed magnetron sputtering. J. Nanoscience Nanotechnology. 11. 1-8.

(105) Neugebauer C. A. **1983**. L. I. Maissed (Ed). Handbook of thin film. McGraw-Hill. Mew York.

(106) Greene J. E. **1993**. D. T. J. Hurle (Ed.) Handbook of Crystal Growth, Vol. 1, Elsevier Science Publishers. Amsterdam. 640.

(107) Jehn H. A. **1992**. W. Gissler, H. A. Jehn (Eds.) Advanced Techniques for Surface Engineering, Brussels, 5.

(108) Martin L. W., Chu Y. H., Ramesh R. **2010**. Advances in the growth and chacacterization of magnetic, ferroelectric, and multiferroic oxide thin films. *Materials Science and Engineering: R: Reports.* 68(4-6):89-133.

(109) Movechan B. A., Demchishin A. V. **1969**. Fig. Met. Metalloved. (USSR), (Phys. Met, Metallogr.), Vil. 28, p.653.

(110) Thornton J. A. **1974**. J. Vac. Sci. Technol. 11, 666.

(111) Messier R., Giri A. P., Roy R. A., **1984**. J. Vac. Sci. Technol. A2, 500.

(112) Fewster P. F. **1993**. X-ray diffraction from low-dimensional structures. Semiconductor science and technology. 8, 1915-1934.

(113) Wang B., Li C., Pang J., Qing X., Zhai J., Li Q. **2012**. Novel polypyrrole-sensitized hollow TiO2/fly ash cenospheres: Synthesis, characterization, and photocatalytic ability under visible light. *Applied Surface Science*. 258(24): 9989-9996.

(114) Zhang Y., Huang Y., Wang Y., Ji X., Shih S., Jia B. **2009**. Study of nano-Ag particles doped TiO_2 prepared by photocatalysis. *J. Nanosci. Nanotechnol*. 9(6): 3904-8.

(115) Carneiro J. O., Teixeira V., Martins A. J., Mendes M., Ribeiro M., Vieira A. **2009**. Surface properties of doped and undoped TiO2 thin films deposited by magnetron spittering. Vacuum 83. 1303-1306.

(116) Tavares C. J., Vieira J., Rebouta L., Hungerford G., Coutinho P., Teixeira V., Carneiro J. O. Fernandes A. J. **2007**. Reactive sputtering deposition of photocatalytic TiO_2 thin films on glass substrates. Materials Science and Engineering B 138, 139-143.

(117) Kubacka A., Ferrer M., Martínez-Arias A., Fernández-García M. **2008**. Ag promotion of TiO2-anatase disinfection capability: study of Escherichia coli inactivation. *Appl. Catal.* B 84(1–2):87–93.

(118) Ashkarran A. A. **2011**. Antibacterial properties of silver-doped TiO2 nanoparticles under solar simulated light. *J. of Theoretical and Applied Physics*. 4-4:1.8.

(119) Yu, B., Leung K. M., Guo, Q., Lau, W. M. and Yang J. **2011**. Synthesis of Ag–TiO_2

composite nano thin film for antimicrobial application. Nanotechnology. 22, 115603 (9pp).

(120) ttp://fys.kuleuven.be/iks/nvsf/experimental-facilities/x-ray-diffraction-2013-bruker-d8-discover. January 2013.

(121) SEM/EDS – Scanning electron Microscopy / Energy Dispersive Spectroscopy, Comparison of V.P. SEM and F.E. SEM Applications. http://www.innovatechlabs.com/analytical-services-electron-microscopy.htm.

(122) Zhu, Yuan Yuan, Ding, Gu Qiao, Ding, Jian Ning, Yuan, Ning Yi. **2010**. AFM, SEM and TEM Studies an Porous Anodic Alumina, 725-734.

(123) Mohammad, Abdulrashid I., Scanning Electron Microscope/energy dispersive X-Ray Spectrometer (SEM/EDS).

(124) http://www.intertek.com/analysis/microscopy/edx/. January 2013.

(125) Vilalta-Clemente, Arantxa, GLoystein, Katherin. **2008**. Principles of Atomic Force Microscopy (AFM), Physics of Advanced Materials Winter School.

(126) Wilson, Robert A., Bullen, Heather A., Basic Theory – Atomic Force Microscopy (AFM), Northem Kentucky University.

(127) Raman, Arvind, Atomic Force Microscopy (AFM), Birck Nanotechnology Center, PURDUE University.

(128) http://www.shimadzu.com/an/spectro/uv/index.html. January 2013.

(129) http://www.vam.ac.uk/content/journals/conservation-journal/issue-01/uv-vis-nir-spectrocopy-what-is-it-and-what-does-it-do/

(130) http://ec.europa.eu/health/opinions/en/energy-saving-lamps/figtableboxes/light-spectrum.htm

(131) http://www.the-scientist.com/?articles.view/articleNo/18797/title/Across-the-Spectrum--Instrumentation-for-UV-Vis-Spectrophotometry/

(132) http://www2.chemistry.msu.edu/faculty/reusch/virttxtjml/spectrpy/uv-vis/uvspec.htm

(133) Zhao L., Wang J., Li Y., Wang C., Zhou F., Liu W. **2010**. Anodic aluminum oxide films formed in mixed electrolytes of oxalic and sulfuric acid and their optical constants. *Physica B*. 405, 456-460.

(134) Physics Mathematics. Proceedings of the Estonian academy of sciences. **2003**. A journal recognized by The European Phycical Society.

(135) Liu L., Liu Z., Bai H., Sun D. **2012**. Concurrent filtration and solar photocatalytic disinfection/degradation using high-performance Ag/TiO_2 nanofiber membrane. *Water Research.* 46: 1101-1112.